UNIVERSITAT POMPEU FABRA

TESI DOCTORAL UPF / 2020

Reconstitution of FMRP-mediated mRNA transport system *in vitro*

Author:

Artem Komissarov

Thesis supervisor:

Dr. Sebastian Maurer

Centre for Genomic Regulation

Cell and Devlopmental Biology Program

July 1, 2020

Abstract

Learning and memory formation are based on the mechanisms of synaptic plasticity. Synaptic plasticity modulates development and strengthening of new neuronal connections, or synapses, upon learning and is based on local protein synthesis next to activated neuronal spines. Thousands of mRNA species are transported from the soma of neuron to dendrites, in order to be translated on demand. The mechanisms of this mRNA transport remain poorly understood.

Mutations of Fragile X-mental retardation protein (FMRP) cause a spectrum of mental retardation disorders. Among other functions, FMRP mediates signal-mediated mRNA transport and local translation in dendrites. In multiple attempts to understand how FMRP is implicated in mRNA transport, there were identified few motor protein candidates. Besides controversy in the literature, none of these motor proteins was demonstrated to bind directly and transport FMRP. In my PhD studies, I employed *in vitro* reconstitution assays, coupled to Total Internal Reflection (TIRF) microscopy, to test, which of the proposed candidate motors can transport FMRP along the microtubules and whether FMRP can co-transport mRNA molecules.

In order to understand the biochemistry of FMRP-mediated mRNA transport, I have purified and tested motor proteins from three Kinesin subfamilies. In this PhD thesis, I am reporting that FMRP binds directly to and is transported by Kinesin-2 motor (KIF3A/C heterodimer), but not by the other tested motors. Mutational analysis of FMRP suggests that its C-terminal region plays the biggest role in Kinesin-2 binding, and that this interaction does not depend on the RGG box region, known to recognise the G-quadruplex structure of FMRP's mRNA targets. These results suggest that mRNA and motor binding by FMRP are not mutually exclusive, and thus FMRP must be capable to mediate mRNA transport. I also show that KIF3A/C motor binds several mRNA targets, with and without G-quadruplex structure, and that G-quadruplex mRNA competes with FMRP for motor binding. These results raise many questions that I address in the Discussion part of the thesis.

This work is the first of its kind, to my knowledge, to systematically test kinesin motor proteins for direct interaction with FMRP and to reconstruct an FMRP transport complex. I conclude that FMRP binds directly to the Kinesin-2 motor and that this complex moves processively along the microtubules. This complex is still missing its cargo, mRNA, which will be investigated beyond the scope of this PhD thesis. I analyse the speeds of used kinesin motors and compare them to the literature. In the end, I discuss

possible reasons why FMRP was not binding the G-quadruplex mRNA in my experimental conditions and outline the caveats of *in vitro* reconstitution assays.

Resumen

El aprendizaje y la formación de la memoria se basan en los mecanismos de plasticidad sináptica. La plasticidad sináptica modula el desarrollo y el fortalecimiento de nuevas conexiones neuronales, o sinapsis, al aprender y se basa en la síntesis local de proteínas al lado de las espinas neuronales activadas. Miles de especies de ARNm son transportadas desde el soma de la neurona a las dendritas, para ser traducidas bajo demanda. Los mecanismos de este transporte de ARNm siguen siendo poco conocidos.

Las mutaciones de la proteína Fragile X-mental Retardation (FMRP) causan un espectro de trastornos de retraso mental. Entre otras funciones, FMRP media el transporte de ARNm inducido por señal y la traducción local en las dendritas. En múltiples intentos de comprender cómo FMRP está implicada en el transporte de ARNm, se identificaron algunos candidatos de proteínas motoras. Además de la controversia en la bibliografía, no se demostró que ninguna de estas proteínas se uniera directamente y transportara FMRP. En mis estudios de doctorado, he utilizado ensayos de reconstitución *in vitro*, junto con la microscopía de reflexión interna total (TIRF), para probar cuál de los motores candidatos propuestos puede transportar FMRP a lo largo de los microtúbulos y si FMRP puede co-transportar moléculas de ARNm.

Para comprender la bioquímica del transporte de ARNm mediado por FMRP, he purificado y probado proteínas motoras de tres subfamilias de kinesina. En esta tesis doctoral, presento que FMRP se une directamente y es transportada por el motor Kinesin-2 (heterodímero KIF3A/C), pero no por los otros motores probados. El análisis de mutaciones de FMRP sugiere que su región C-terminal juega el papel más importante en la unión con Kinesin-2, y que esta interacción no depende de la región de RGG box, conocida por identificar la estructura de G.quadruplexde de los ARNm diana de FMRP. Estos resultados sugieren que FMRP es capaz de unirse al motor y transportar ARNm simultáneamente. También muestro una observación de que el motor KIF3A/C se une a varios ARNms, con y sin estructura de G-quadruplex, y que el ARNm con G-quadruplex compite con FMRP por la interacción con la proteína motora. Estos resultados plantean muchas preguntas que abordo en la parte de Discusión de esta tesis.

Este trabajo es el primero de su tipo, en mi conocimiento, para probar sistemáticamente la interaccion directa de FMRP con las proteínas motoras de kinesina y para reconstruir un complejo de transporte de FMRP. Concluyo que FMRP se une directamente al motor Kinesin-2 y que este complejo se mueve procesivamente a lo largo de los microtúbulos. A este complejo todavía le falta su carga, ARNm, que se investigará más allá del

alcance de esta tesis doctoral. Analizo las velocidades de los motores de kinesina utilizados y los comparo con la bibliografía. Al final, discuto las posibles razones de por qué FMRP no se estaba uniendo el ARNm de G-quadruplex en mis condiciones experimentales y describo los escollos en utiliza de los ensayos de reconstitución *in vitro*.

Автореферат

Здатність до навчання та формування пам'яті базуються на пластичності нервових з'єднань, або синапсів. Механізми синаптичної пластичності контролюють розвиток та розбудову нових синапсів під час навчання, та, у свою чергу, залежать від локального синтезу білку в неопосередкованій близькості до активованих дендритних шипиків. Тисячі молекул мРНК транспортуються з соми, або тіла нейрону, до дендритних закінчень, щоб забезпечити біоситез білку після стимуляції нервовим імпульсом. Механізми транспорту молекул мРНК залишаються погано дослідженими.

Мутаціїї в білку Fragile X-mental retardation (FMRP) призводять до цілого спектру нервово-дегенеративних розладів. Поміж інших функцій, FMRP опосередковує транспорт та трансляцію мРНК у дендритах після нервової стимуляції. Завдячуючи численним дослідженням ролі FMRP у транспорті мРНК, було ідентифіковано декілька кандидатів білків-моторів, які могли б забезпечити транспорт FMRP. Окрім того, що результати цих досліджень часто є суперечливими, досі не було доведено здатність жодного з цих моторів напряму зв'язуватись з FMRP та забезпечувати його транспорт. Задля того, щоб протестувати, який з потенційних білків-моторів може транспортувати FMRP по мікротрубочках, а також дослідити можливості FMRP у транспорті молекул мРНК, у моїх кандидатських дослідженнях я використовував метод реконституції, або відтворення, молекулярних комплексів *in vitro*.

Для того, щоб вивчити біохімію мРНК транспорту за участю FMRP, я очистив та випробував білки-мотори з трьох підродин Кінезинів. У цій дисертації, я доповідаю, що FMRP неопосередковано зв'язується та транспортується Кінезином-2 (гетеродимером KIF3A/C), але не іншими протестованими моторами. З мутаційного аналізу FMRP випливає, що його С-кінцевий фрагмент грає найбільшу роль у зв'язуванні Кінезина-2, а також що ця взаємодія не залежить від RGG box фрагменту, який відповідає за розпізнавання G-квадруплексної структури, притаманної молекулам мРНК, що зв'язуються з FMRP. Ці результати вказують на те, що FMRP має бути спроможним транспортувати мРНК у складі комплексу з мотором. Я також демонструю спостереження, що KIF3A/C мотор може зв'язувати декілька таргетних мРНК, з та без G-квадруплексу, а також що G-квадруплексна мРНК конкурує з FMRP за зв'язування з мотором. Ці результати залишають багато запитань, які я обговорюю в Дискусійній частині дисертації.

Ця робота є першою, до мого відома, роботою з систематичного тестування Кінезинів щодо їхньої взаємодії з FMRP та *in vitro* реконструкції транспортного комплексу FMRP. В результаті цієї роботи я роблю висновок, що FMRP неопосередковано зв'язується з Кінезин-2 мотором та що цей комплекс процесивно рухається вздовж мікротрубочок. Цьому комплексу все ще недостає вантажа, мРНК, що буде надалі досліджуватись поза межами цієї дисертації. Я аналізую швидкості руху досліджених кінезинів та порівнюю їх з літературними даними. У заключення, я обговорюю можливі причини, чому FMRP не впізнавав G-квадруплексні мРНК у моїх експериментальних умовах та звертаю увагу на підводні камені метода молекулярної реконструкції *in vitro*.

Table of Contents

List of figures

List of tables

Glossary and abbreviations

+TIPs	– plus-end microtubule tracking proteins
82-FIP	– 82 kDa FMRP-interacting protein
a.u.	– arbitrary unit(s)
CaMKIIα	– Calmoduline kinase II α mRNA
CYFIP	– cytoplasmic FMRP-interacting protein
FMRP	– fragile X-mental retardation protein
FRET	– Förster resonance energy transfer
FXR1/2	– Fragile X-mental retardation syndrome-related protein 1 or 2
FXS	– Fragile X-mental retardation syndrome
G4x	– G-quadruplex
IP	– immunoprecipitation
KAP	– kinesin associated polypeptide
KH (domains)	– hnRNP K homology (domains)
KHC	– kinesin heavy chain
KHL	– Kinesin Heavy Chain
KLC	– Kinesin Light Chain
KLC	– kinesin light chain
KO/KD	– knock out / knock down
LTD	– long-time depression
MAPs	– Microtubule-associated Proteins
NLS	– nucleus localization sequence
NUFIP	– nuclear FMRP-interacting protein
PEG	– polyethylene glycole
PLL	– poly-L-lysine
POI	– protein of interest
(m)RNP	– (messenger) RiboNucleoProtein (complex)
RPB	– RNA binding protein
smPIFE	– single molecule protein-induced fluorescence enhancement
SiMPull	– single molecule pull-down
TIRF(M)	– Total Internal Reflection Fluorescence (Microscopy)
WB	– Western blotting
Y2H	– yeast 2 hybrid assay
Zipcode	– a specific stretch of nucleotides inside of mRNA sequence recognised by a corresponding RNA binding protein

Chapter 1

1. INTRODUCTION

This PhD Thesis work stands on three overlapping fields of natural sciences: protein biochemistry, RNA biology and microscopy. However, making an introduction solely on these subjects would be very technical and not fulfilling.

Instead, I am inviting you to a hike through an area, where three mountains meet: protein biochemistry, RNA biology and Neuroscience. Although neuroscience was not the mountain I was trying to climb during my research, it is high enough to overlook protein and RNA biochemistry of my project from above. From the Neuroscience point of view, physiological sense of FMRP within an agglomerate of kinesin motors and mRNAs gains special depth and much higher functional relevance.

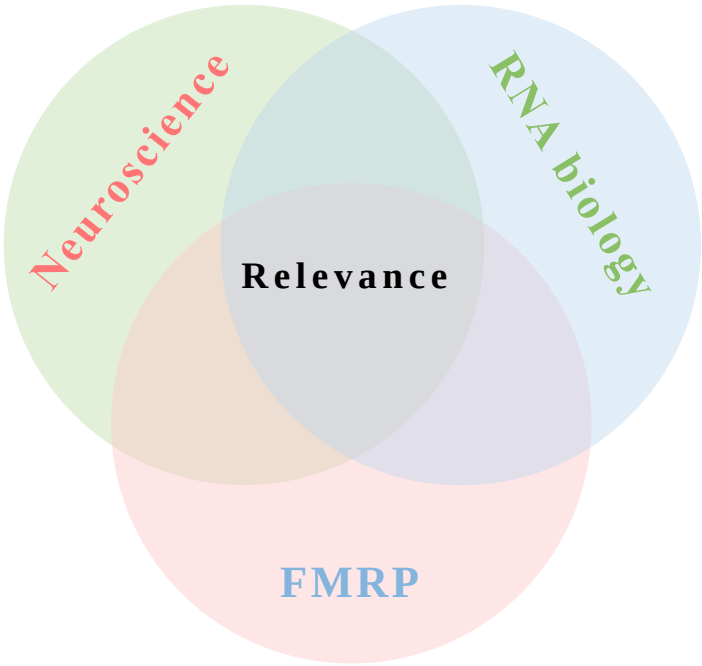

1.1 The logics and principles of mRNA transport

To sustain complexity of the living organisms, cells have to express genes in a precise spatiotemporal manner, fulfilled by numerous global and fine-tuning regulation mechanisms. The majority of the mechanisms regulating gene expression operate on the post-transcriptional level. The best-studied examples include post-transcriptional mRNA modifications[1,2], 5' and 3' mRNA degradation[3], regulation of the bulk and message-specific translation[4], etc. In the last two decades, another set of regulatory gene expression mechanisms caught the interest of researchers – namely mRNA transport, localisation and local translation.

1.1.1. mRNA transport and localisation are evolutionary conserved mechanisms

Specific localisation of the RNA messages was reported in the major kingdoms of life: bacteria[5,6], plants[7], fungi[8], animals[9], where it plays many different, yet indispensable roles. For instance, during mitosis of the *S. cerevisiae*, *ash1* mRNA is transported to the tip of the daughter cell, where upon its translation, the Ash1p protein restricts the mating type conversion of the budding daughter cell[10,11]. Localisation of maternal mRNAs forms polarity axes of the egg in *Drosophila*: *bicoid* mRNA marks the anterior pole, *gurken*, *nanos*, *staufen* and *oskar*[12] the posterior one; later in development *gurken* accumulates on the dorsal pole forming the dorso-ventral axis[13]. Accumulation of the *Vg1* mRNA on the vegetal pole of *Xenopus* egg[14] marks the dorsal pole of the future embryo and triggers formation of the dorsal mesoderm[15]. Transport of *β-actin* mRNA to the leading edge and protrusions of mammalian fibroblasts[16] mediates their motility[17]. And finally, a failure to localise *camkIIα* mRNA to dendrites leads to reduction in associative fear conditioning and object recognition memory, as well as impairments in spatial memory in mice[18].

These (Fig. I.1) and many other examples clearly demonstrate that mRNA transport and localisation, while being widely represented among different forms of life, can play a plethora of distinct physiological roles. Despite being diverse, the mechanisms of controlled and regulated asymmetrical mRNA distribution often are based on the same principles, which will be the focus of this subchapter.

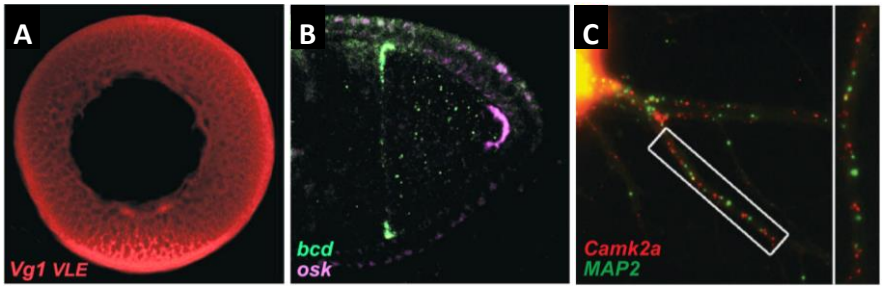

Fig. I.1. mRNA transport and localisation as evolutionary conserved mechanisms

A. Injected fluorescent RNA transcribed from the *Vg1* vegetal localization element is localized to the vegetal cortex (bottom) of a stage III *Xenopus* oocyte. **B.** *bicoid* (green) and *oskar* (magenta) mRNAs accumulate, respectively, at the anterior and posterior poles of a *Drosophila* oocyte. **C.** *camk2a* (red) and *map2* (green) mRNAs are localized in dendrites of cultured mammalian hippocampal neurons. Boxed area is shown at higher magnification on the right. Pictures adapted from[19].

1.1.2. Why transport mRNA?

There are two main reasons for transporting molecules, molecule complexes or organelles: either to deliver them into places that are poorly accessible by plain diffusion, or to break diffusion-generated gradients in a controlled manner. The previous examples represent either of these cases.

What are the advantages of transporting mRNAs over proteins? First of all, every single copy of a localised mRNA molecule can be translated multiple times into proteins, creating local centre and the gradient of protein diffusion. mRNA transport can spare substantial amounts of ATP molecules, comparing to transport of the single protein molecules. Second, localised mRNAs can be translated on demand[20,21], adding an additional dimension of regulation – time. A typical example of this case is stimulus-induced mRNA translation in neurons[22]. Third, local translation can create high protein concentration gradient on spot, increasing the probability of protein complexes assembly[23]. Fourth, new data suggest that locally translated proteins can be post-translationally modified by locally distributed modifying enzymes[24]. It makes them functionally different from the cytoplasm-translated proteins. Lastly, local protein synthesis spares proteins' half-life[25] to fulfil their function, as well as reduces the risk of protein degradation *en route*.

1.1.3. The three major modes of long-distance mRNA transport

Currently, there are known three major mechanisms of long-distance mRNA transport: based on hitchhiking the vesicles that are transported along the microtubules[26], by myosin carrying mRNA on the actin meshwork and via kinesin/dynein transport along the microtubules.

The best-studied example of the **vesicle-mediated mRNA transport** is represented by *Ustilago maydis*. To propel in the tissue of infected corncob, this parasitic fungus transports *cdc3* mRNA molecules on endosomes to the tips of its hyphae, where these messages undergo translation and the nascent proteins help extending the hyphae[27,28].

Another major mechanism of **mRNA transport is based on actin-myosin motility**[29]. Myosin-Va plays a direct role in transport of various mRNA-protein complexes[30] in mammalian neurons[31–33], including transport of the key RNA-binding protein (RBP) for my thesis work, FMRP[34]. ZBP1/Myosin-Va-mediated[24] transport[35] of β-*actin* mRNA, for example, directs fibroblast movement by locally translating b-actin[36] that stabilises focal adhesions[36,37].

The third central mechanism of active **mRNA transport** is **based on kinesin and/or dynein motility along the microtubules**. Both kinesins and dyneins are molecular motors that convert the energy of ATP into motion along the microtubules. Both, kinesins[38,39] and dyneins[39–41] associate with multiple mRNA species and transport them in various cellular environments. The motility of vesicles also depends on kinesin/dynein movement along the microtubules[42], yet all the work described in this thesis refers to RNA-motor interactions, mediated solely by adaptor proteins, without membranous structures. Kinesin-based mRNA transport mechanism is the focus of this PhD Thesis and is deeper discussed in the next subchapter.

1.2. Kinesin-based mRNA transport

RNA motility is based on association of multiple molecules into large molecular complexes. These complexes typically consist of three principal components: a motor protein, an RNA-binding protein (RBP) and an mRNA[43,44]. Some of the motors require an additional adaptor protein that is responsible for cargo loading and cargo-dependent motor activation[45]. Here I discuss each of the major components in more detail.

1.2.1. Microtubules

Together with actin and intermediate filaments, microtubules represent one of the three classes of cellular cytoskeleton. What all of these three classes have in common, is their modularity: they form fibrils from polymerised mono- or oligomers. Microtubules are built from α- and β-tubulin heterodimers that autonomously assemble into typically 13 protofilaments. The protofilaments interact laterally, closing into a hollow semi-rigid tubular structure – microtubule (Fig. I.2, B). Typically, microtubules have the B conformation with diameter of ~25 nm. Due to their modular structure, microtubules have two ends, one exposing solely α-tubulin, the other only β-tubulin. These ends are called minus- ad plus-ends respectively. The surface of the microtubules is called lattice and it serves as a binding platform for dozens of microtubule-associated proteins (MAPs). MAPs can function as microtubule stabilisers (Map2, Map4), destabilisers (katanin, Kinesin-13), plus-end tracking proteins (+TIPs, like EB1[46], APC, CLIP-170), minus-end trackers (γ-TURC), bundlers and cross-linkers (Map65), and finally motor proteins[47].

Microtubules have a plethora of functions: they form mitotic spindles that separate chromosomes during the anaphase, they comprise cilia and flagella needed for cell communication and motility, microtubules work as rails for directed transport of various organelles and molecules, establishing cell polarity. In this work, I am interested in microtubules as the means for transport of molecules in neurons. The readers interested in more details are kindly directed to an excellent review[47].

Microtubules naturally undergo cycles of sporadic polymerisation and disassembly, called growth and catastrophe. In order to keep microtubules steady, in my studies I have extensively used *taxol*, a drug that stabilises microtubules by binding directly to the β-tubulin molecules[48].

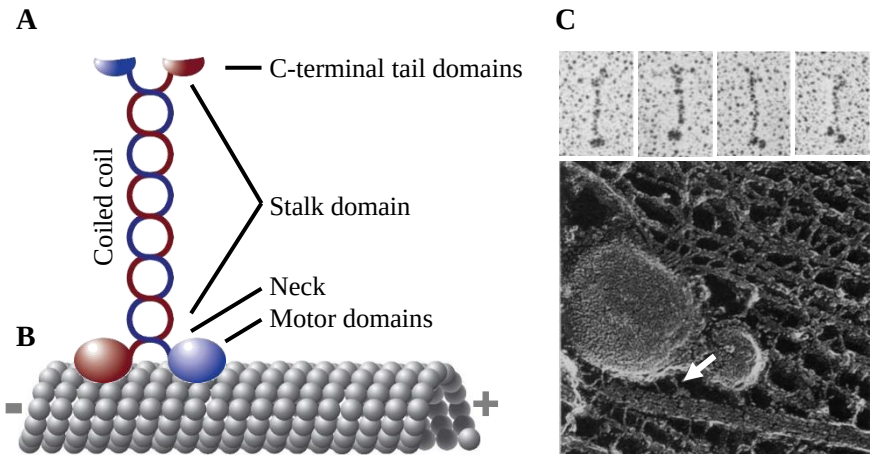
A
C-terminal tail domains
Coiled coil
Stalk domain
Neck
Motor domains
B
-
+
C

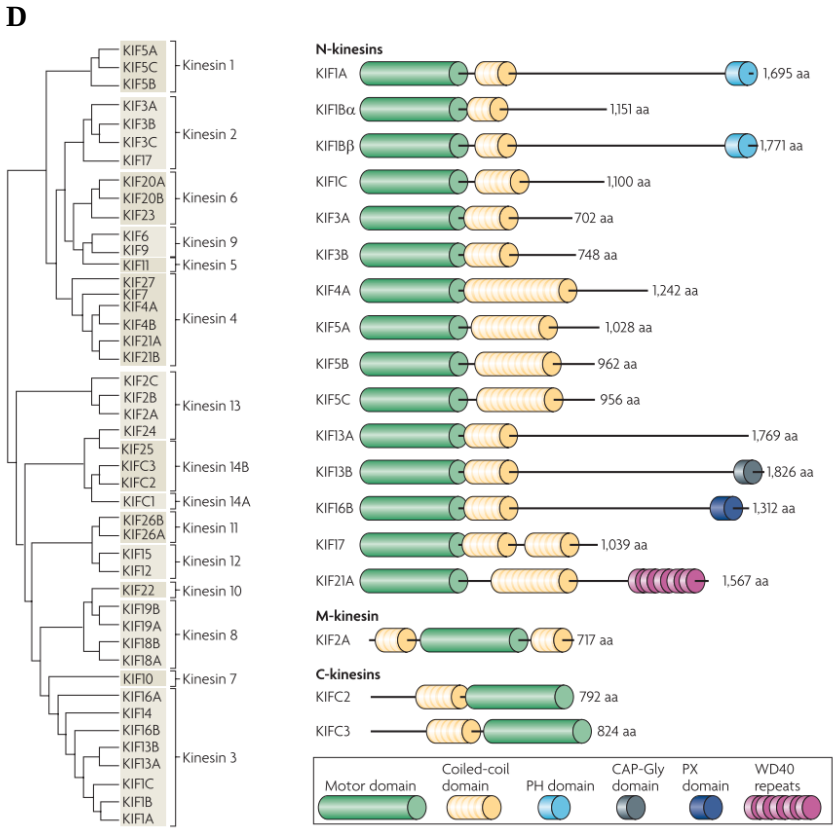
D
KIF5A
KIF5C
KIF5B
Kinesin 1
KIF3A
KIF3B
KIF3C
KIF17
Kinesin 2
KIF20A
KIF20B
KIF23
Kinesin 6
KIF6
KIF9
Kinesin 9
KIF11
Kinesin 5
KIF27
KIF7
KIF4A
KIF4B
KIF21A
KIF21B
Kinesin 4
KIF2C
KIF2B
KIF2A
Kinesin 13
KIF24
KIF25
KIFC3
KIFC2
Kinesin 14B
KIFC1
Kinesin 14A
KIF26B
KIF26A
Kinesin 11
KIF15
KIF12
Kinesin 12
KIF22
Kinesin 10
KIF19B
KIF19A
KIF18B
KIF18A
Kinesin 8
KIF10
Kinesin 7
KIF16A
KIF14
KIF16B
KIF13B
KIF13A
Kinesin 3
KIF1C
KIF1B
KIF1A
N-kinesins
KIF1A
1,695 aa
KIF1Bα
1,151 aa
KIF1Bβ
1,771 aa
KIF1C
1,100 aa
KIF3A
702 aa
KIF3B
748 aa
KIF4A
1,242 aa
KIF5A
1,028 aa
KIF5B
962 aa
KIF5C
956 aa
KIF13A
1,769 aa
KIF13B
1,826 aa
KIF16B
1,312 aa
KIF17
1,039 aa
KIF21A
1,567 aa
M-kinesin
KIF2A
717 aa
C-kinesins
KIFC2
792 aa
KIFC3
824 aa
Motor domain
Coiled-coil domain
PH domain
CAP-Gly domain
PX domain
WD40 repeats

1.2.2. Kinesin motors

The superfamily of kinesin genes is very versatile and comprises 45 motors in mice and humans, classified into three large groups according to the position of their motor domain, or distributed into 14 families that reflect the evolutionary relatedness of the kinesins (Fig. I.2, D)[49,50]. Despite an impressive variety of kinesins, all of them have four essential functional domains: a motor domain, a neck, a stalk and a C-terminal tail domain (Fig. I.2, A, C). The motor domains are globular and share high homology, they contain a microtubule- and ATP-binding moieties. These motor domains demonstrate velocities of 200-1500 nm/s *in vitro*[50]. The rest of the sequence is less conserved. Necks serve to provide the motor domains with some flexibility relatively to the stock domains that form a sturdy helix upon dimerization of two motor molecules. The tail domains demonstrate a wide sequence diversity that permits recognition and transport of various cargoes.

The most important cargoes are represented by synaptic vesicle precursors in axons (transported by KIF1A and KIF1Bβ), mitochondria (by KIF5 and KIF1Bα), clathrin vesicles (by KIF13A), as well by less obvious cargoes like oligomeric tubulin (by KIF5), NMDA (by KIF17) and AMPA receptors that are transported into dendrites (by KIF5), large RNA-protein complexes (by KIF5 and KIF3). This excellent review provides with more details[50]. Out of the wide variety of kinesin proteins, in my thesis I was mostly interested in the first three subfamilies. I am inviting you to discuss them in more detail.

Fig. I.2. General principles of kinesin-based mRNA transport

A. Kinesins consist of three main functional modules: motor domains that bind microtubules and change conformation upon ATP hydrolysis, stalk region made from coiled-coil domain that transforms conformational changes of motor domains into directed motion and the C-terminal domains, responsible for cargo loading or adaptor protein recognition. **B.** Microtubules are long dynamic structures with plethora of indispensable functions, among which is stipulation of organelle and molecule transfer within living cells. +/- mark the microtubule plus- and minus-ends correspondently. **C.** Low-angle rotary shadowing electron microscopy reveals kinesins in function. Above: photographs of KIF5 (Kinesin-1 or KHC). Below: a quick freeze-deep electron micrograph of a mouse axon. A membranous organelle is linked to a microtubule thorough a molecule resembling kinesin (white arrow). Borrowed from[51]. **D.** The structure and phylogeny of the major mouse kinesins[49].

Kinesin-1

Kinesin-1 motor, also known as conventional kinesin, functions in the form of dimers, consisting of two heavy chains (KHCs), ~117 kDa each. Mammalian Kinesin-1 family encompasses three genes encoding ubiquitously expressed KIF5B and neuron-enriched KIF5A and KIF5C motors that are known to form three forms of heterodimers[52]. However, alternative studies suggest that KIF5 motors in the mouse brain form exclusively homodimers[53].

Besides the heavy chains, Kinesin-1 holoenzyme includes two Kinesin Light Chains (KLCs), ~69 kDa each. KLCs serve as cargo binding adaptors, forming a tetrameric protein of ~370 kDa. Kinesin light chains bind the C-termini of the KHC stalk regions, which are also the most variable regions among the KHC versions (Fig. I.3, A). In human, four KLC forms are expressed, KLC1-4. IP studies from murine brain demonstrated that each of the three combinations of KHC heterodimers bind KLC1 or KLC2[53], creating at least six versions of Kinesin-1 holoenzyme. Furthermore, KLC1 was shown to have different splice-isoforms, increasing the number of possible holoenzyme combinations that might target different cargoes. KLC consists of three domains: the N- terminal (coiled-coil / heptad repeat domain) that binds to KHC, a tetratricopeptide repeat (TPR), and the C-terminal domain. The TPR and C-terminal domains are responsible for cargo binding. These TPR domains consist of multiple tandem repeats of 34 amino acids and serve as a protein-protein interaction platform[54].

In its free state, KIF5 was shown to be autoinhibited[55–58]; cryo-EM studies after photo-crosslinking have demonstrated that coiled-coil domains bend in their neck region and fold double, thus permitting the QIAKPIRP amino acid sequence of Kinesin-1 C-terminal region to block ADP release by the motor domains, inhibiting its activity[58] (Fig. I.3, B). In the absence of cargo, KLC seems to inhibit MT-binding activity of KHC, involving the heptad repeats of the N-terminal region of KLC and the C-terminal parts of the coiled-coil stalk/tail region[55]. Surprisingly, some cargo proteins' sequences as short as 10 amino acids suffice to activate KIF5 through the 2-5 TPR domains of KLC1[56]. Furthermore, there are also evidence that KLC itself can be autoinhibited and that this autoinhibition is released upon cargo binding[59]. These data demonstrate how complex is the regulation of Kinesin-1 holoenzyme activation. These physiological mechanisms might serve to ensure that Kinesin-1 does not waste ATP for cargo-less motility along the microtubules.

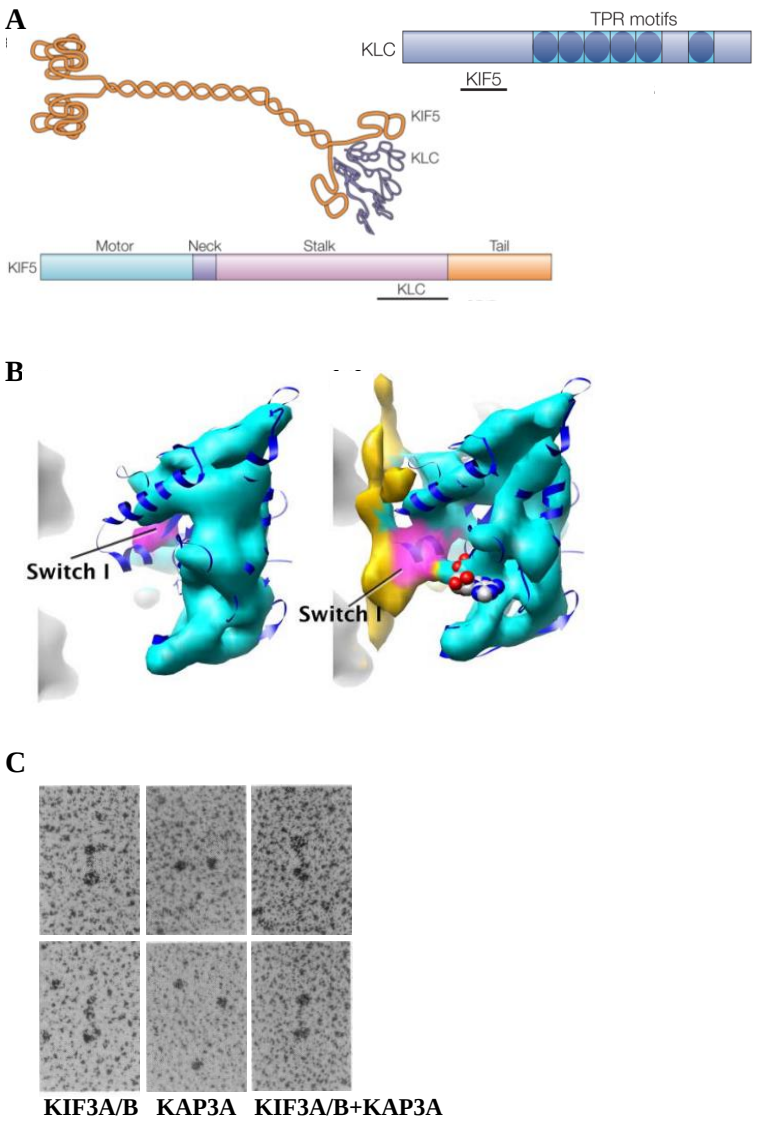

Fig. I.3. General principles of kinesin-based mRNA transport

A. A schematic model and binding domains of KIF5 and KLC. Adapted from[50]. **B.** CryoEM map demonstrates how the motor domain of Kinesin-1, bound to the microtubule lattice (left) is blocked by the tail domain, autoinhibiting the motor (right). Microtubule is represented in grey, Kinesin-1 motor domain in cyan and the tail in yellow. Switch I notifies the contact surface between the motor and tail domain (highlighted in magenta). The authors of this article[58] speculate that the tail domain blocks the exit for the ADP molecule (space-filling model on the right), locking the ATP hydrolysis cycle. **C.** Low-angle rotary-shadowing electron micrographs demonstrate heterotrimerisation of recombinant Kinesin-2 with its adaptor KAP. Borrowed from[60].

Kinesin-2

Mammals have four Kinesin-2 genes, encoding KIF3A, KIF3B, KIF3C and KIF17. KIF3s form two variants of heterodimers in vivo: KIF3A/B and KIF3A/C[61], KIF3B/C heterodimer was not found *in vivo*[62,63]. Although heterodimerisation was reported to be preferential over homodimerisation, homodimerisation can happen in specific circumstances, for example of KIF3C/C upon neuronal injury[64]. Interestingly, different Kinesin-2 heterodimers exert different speeds: KIF3AB was reported to travel at speed of 224 nm/s[65] or 590 nm/s[60], KIF3A/C at 169 nm/s[65], while KIF3C/C homodimer was moving at 7,5 nm/s[64] (for more information, please refer to Table 5, p.96). The processivity, or an average travel distance before the motor detaches from a microtubule, also differs between the dimers: KIF3A/B run length reaches 1,62 um, while for KIF3A/C it is around 1,23 um[65].

In contrast to Kinesin-1 motors, Kinesin-2 has only one common adaptor, Kinesin Associated Polypeptide 3 (KAP3) that together with KIF3A/B forms a trimeric holoenzyme (Fig. I.3, C). KAP3 primarily consists of armadillo repeats, which are responsible for specificity of KIF3A/B-KAP3 and KAP3-cargo interactions. In contrast to KLC, KAP3 was shown not to influence motility of Kinesin-2 motor[60].

Although KAP3 is known to have two isoforms, KAP3A and KAP3B, in this study we used only isoform A. Our recent paper provides evidence of cargo (APC and an mRNA) activating KIF3A/B/KAP3 motor, significantly and essentially increasing the number of run events on the microtubules *in vitro*[43]. This finding coincides with the data on Kinesin-1 motor that as well requires cargo loading for its activation. There is evidence that another Kinesin-2 motor that we will not discuss further, KIF17, is also autoinhibited[66]. These data imply that the autoinhibition of motor proteins can be rather a common mechanism than exception.

Kinesin-3

The most interesting to my project motor from this kinesin subfamily, KIF1B, is known to transport mitochondria (KIF1Bα)[67] and synaptic vesicle precursors (KIF1Bβ)[49]. What makes this motor special is that KIF1B functions as a monomer[67]. KIF1B was measured to have a running speed *in vitro* of 660 nm/s [67] or 750 nm/s for the motor domain only[68]. In this work, I was working with KIF1Bβ, which differs from KIF1Bα by the C-terminal region that defines the cargo specificity of these two motors.

1.2.3. RBPs, mRNAs and their zip-codes

RNA-binding proteins, or RBPs, is the next principal component participating in mRNA transport. RBPs recognise their mRNA targets already in the nucleus or after their export to the cytoplasm and mediate binding to the relevant motor proteins that fulfil the transport function. RBPs recognise their target mRNA molecules by specific sequences, called zip-codes, in analogy the with postal codes that allow quick package sorting according to its destination.

For example, zip-code-binding protein 1 (ZBP1) recognises a 54-nt long zip-code of the *β-actin* mRNA and is necessary for localisation of *β-actin* to neuronal dendrites as well as for growth of dendritic protrusions after BDNF stimulus[69]. Translocated in liposarcoma (TLS) protein is transported to neuronal dendrites in response to mGluR5 stimulation in a complex with its target *Nd1-L* mRNA, presumably associating with multiple zip-codes in its 3'-UTR[70]. Zip-code recognition can be either based on plain mRNA sequence (e.g. ZBP1 with *β-actin* mRNA) or a secondary structure (Staufen and *bicoid* mRNA[71], She2p/She3p and *ASH1* mRNA[10]). For more examples, please refer to this excellent mRNA zip-code review[71].

RBPs can possess a set of different domains that mediate target mRNA recognition. In order to bind *β-actin* mRNA, ZBP1 utilises K-homology (KH) domains[69]. TAR DNA binding protein (TDP-43) binds its target mRNAs, recognising UG/GU motifs with its RRM1 and RRM2 domains[72]. A curious reader can find more examples here[73]. In order to identify and characterise minimal zip-code sequences or their secondary structures, there have been done multiple studies *in vitro*. As you will see in the last subchapter of the Introduction (1.4.4), known RBP-motor interactions stand on a much weaker basis. Cells have multiple examples of redundant mechanisms, which can make the results from classical KD/KO experiments questionable. At the same time, there have been done very scarce studies on RBP-motor protein interactions *in vitro*, seriously limiting our understanding of mRNA transport processes.

In this subchapter, we have discussed the major elements participating in kinesin-based mRNA transport. Different classes of kinesins transport dozens of RBP species along the microtubules. RBPs recognise mRNA targets and link them to the corresponding motors. In the next subchapter, we will project the principles discussed here, into neuronal environment and see what roles mRNA transport plays in learning and memory formation.

1.3. Specifics of mRNA distribution in mammalian neurons

Neurons count to the most complex cells in our bodies. The body of a neuron, soma, extends into two functionally and structurally different types of protrusions: dendrites and axons (Fig. I.4, A). We know from the textbooks that axons send the signals, while dendrites mostly receive them. Such structure creates directed flow of information from dendrites through the soma to axons, which is possible due to polarisation of neuronal cells.

1.3.1. Memory formation and learning are based on synaptic plasticity

Communication between the neurons takes place through complex mushroom-shaped structures called neuronal spines (Fig. I.4, B). Spines transfer the signals through synapses (Fig. I.4, D). Neuronal spines are very dynamic. Motor learning of mice leads to formation of clusters of novel dendritic spines in between 1-4 days after training[74] (Fig. I.4, C). Currently it is believed that memories (and acquired skills) are stored in populations of neurons that overlap with their dendritic branches and form clusters of inter-neuronal synaptic connections. These clusters encode for memories, related in time, space or context[75]. Learning and memory formation, therefore, is based on neuronal rewiring – constant formation, maintenance (hours to many years) or removal of synaptic contacts[76].

Rewiring, in turn, is assisted by another mechanism of learning and memory formation – synaptic plasticity. Synaptic plasticity modulates "decisions", whether the newly formed spines should be strengthened (long-term potentiation, or LTP) or diminished and finally removed (long-term depression, or LTD). LTP is an increase of synaptic strength that happens after high-frequency stimulation of the synapse. LTD has the opposite effect, taking place after long periods of stimulation at lower than the baseline stimulation frequencies. LTP consists of two phases: an early phase, displayed by activation of kinase activity for 0,5-3 h, and a late phase, which induces changes in the gene expression for many hours after the stimulus. In concert with this, it was shown that RNA synthesis and protein translation inhibitors block long-lasting forms of LTP and, subsequently, memory formation[77].

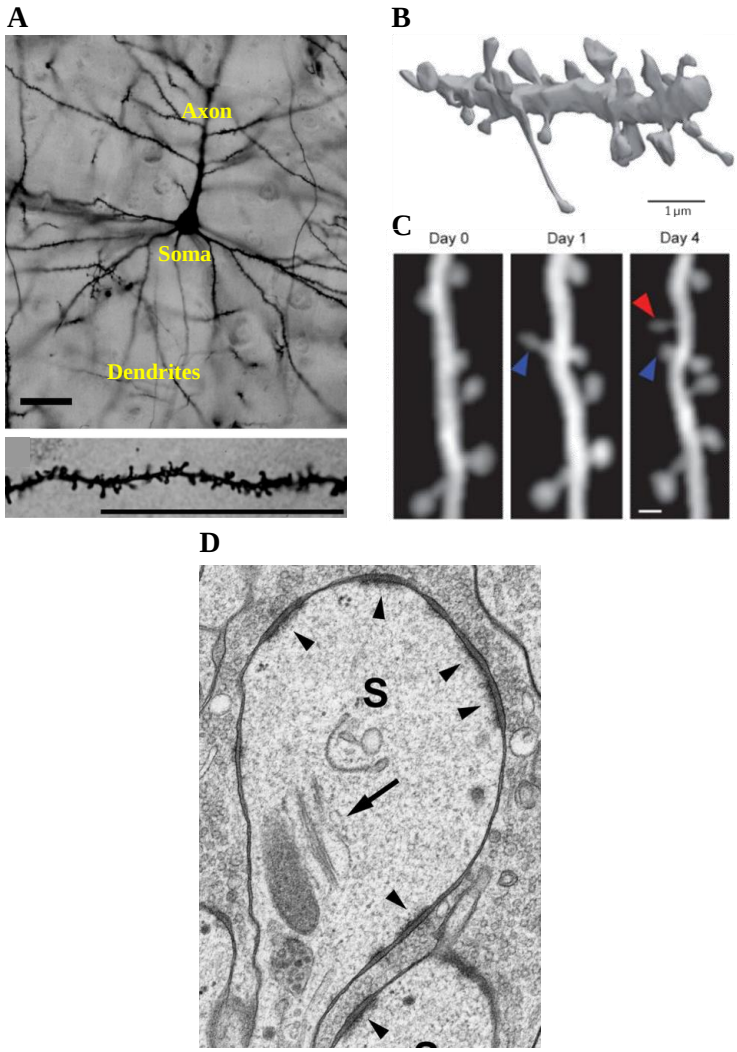

Fig. I.4. Memory formation and learning are based on synaptic plasticity

A. An electron micrograph of a pyramidal neuron of human prefrontal cortex[78]. Above – a typical neuron that forms a dendritic tree, which serves to receive signals from the other neurons, soma that contains the nucleus, and an axon, a long protrusion that transmits signals to the other neurons. Below – an expanded photograph of a single dendrite. Small mushroom-shaped structures along the dendrites are called dendritic spines. Scale bars: 50 um. **B.** A three-dimensional reconstruction of a segment of a CA1 pyramidal neuron apical dendrite demonstrates the variability of dendritic spine morphology[79]. **C.** Motor learning induces new spine formation between 1 (blue arrow) and 4 days (red arrow) after training[74]. **D.** Large complex spine of a CA3 pyramidal cell[80]. The arrow points to the smooth endoplasmic reticulum, arrowheads indicate synapses. Scale bar: 200 nm.

1.3.2. Local protein translation upon synaptic activation

Three decades ago, it was already known that late, but not the early stages of LTP, are blocked upon global inhibition of protein synthesis with anisomycine[81]. Later it became evident that inhibition of protein synthesis locally in neuronal protrusions is enough to block the LTP[82]. Nowadays it is widely accepted that LTP is dependent on nascent proteins that are translated next to stimulated spines and serve as building blocks for synaptic strengthening and remodelling[79,83].

Local protein translation would require localisation of corresponding mRNAs, ribosomes, translation regulating enzymes and corresponding cytoskeletal infrastructure next to or inside the spines. Deep sequencing of synaptic neuropil of rat hippocampus has revealed over 8,4 thousands of transcripts, 2,5 thousand of which were significantly enriched in dendrites or axons[84]. Synaptic transcriptome studies identified over 1000 transcripts encoding essential for synaptic functioning proteins[85]. Using mRNA reporters, a very elegant study allowed to visualise local mRNA translation in murine RGC neurons[86]. Ribosomes[87,88], endosomes and mitochondria[89] were also shown to co-localise with mRNA granules in mice axons, fulfilling all the necessary conditions for distant from the soma protein synthesis. Plenty of other studies have established that mRNAs end up in dendrites and axons. The mechanisms of this transport, however, remain poorly understood[90].

1.3.3. A sushi-belt model of dendritic mRNA distribution

Neuronal cells together with their protrusions can be extremely long, e.g. sciatic nerve in humans can reach over 1 m in length. Simulation studies have demonstrated that plain diffusion could sustain neuronal structures only up to few hundred micrometres from the soma[91]. In order to overcome these limitations, build and sustain the complexity and dynamic properties of synapses along the dendrites and axons, neurons form a complex cytoskeletal network, represented by all three classes of cytoskeletal elements[92,93]. Microtubules are the most interesting for us, since they serve for transport of various organelles, proteins, ribosomes as well as mRNAs[89]. Neuronal mRNA transport has been associated with a handful of motor proteins: Kinesin-1[38,94], Kinesin-2[38], Kinesin-3[95], Dynein[44,94] and Myosin[31,96–98]. For more examples, please refer to these excellent reviews[22,90,99]. Although we know many motor protein candidates, RBPs and the mRNAs that are transported, it is still unclear how mRNA transport functions on molecular level. Furthermore, how does the soma of a neuron "know" that a specific mRNA species might be needed next to a spine located millimetres away? The so-called "Sushi belt model" explains it.

The "Sushi belt model" was published by Michael Doyle and Michael Kiebler in 2011[100]. According to this model, the soma "does not need to know" when and where the mRNAs have to be delivered to distinct synapses. Instead, all kinds of destined for dendrites or axons messages are constantly carried back and forth by the motors and are pulled to a spine on demand, exactly like a customer pics up a sushi from the running belt (Fig.I.5). An absolutely terrific study[21] has proven this model to be true. By fusing GFP to endogenously expressed *β-actin* mRNA via MS2 loops, the authors could observe behaviour of these mRNAs in the dendrites of murine hippocampal neurons. At the same time, they transfected the cells with virus that allowed to express light-triggered ion channels, which permit spot-restricted glutamate uncaging, thereby mimicking synaptic activation. In the normal state, *β-actin* particles moved bidirectionally. Local glutamate uncaging in 3x10 pulses on 6 spots of the distal dendritic regions over 100 um from the soma, led to accumulation of the *β-actin* mRNA near the uncaging location in a 15 min timespan (Fig. I.6). Remarkably, this mRNA recruitment was persistent for at least 2 h. The authors also show that the recruited *β-actin* mRNA molecules were undergoing translation after the stimulus and that the nascent b-actin protein was built into the local spines. A similar stimulus-induced translocation to the spines was reported for proteins, well known to bind and transport mRNAs, like Pur α[96] and TLS[101]. Such mechanisms make even more sense when matched with the observations that dendritic microtubules can enter dendritic spines upon spine stimulus[93].

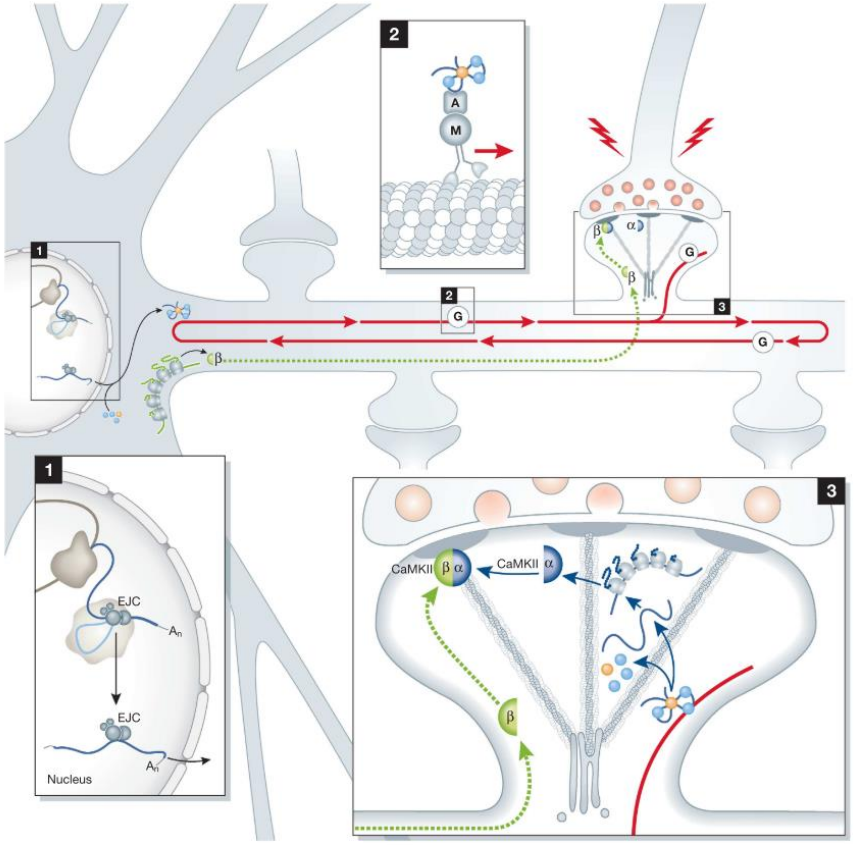

Fig. I.5. Sushi-belt model of mRNA transport

Upon mRNA transcription, splicing and export through the nuclear pores (**1**), mRNAs are recognised by corresponding RBPs and form motile complexes, or granules, with the motor proteins. These complexes are then bidirectionally transported along the microtubules inside dendritic shafts (**2**). Synaptic stimulus promotes microtubule entering into the activated spine and triggers localisation of mRBP granules (**3**). Upon repetitive stimulus, mRNAs are unmasked and translated into proteins that strengthen activated spines. Interestingly, some components of the protein complexes are delivered from the soma autonomously. For example, CaMKIIβ peptide requires locally translated CaMKIIα peptide to form fully functional complex. A – adaptor, M – motor, G – granule. Borrowed from[100]

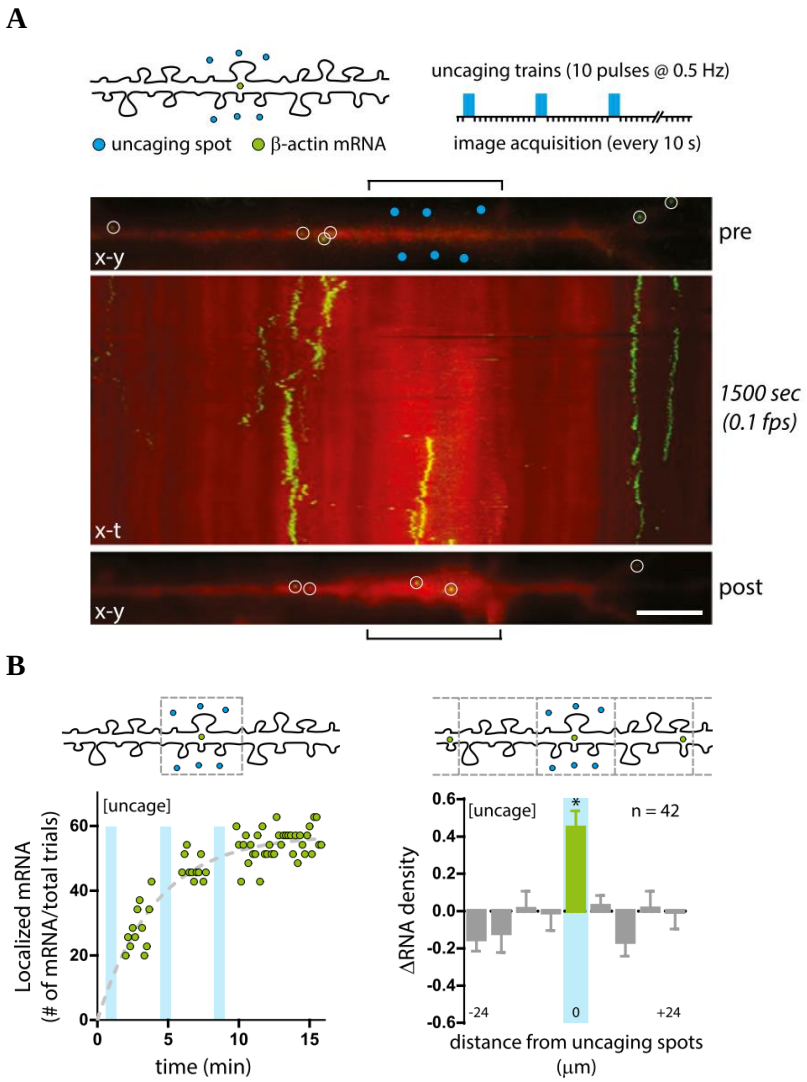

Fig. I.6. Bidirectionally transported mRNAs are anchored to the stimulated spot of dendritic shaft

A. Glutamate uncaging leads to *β-actin* mRNA localization to the induced spot. Rapid laser pulses (blue bars on top right) triggered glutamate uncaging on chosen spots (blue circles) around a dendrite (red). In terms of 15 min, *β-actin* mRNA granules (green) switched from bidirectional and diffusive movements (a distance/time plot, or kymograph, in the middle) to an anchored state next to the uncaging location. Scale bar: 5 um. **B.** Dynamics of the post-stimulus *β-actin* mRNA accumulation. Cyan bars represent glutamate uncaging pulses. **C.** *β-actin* mRNA density over distance from the uncaging location plot. $p<0,05$ relative to the other segments. Error bars indicate SEM. Adapted from[21].

1.3.4. RBPs bridge the gap between nucleus and spines

Now, as we know that localised mRNAs are constantly redistributed along the dendrites, recruited to and translated inside the stimulated spines, we can discuss, how these messages are delivered and distributed along the shafts of a dendritic tree.

Studies on dendritic mRNA granules' composition have identified dozens of RBPs[38,102–105]. Surprisingly, these mRBP granules shared only about one third of the protein components[102], which implies that different RBPs can have various functions in terms of mRNA recognition, determination of transport destinations, regulation of mRNA translation etc. Among many other functions, RBPs ensure that their target mRNAs are not translated before synaptic stimulus. ZBP1, for example, known to transport *β-actin* mRNA mentioned above, inhibits its translation and releases this inhibition upon phosphorylation by Src kinase[24]. Such phosphorylation reactions are dependent on kinases, activated through the signalling cascades, which in their turn are launched upon synaptic activation. Release of mRNA translation blockade is called mRNA unmasking.

Another example of a high-impact RBP that is responsible for mRNA transport in a translationally repressed state is FMRP. Upon DHPG stimulus, FMRP is indispensable for dendritic localisation of *map1b* and *camkIIα* mRNAs[106], as well as for translation of *camIIα*, *psd-95*, *nmdar* and *β-actin* mRNAs[20,107]. DHPG-stimulated activation of mGluR1 leads to S6K1-mediated phosphorylation of FMRP (by serine 499) in murine hippocampal neurons in timely manner[108]. However, in contrast to ZBP1, the role of FMRP phosphorylation still remains unknown[109,110], as well as how FMRP releases its masking. It is also unclear, how FMRP can stipulate transport of its target mRNA molecules from soma to the dendrites. We will see in the next chapter that FMRP is associated with a set of various motor proteins that could fulfil the transport function, yet in a very controversial and disputable manner. Furthermore, mutations in *Fmr1* gene cause a handful of neuronal disorders, which makes this protein very important also from the medical perspective. These open questions make FMRP one of the most interesting RBPs in the field of mRNA localisation and local translation, this is why FMRP was chosen as the focus of my mRNA transport studies.

1.4. FMRP: Fragile X-mental Retardation Protein

1.4.1. FMRP as a high-impact RNA binding protein

Fragile X-mental Retardation Protein is known to cause a syndrome of the same name (FXS) upon mutation in its gene. X-mental retardation is characterised by mild to severe mental retardation, subtle connective tissue abnormalities, hyperactive and attention deficit disorder and autistic-like behaviour[111]. This syndrome was shown to be caused by expansion of the CGG repeats in the 5'-UTR of the *fmr1* gene, while severity of this disorder positively correlates with the length of these expansions[112]. The *fmr1* gene and FMRP have also been associated with the other disorders, such as fragile X-associated tremor ataxia syndrome (FXTAS), primary ovarian insufficiency (FXPOI), and autism spectrum disorder (ASD)[112].

FMRP is well known and has been intensively studied as a regulator of translation. The most research works report FMRP to be a negative regulator of translation, whereas FMRP can function by stalling translating ribosomes on its target mRNAs[107,113], inhibiting translation initiation via CYFIP1 and eIF4E proteins[114]. However, there are also reports that FMRP can positively regulate translation, either directly[115] or by recruiting auxiliary proteins[116]. Later reports have linked FMRP with multiple stages of mRNA life, starting with alternative splicing of its mRNA targets in the nucleus[113], export of the (N^6-methylated) mRNAs from the nucleus[117], control of mRNA stability[118], mRNA transport[119], and even indirect regulation of DNA methylation[113]. It makes FMRP a hard protein to study with traditional biochemistry methods, since classical KO or KD can cause multiple effects on different levels of cellular physiology. Therefore, *in vitro* approach that we use is our lab could be a great tool to help separate these multiple functions of FMRP one from another.

Although a great progress has been made in understanding FMRP functions, the role of FMRP in neuronal mRNA transport has just started being elucidated. We will discuss this topic in detail after focusing on what is known about the domain structure of FMRP and the molecular mechanisms that they stipulate.

1.4.2. FMRP: structure meets the functions

The *fmr1* gene is expressed ubiquitously, it comprises 17 exons spanning 38 kb of Xq27.3[120]. These exons allow for generation of 12 different *Fmr1* mRNA isoforms in the murine brain, whereas the isoform 1 is the full-length transcript that also represents 97% of amino acid sequence identity with a human orthologue[121]. The expression levels of these isoforms depend on mouse development stages as well as the regions of the brain, thus to keep our research as general and case-independent as possible, all the experiments were conducted with the full-length protein, represented by the isoform 1 (ISO1).

The N-terminal part of FMRP consists of two Agenet domains, encoded by exons 1-4. Each of these domains comprises four Tudor repeats, folding into a bent four-stranded antiparallel β-sheet[122]. These folds bear hydrophobic pockets that, by analogy with Tudor domains of other proteins, are supposed to mediate protein-protein interactions[122]. The first Agenet domain was proposed to bind non-coding *BC1* RNA[123], which recruits FMRP to specific subsets of its mRNA targets[124]. The second Agenet domain was shown to be responsible for binding 82-FIP[122], a protein binding translating polysomes in the brain[125]. The latter study also demonstrates by the yeast-two-hybrid (Y2H) assay that the N-terminal region of FMRP (aa 1-134) binds NUFIP1, another FMRP-interacting proteins capable to bind poly-U/G RNA[126], as well as CYFIP2[127]. Besides NLS sequence[128], the N-terminal part of FMRP also binds an important FMRP paralogue that we will discuss later, FXR2[129]. And finally, a resolved crystal structure of the N-terminal region of FMRP demonstrated that FMRP can dimerise via Ile106[130]. All these evidence imply that the N-terminal part of FMRP (aa 1-218) functions as a protein-protein interaction platform, mediating interactions between FMRP and its multiple partner proteins (Fig. I.7).

The central region of FMRP is harbouring two KH domains, named for their homology to hnRNP K protein. Throughout the tree of life, KH domains are responsible for RNA and ssDNA recognition, binding to 4-bases long nucleotide stretches with low micromolar affinity[131]. There had been attempts to device consensus sequences reflecting KH domains' specificity, although they were not very convincing[132]. Attention to FMRP KH domains increased after there had been described a point mutation in the KH2 domain (Ile367Asn), leading to a severe X-mental syndrome, not linked to the CGG repeats[133]. Subsequent research has demonstrated that an analogues mutation in murine FMRP (Ile304Asn) leads to inability of FMRP to associate with actively translating polysomes, shifting FMRP to the monosome fractions[134,135]. Introduction of a corresponding mutation to

the KH1 domain (Ile241Asn) leads to a similar effect[110,135]. On the example of hnRNP K, it was confirmed that multiple KH domains can have additive effect on RNA recognition efficiency[134]. Structure studies demonstrate that these isoleucine residues form hydrophobic cores of the KH domains[137].

The C-terminal FMRP region harbours the well-studied RGG box and few other interaction regions. RGG box binds a G-quadruplex structure of its target mRNAs[109,110,138,139] and is indispensable for their dendritic localisation[140]. The latter study also demonstrates that RGG box binds a distinct to KH domains set of mRNA targets, implying that RGG box is responsible for mRNA transport and localisation function of FMRP, while the KH domains rather regulate mRNA translation. Studies with the RGG-binding RNA aptamer *sc1* have shown that RGG box utilises positive charges of the side chains of its multiple arginine amino acids[141], located in a short, near 12-residue stretch that has a type I β-turn conformation[142] (Fig. I.8).

Besides the RGG box, FMRP C-terminus contains important phosphorylation sites. Ser500 of hFMRP (Ser499 in mouse), for example, is a conservative among animals amino acid that was shown to be phosphorylated in human. Ser500 phosphorylation promotes FMRP homodimerisation and poly-U RNA binding[143]. From this analysis, we can learn that FMRP is a very complex protein that due to its multifaceted functions possesses a high number of motifs and interaction surfaces that permit binding to various proteins, mRNA molecules and even homo- and heterodimerisation with the homologues proteins.

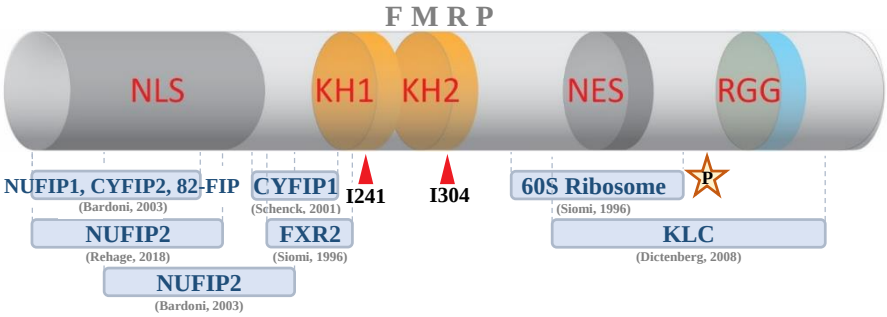

Fig. I.7. FMRP domain and interaction map

FMRP N-terminal domain is primary responsible for inter-protein interactions. KH1/2 domains together with the RGG box bind mRNAs. NLS and NES – nuclear localization and export sequences, correspondently. FMRP-interacting proteins are mapped according to the region of FMRP they bind or were shown to interact. Red triangles map two isoleucine residues that are crucial for KH domains' functionality. A star marks a conservative phosphorylation site (S499) with yet not fully understood function.

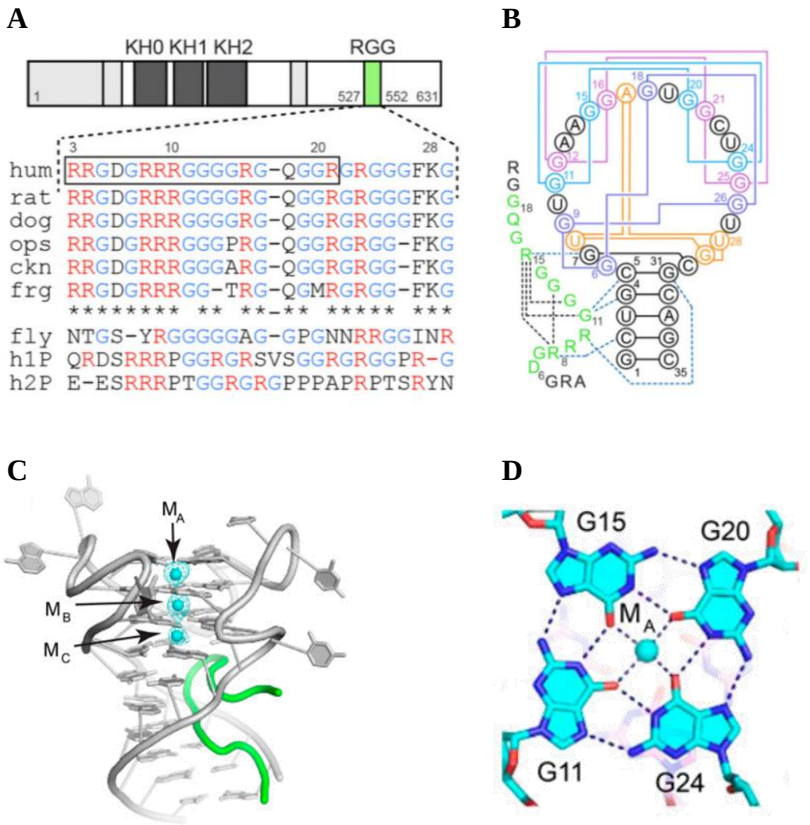

Fig. I.8. RGG box of FMRP recognizes a complex G-quadruplex fold

A. FMRP RGG box is very conservative between different species and in comparison to somatic homologues of FMRP. h1/2P – FXR1/2 proteins (please refer to 1.4.5. block). **B.** A scheme of a secondary structure of an artificially evolved RGG-binding sc1 RNA aptamer. RNA (grey) is recognised by the RGG peptide region (green) through the hydrogen bonds (dashed lines). Blue dashed lines represent base-specific interactions. **C.** A crystal structure of the sc1 RNA Q-quadruplex (grey) interacting with the RGG box protein fragment (green). Cyan spheres represent K^+ ions that are necessary for the G-quadruplex formation. **D.** G-quadruplex structure seen from above. Guanines form tetrads, which hold potassium ions by coordination bonds. Exported from[142].

1.4.3. Roles of FMRP in synaptic plasticity

FMRP was known to bind hundreds of mRNA species in the brain[144]. More recent PAR-CLIP data revealed ~6000 mRNA targets of FMRP for both ISO1 and ISO7[132]. Thousands of target mRNA species were also reported in other HITS-CLIP studies[107,145]. Based on this, FMRP was thought to be responsible for correct mRNA localisation in the dendrites. However, it became evident that plain FMRP KD/KO does not lead to dendritic mRNA mislocalisation. Instead, FMRP KO leads to its target mRNA mislocalisation only upon neuronal stimulation. For example, FMRP is responsible for *camkIIα* and *map1b* mRNA transport upon DHPG stimulus[106] (Fig. I.9).

Besides stipulating correct localisation, FMRP was shown to regulate translation of thousands of mRNAs in the brain[107]. For example, FMRP unmasks *nlgn1-3*[146] and *fmr1* mRNAs in mGLuR-stimulated dendrites[147]. Another study demonstrated a short-term release of FMRP/CYFIP1-mediated translation inhibition upon DHPG stimulation in hippocampal and cortical synaptoneurosomes[114]. The Gene Ontology analysis of FMRP-regulated messages has shown enrichment for synaptic transmission, neuron projection and GTPase signalling functions[107]. The role of FMRP in synaptic plasticity is backed up by the evidence of enhanced long-term synaptic depression (LTD), induced by DHPG stimulation of mGLuR in hippocampus of *fmr1*-KO mice[148]. Another characteristic feature of FMRP-deficient mice is an increased percentage of long thin dendritic processes of cortical neurons, reminiscent of protospines[148], which links FMRP to synaptic maturation processes.

These data direct us toward understanding how through binding, transporting and regulating translation of its target mRNAs, FMRP plays role in synaptic plasticity, learning and memory formation. To see a bigger picture about the functions of FMRP in neuronal homeostasis, I am directing an interested reader to a comprehensive review[149].

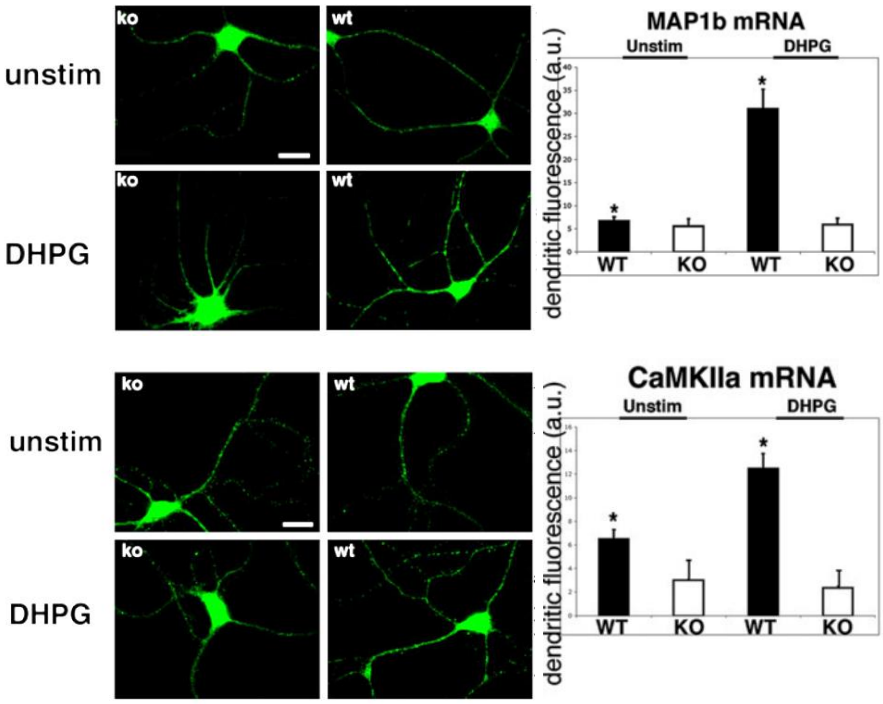

Fig. I.9. FMRP stipulates stimulus-induced dendritic mRNA localisation

FMRP KO does not significantly alter dendritic mRNA localisation in resting murine hippocampal neurons. However, FMRP KO neurons fail to localise FMRP-associated mRNAs upon DHPG stimulus. $p<0,001$ and $p<0,01$ for *map1b* and *camkIIα* mRNAs correspondently. Adapted from[106].

1.4.4. Dendritic FMRP transport. Missing gaps in the knowledge

After it became evident that correct dendritic localisation of some mRNAs is dependent on FMRP and that this localisation is regulated in time, more effort has been done to understand, how FMRP can be transported to the dendrites. Plenty of kinesins, dynein and myosin motors were known to be implicated in the vesicle and organelle transport along the microtubules or actin, however not in relation to FMRP-mediated mRNA transport. There has been many studies done in this direction, below I am summarising the ones which are the most informative and that were used as the cornerstone data for my PhD project.

Davidovic L., et.al. paper[150] claims that FMRP is transported by Kinesin-2 motor, KIF3C (Fig. I.10). First, they demonstrate with the Y2H screen that human FMRP binds the C-terminus (aa 403-792) of the mouse KIF3C motor, implying a direct interaction. They also confirm this interaction with a pull-down assay, using either *in vitro* translated or endogenous FMRP. They show that FMRP and KIF3C co-localise in cultured primary hippocampal neurons and that an overexpression of GFP-FMRP together with RFP-KIF3C-ΔN , which is missing its N-terminal motor domain, leads to decrease of the GFP-FMRP granules' maximal transport distances.

Dictenberg J.B., et.al. paper[106] demonstrates data that FMRP can be transported by Kinesin-1 motor, KIF5, through its adaptor protein KLC. First, the authors show that GFP-FMRP, overexpressed in cortical murine cells, pulls down Kinesin-1, but not Kinesin-2 motor. mGluR activation caused an increase in FMRP-KIF5 association (WB). Another IP has demonstrated that KLC pulled FMRP down by its C-terminus (aa 386-585), but not by the other fragments. Fluorescence recovery after photobleaching (FRAP) analysis has shown a 5-fold increase in recovery time of dendritically localised GFP-FMRP, when overexpressed with TPR domain of KLC (TPR domain is able to bind cargo, but not KHC). Moreover, this cell line showed a 2-fold decrease of *camkIIα* and *fmr1* mRNAs localization to dendrites. Next, the authors state that upon FMRP KO, a range of mRNAs reduce their association with KIF5 (IP and q-PCR); these messages represented genes, involved into synaptic remodelling, synaptic signalling (*camkIIα, rsg5*) and structure maintenance (*map1b, sapap4*). Finally, overexpression of the C-terminal FMRP fragment led to a 2-fold decrease of *camkIIα* and *sapap4* localisation to dendrites. These data suggest that FMRP-KLC association is necessary for dendritic localisation of distinct mRNA targets and that this localisation is probably based on Kinesin-1 motility.

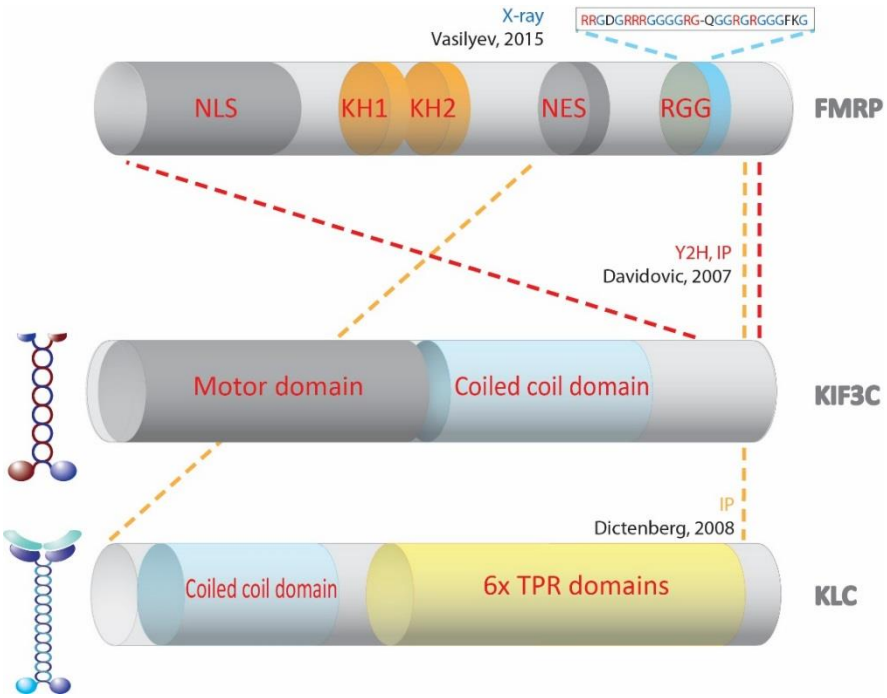

Fig. I.10. Major motor candidates for FMRP transport

Search for the motor proteins that can be responsible for FMRP transport led to contradicting results. Davidovic L., et.al. use yeast-2-hybrid screen to identify an interaction between FMRP and the C-terminus (aa 403-792) of KIF3C motor. These proteins also interacted in a pull-down assay and co-localised in living cells. Dictenberg J.B., et al. utilise an IP, confirmed by various experiments in cells that FMRP C-terminus (aa 386-585) binds Kinesin Light Chain adaptor, but not Kinesin-2.

Ling S.-C., et.al.[39] published a study, where they show that dFMRP associates with KHC, but not with KLC. Using the S2 cells of *Drosophila* origin, the authors report a dramatic reduction of overexpressed GFP-FMRP motility and run length upon KHC, but not KLC, KD. GFP-FMRP IP also pulled down KHC, but not KLC, confirming their previous observation.

Charalambous D.C., et.al[151] observed an association of FMRP-containing granules with KIF1Bβ motor in murine hippocampal dendrites. The authors pulled down an endogenous KIF1Bβ motor from the mouse brain and identified with the WB associated with it RBPs, such as Pur α, FMRP and FXR2 (see below), as well as KIF3A motor. They demonstrated that these proteins also co-localise in dendrites of cultured murine hippocampal neurons. Based on the evidence that KIF1Bβ accumulates in

synaptoneurosomes upon stimulus with multiple mediators and KCl, the authors speculated that KIF1Bβ might be involved in a stimulus-mediated mRNA transport.

The works discussed above are not the only ones in the field. What they all have in common, is that they are based on well established, but not always optimal methods, like IP/WB, confocal microscopy and KD/KO studies. These techniques provide with information about the members of protein/RNA complexes, whether they play a role in transport or complex formation, whereas the information about direct interactions is missed. We cannot judge from an IP, whether the interaction of interest is direct or mediated by a yet unknown protein. A good illustration of this problem is a paper of Kanai Y., et.al.[38]. The authors perform an IP on KIF5 tail and do tedious work identifying dozens of associated RBPs and motor proteins by WB. However, upon addition of RNAse, the vast majority of the identified interactors vanish from the nitrocellulose paper. Plenty of similar studies that are performed less carefully, put the reader under the risk of drawing false conclusions due to limitations of the methods. Performing an IP, one also has a chance to identify only those proteins, which are expected and are backed-up by corresponding antibodies. Furthermore, the majority of antibodies cannot distinguish between homologues or highly identical proteins, like FMRP, FXR1 and FXR2 (see later). Finally, using IP/WB, we can hardly identify, which of the proteins in the complex are minimal, yet essential for its function.

There is only one study, to my knowledge, that shows directly that FMRP can be actually transported[86]. The authors electroporated EGFP-FMRP into the radial glia cells (RGCs) of the embryonic murine brain and demonstrated a video of FMRP transport from cell body to the endfoot of a neuron. In spite of having access to multiple studies of FMRP and its potential carrier motors, the results remain controversial and non-conclusive. We still do not know which of the motors binds FMRP directly and is responsible for FMRP transport. Furthermore, it remains unknown, whether FMRP transports its target mRNAs directly or plays some auxiliary role in the mRNA distribution mechanisms.

1.4.5. FMRP paralogues FXR1 and FXR2

FMRP does not fulfil its functions alone, but often together with FXR1/2 proteins. FXR1 and FXR2 (Fragile X-mental Retardation syndrome-related proteins 1 and 2) are autosomal paralogues of FMRP. Both FXR1 and FXR2, like FMRP, have two KH domains and an RGG box, sharing among different domains a 70-86% amino acid sequence identity with FMRP (~60% identity as a whole), with only a 6% identity in the C-termini[152,153]. FMRP and FXR1/2 also have similar Tudor domains in their N-terminal regions, which implies that they could share some protein binders[154].

Besides having very similar amino acid sequences, FMRP and FXR1/2 interact in the Y2H assay and pull each other down in the IP/WB assays[153]. FMRP heterodimerises with FXR2 through aa 171-211[129], without overlapping with the KH domains or the RGG box, entailing that this heterodimerisation can be a mechanism of mRBP granule formation. Indeed, FMRP forms granules with FXR1, FXR2, *ctnnb1* (β-catenin) and *apc* mRNAs in murine brain[155]. FXR1/2 associate with heavy polysomes together with and independently from FMRP[129], supporting the idea that FXR1/2 can have their proper regulatory functions regulating mRNA translation. Studies with RNA aptamers have demonstrated that FXR1/2 can bind G-quadruplex RNA independently from FMRP[156]. In hippocampal extracts, FMRP seems to recruit FXR2 to the endogenous *psd95* mRNA, where FXR2 positively regulates it's DHPG-stimulated translation[116]. These data suggest that FXR2 plays a similar role to FMRP, probably fulfilling redundant functions.

Interesting is that FXR2 KO mice exhibit learning and cognitive deficits, similar to the FMRP KO mice[157,158]; furthermore, FMRP and FXR2 have an additive effect on dendritic maturation in neurons[158]. Ability of FXR1/2 proteins to bind mRNA and regulate its stimulus-induced local translation in dendrites together with FMRP, makes these proteins interesting for my studies. Ability to heterodimerise with FMRP poses even more questions about functions of FXR1/2 proteins and their functional relationship with FMRP. Do they strengthen each other's effects or fine-tune spatio-temporal regulation of synaptic translation? And finally, since KIF3C motor can interact with FXR1/2 directly[150], does it mean that these autosomal paralogues of FMRP can bear independent from FMRP functions?

1.5. Research Goals

The aim of this introduction was to demonstrate the scientific value of this project. One of the biggest mysteries in biology is how our neurons function, letting us learn and form memories. These processes are based on the mechanisms of synaptic plasticity, which in turn rely on mRNA transport and local translation that are tightly regulated in space and time. On the other hand, out of hundreds of RBPs, implicated in mRNA transport, we have focused on one of the best studied yet still poorly understood – FMRP. This protein is multifaceted in its functions in mRNA life, following its targets from the nucleus all the way to dendritic spines and regulating their local translation. So far we do not have mechanistic understanding of how, and if, FMRP can transport mRNA molecules from neuronal soma to the dendrites. Most of the attempts to identify the putative motors, responsible for this transport, have led to a big controversy in the field.

To solve this ambiguity, as well as to push the boundaries in our understanding of the mechanisms, governing FMRP transport, we have outlined the following questions for my PhD project:

1. **Which motor(s) can transport FMRP?**

2. **Can FMRP carry mRNA while being transported?**

3. **Which FMRP domains are responsible for its own and the target mRNA transport?**

I have discussed above the drawbacks of traditional biochemical methods that led to the present controversies in the field. To answer these research questions, we chose *in vitro* reconstitution assays, the benefits of which are discussed in the next subchapter.

1.6. Introduction to the key methods

1.6.1. The power of *in vitro* reconstitution assays

Giving the credit to the classical biochemistry methods, like IP, WB, KO/KD in the cell lines, fluorescent microscopy, they allowed generating knowledge of the state of the art. These techniques have done a great job identifying the most common components of the molecular complexes, yet leaving a gap in understanding direct interactions involved, as well as their biophysical parameters. For example, in a work already mentioned above, published by Kanai et al.[38], the authors identify a set of RBPs associated with the KIF5 motor. IP combined with WB produces yes/no quality of information, but does not help us understand direct interactions between the molecules, making it hard to identify the core components of the complex as well as to learn which of them are minimal and essential. The authors go deeper with their methods and include RNAses and salt gradients into their pull-down assays, which helps to rule out RNA-mediated interactions in the complex. However, the questions of mechanistic understanding of the interactions inside the complex are left unsatisfied.

Another important drawback of conventional IP/WB methods is their absolute dependence on the quality of antibodies. Leaving out potential issues with unspecific binding, commercial antibodies often fail to recognise protein homologues. For example, in another key study performed by Dictenberg et al.[106], it remains unclear, which out of the three Kinesin-1 versions (A, B or C) is the target of the antibodies, used for KHC immunoprecipitation[106]. Another relevant example is the FMRP itself: its paralogues, FXR1 and FXR2, share over 60% of protein sequence similarity with FMRP[154]. Furthermore, these three proteins heterodimerise in different combinations[116,129,159], which makes the specificity of commercially available antibodies very questionable. Our colleagues in the field support the concern that we have no idea how specific the a-FMRP antibodies really are (verbal communication). It makes some of the results questionable.

Studying RNA transport in neurons by knocking proteins out is an even more challenging task. KO/KD of the kinesin motors influences not only mRNA transport, but also transport of the vesicles and signal molecules that can lead to global effects upstream to hampered mRNA transport, like defects in cell polarity and neurite development[160,161]. The above-mentioned limitations can be mitigated using approaches of a new generation – the *in vitro* family of methods. The most basic in vitro techniques were established decades ago, like EMSA assays for protein-nucleic acid interactions.

The novel *in vitro* techniques are much more complex. They provide with the data of a single-molecule level quality and allow combination of various advanced techniques for single-molecules studies, like smPIFE and SiMPulls[162]. *In vitro* reconstitution assays have been utilised to study protein translation[163,164], regulation of dynamics of the microtubules[46,165] etc. A beautiful *in vitro* tug-of-war study on actin-dynein intersections has confirmed that by default, the direction of movement depends on the prevailing force between the associated motors, while some proteins, like Map7, resolve tug-of-war between Kinesin-1 and Dynein by increasing binding rate of Kinesin motor to the microtubules[42]. In terms of the mRNA transport field, *in vitro* reconstitution assays have been very informative, helping us to learn that not only can mRNA cargos activate the motors like Kinesin-2[43] and Myosin V[44,166], but also recruit additional motor units to the complex, for example Dynein/Dynactin[167].

For my PhD project, I have been using an *in vitro* motility reconstitution assay, linked to the Total Internal Reflection Fluorescence (TIRF) microscopy (Fig. I.11). This method allows to study mRNA transport complexes on a single- or near-single-molecule level quantitatively, taking the complex motility as a readout. It is based on combining individually purified and fluorescently labelled components in a microscopic chamber and their visualisation with TIRFM. The microscopic chamber consists of a biotinylated PLL PEG-coated coverslip attached via sticky tape to a PEG-neutralized glass slide (Fig. I.11, A). The system includes *in vitro*-generated taxol-stabilized microtubules that include fluorescently labelled and biotinylated, next to the normal, tubulin dimers. First, the microtubules are attached to the biotinylated coverslip via neutravidine molecules. Next, all the other molecules are pre-mixed and pre-incubated on ice for 10-15 min, diluted down to nM-pM concentrations and added into the chamber. Then the chamber is sealed with transparent nail polish and positioned for the TIRFM (Fig. I.11, B).

The assay allows to study motility of the added components in real time with near-single-molecule resolution. The other important advantages of this method are:

1. Full control over presence and concentrations of the components. In contrast to live cell-based assays, this *in vitro* assay cuts out all indirect interactions between the molecules. When a cell-based assay might still show an interaction between unknown components, an *in vitro* assay completely prohibits it. Moreover, this feature allows for building up the chain of interactors from the motor proteins up to the cargo molecule(s) step by step. At the same time, it makes a flaw of the assay – in order to reconstitute a

complex, one has to be aware of the full chain of necessary interactors.

2. Having three high-speed cameras, our TIRF microscope permits studying up to four distinct fluorescently labelled molecules at the same time. Due to its high sensitivity and space-time resolution, the assay permits investigation of stoichiometry of the interactors.

3. High-throughput analysis. Throughout the course of each recorded movie, decades to hundreds of motile particles can be analysed. Since every experiment can generate two movies or more, three repeats of every experimental set up satisfy the requirement for objective statistical analysis.

4. A plethora of valuable information, extracted from one assay. Such an *in vitro* assay is a perfect tool to measure the speeds of running motor proteins or to study intensity distributions of the particles. Last but not least, this assay allows for investigation how addition of different molecules can influence the whole complex assembly.

The main drawback of the assay is its high complexity that leads to difficulties with troubleshooting and permits studying only one condition at a time. Also, the assay is extremely sensitive to subtleties in handling and a thorough training is required. Nevertheless, the specifics mentioned above make this *in vitro* reconstitution assay a perfect tool to address the questions of my project's focus.

Fig. I.11. TIRFM-based *in vitro* reconstitution assays

A. A simplified scheme of the assay. Components are mixed together at desired concentrations, incubated for 15 min and are flown into the microscopy chamber (a scheme and a photo below). **B.** Sealed chamber is then imaged at the TIRF microscope. **C.** The lasers are set at a critical angle, whereby the light is fully reflected back to the objective, leaving an evanescent wave, or field, which excites fluorophores of the molecules of interest in a close vicinity to the glass surface. Taxol-stabilised, fluorescently and biotin-labelled microtubules are fixed to the biotinylated coverslip through the streptavidin molecules.

A

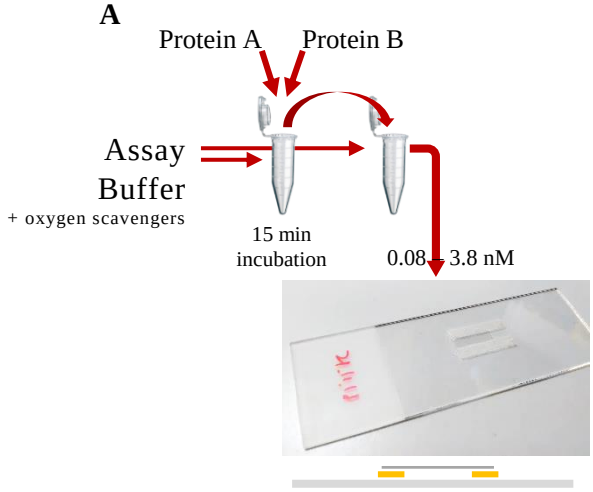
Protein A
Protein B
Assay
Buffer
+ oxygen scavengers
15 min
incubation
0.08 – 3.8 nM

B

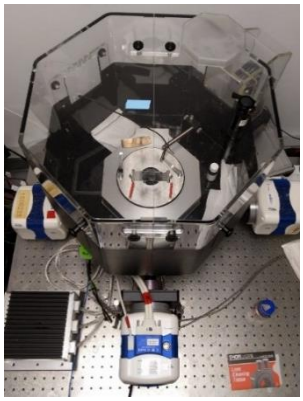

C

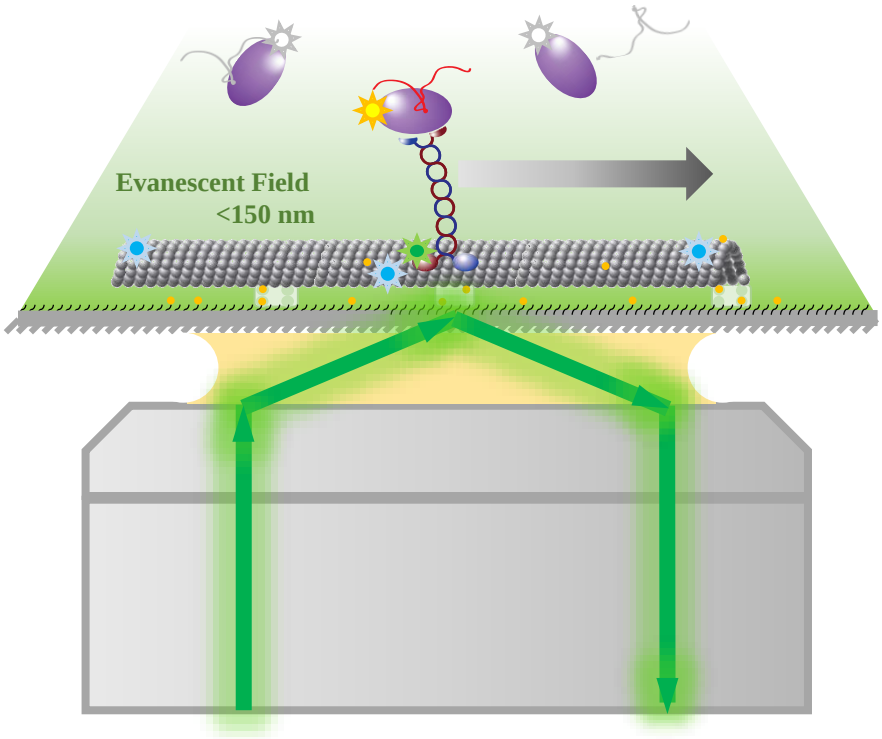
Evanescent Field
<150 nm

1.6.2. TIRF Microscopy

Total Internal Reflection Fluorescence Microscopy is a special microscopy technique that allows for illumination of a sample with an extremely shallow depth (100-200 nM) beyond the glass (Fig. I.11, C). This effect is achieved by picking a very sharp angle of light attack relatively to the glass surface, called a critical angle. When the critical angle is achieved, the light beam fully reflects back from the oil-glass interface (due to the difference of refractive indexes), before illuminating the sample directly. Therefore this reflection is called *total internal reflection*, hence the name of this microscopy technique. Although the beam does not reach the sample, it leaves an electromagnetic field of the same frequency that penetrates the sample. Since the intensity of this penetrating field decays exponentially over the distance from the glass surface, it was called *evanescent* wave, or field. The depth of the evanescent wave depends on the incident light angle, the wavelength of the laser used, as well as the refractive index differences, reaching up to 200 nm in depth.

Why use this technique? As mentioned in this excellent TIRF review[168], TIRFM offers a few major benefits, among which:

1) An excellent signal-to noise ratio due to (theoretically) up to 2000-fold lower background than in conventional epifluorescence microscopy;

2) TIRFM permits no out-of-focus light, thus no deconvolution post-processing algorithms are needed;

3) In contrast to conventional confocal microscopy, TIRF microscopes illuminate all the field of view at a time, thus the speed of recording is limited only by the brightness of the fluorophores used and sensitivity of the light detectors;

4) If used for cellular studies, TIRFM permits less exposure to light, increasing the life span of a living sample;

5) TIRFM can be combined with other advanced fluorescence-based assays, like bleaching step analysis[43], FRET[169–171] and smPIFE[162].

There are two common configurations of the TIRF microscopes: prism- and objective-based, depending how the light is directed to create the evanescent field. In our laboratory, we are using objective-based microscope, where the reflected light goes back through the objective, permitting an easy switching between epifluorescence and TIRF modes.

Although TIRFM has been used traditionally for the cells surface studies, like exo- and endocytosis, cell-substrate contact formation, cellular motility, during the last years, the advantages of TIRFM have been deployed for the next-generation *in vitro* assays, like SiMPulls[172] and *in vitro* reconstitutions[46]. In the Results chapter, I will gladly share with you my results, obtained with this exceptional technique.

1.6.3. The chemistry of SNAP labelling

Since TIRF microscopy requires the biomolecules to be fluorescently labelled, in our laboratory we are using the SNAP tag technology for highly efficient and tag-specific fluorescent labelling of our proteins. The SNAP tag was developed from the O^6-alkylguanine DNA alkyltransferase of human origin that was subjected to directed evolution and mutagenesis to reduce its size, improve labelling kinetics and specificity.

SNAP tag transfers an alkyl group from O^6 of an alkylguanine substrate to a cysteine residue in its active site. Fusing fluorescent dies to the O^6-benzylguanine linker allowed for using optimised SNAP tag for site-specific fluorescent labelling of the proteins of interest, fused to the SNAP protein. SNAP protein has a rapid dye binding kinetics ($k = 2{,}8 \times 10^4\ M^{-1}\ s^{-1}$), is relatively small (19,4 kDa) and very stable[173]. SNAP-dye conjugation is also irreversible. Currently a wide variety of SNAP-compatible fluorescent dyes is commercially available[173].

Chapter 2

2. MATERIALS AND METHODS

2.1. Tubulin production

Tubulin was purified from bovine brains according to the previously published protocol[174]. This protocol consists of two cycles of tubulin polymerisation and depolymerisation in high molarity PIPES buffer (Fig. M.1, A). The utilised strategy allows to accumulate functional tubulin dimers, capable of repeated (de)polymerisation cycles, while removing damaged tubulin dimers with all the accompanying contaminant proteins. Dilution of the final depolymerised tubulin in desired buffer volume permits production of highly concentrated tubulin. Processing six bovine brains usually gave a final yield of 0,6 mg of tubulin. Some of the tubulin was snap-frozen and stored in liquid nitrogen in 10 µl aliquots at 185 µM concentration for taxol-stabilised MT preparation, the rest was snap-frozen and stored in 3 ml aliquots for future labelling. Tubulin purity was assessed by SDS-PAGE (Fig. M.1, B).

Tubulin was labelled with EZ-Link™ NHS-Biotin (ThermoFisher) or ATTO 390 NHS-ester (ATTO-TEC GmbH), according to the guidelines from the Mitchison lab. In short, the general procedure involved labelling of already polymerised tubulin, ensuring protection of the surfaces, necessary for MT assembly. Labelling was performed at high pH to foster the NHS (succinimidyl) ester conjugation reaction. After the labelling reaction, a cycle of polymerisation / depolymerisation was performed to collect only functional tubulin dimers and to remove unreacted dye or biotin esters.

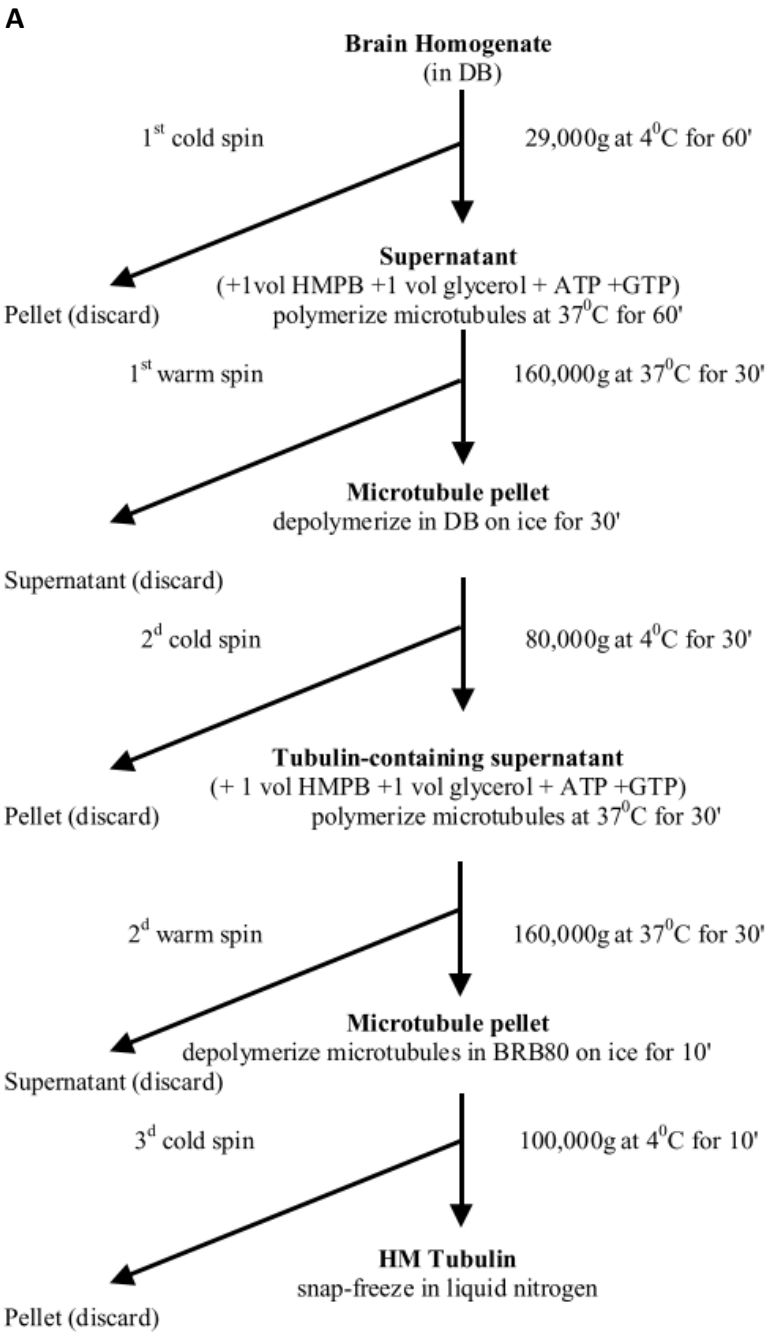
A
Brain Homogenate
(in DB)
1st cold spin
29,000g at 4⁰C for 60'
Supernatant
(+1vol HMPB +1 vol glycerol + ATP +GTP)
Pellet (discard)
polymerize microtubules at 37⁰C for 60'
1st warm spin
160,000g at 37⁰C for 30'
Microtubule pellet
depolymerize in DB on ice for 30'
Supernatant (discard)
2d cold spin
80,000g at 4⁰C for 30'
Tubulin-containing supernatant
(+ 1 vol HMPB +1 vol glycerol + ATP +GTP)
Pellet (discard)
polymerize microtubules at 37⁰C for 30'
2d warm spin
160,000g at 37⁰C for 30'
Microtubule pellet
depolymerize microtubules in BRB80 on ice for 10'
Supernatant (discard)
3d cold spin
100,000g at 4⁰C for 10'
HM Tubulin
snap-freeze in liquid nitrogen
Pellet (discard)

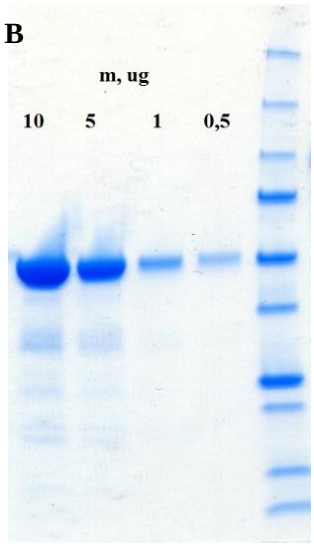

Fig. M.1. Tubulin extraction protocol.

A. Freshly collected into the cold PBS bovine brains were pealed, blended with the tubulin buffer, filtered and centrifuged. Tubulin in the supernatant was subjected to few polymerisation-depolymerisation cycles in order to enrich for intact tubulin molecules. In the last step, the tubulin was resuspended in the volume, resulting in tubulin concentration of 20 mg/ml, aliquoted and snap-frozen in the liquid nitrogen. Based on the published protocol[174]. **B.** The final gel demonstrates purity and intact state of protein in the last tubulin prep.

2.2. Protein production

Protocols for purification of various proteins have been evolving over the course of my PhD work. Here I am providing with the latest versions of the protocols to avoid unnecessary information overcrowding and redundancy.

2.2.1 Protein overexpression in *E. coli*

BL21 AI chemically competent *E. coli* cells (Invitrogen) were transformed with 1 µl of the plasmid carrying a corresponding expression cassette. Cells were incubated on ice for 30 min, heat-shocked for 30 s at 42°C and incubated for 2 min on ice. 250 µl of pre-warmed to 37°C SOC medium was added and cells were incubated for 60 min at 37°C, shaking at 350 rpm. 50-150 µl of transformed cells were plated on agar containing 50 µg/ml kanamycin or 100 µg/ml ampicillin and incubated O/N at 37°C. The next day, one colony was hand-picked by a pipette tip and moved into 100 ml LB medium with corresponding antibiotic and incubated O/N at 37°C, 350 rpm. The next morning, cells were diluted 1:50 into 300 ml of a fresh pre-warmed LB medium and incubated on the shaker until reaching OD=0,8.

Next, cells were diluted 1:50 into 6x5L flasks, containing 1L of fresh LB medium and left incubated in the same conditions. Upon reaching OD=0,8 the media were supplemented with final concentrations of 0,1% arabinose and 1 mM IPTG. Cells were incubated at 18°C for 16 h until collection. Cells were harvested in the morning by centrifuging at 4000 g for 20 min at 4°C (JLA 8.1000 rotor, Avanti® J-26XP centrifuge, Beckman Coulter). The pellets were resuspended in 20 ml PBS and centrifuged at 4000 g for 20 min at 4°C in 50 ml falcons. Pellets were flash-frozen in liquid nitrogen and kept at -80°C until used. Before centrifuging and freezing, 1 ml of sample was collected for the final validation of protein expression by SDS-PAGE. Bacterial cultures were grown in an incubator shaker (INFORS HT multitron). Unless otherwise stated, cell suspensions were centrifuged with an Eppendorf 5810 R centrifuge.

2.2.2. Protein overexpression in *S. frugiperda*

Sf21 cells were sustained in Sf-900™ II SFM medium (ThermoFisher). Upon reaching the cell density of $0,5x10^6$ cells/ml, the cells were transfected with corresponding bacmids in 6-well plates (Greiner), using InsectGeneJuice® Transfection Reagent (Novagen) and incubated at 28°C for 3 days. Next, 3 ml from each well were collected to obtain the V_0 virus stock, which was and stored at 4°C protected from light. Cells were compensated with 3 ml of fresh medium and kept at 28°C for 3 more days. Cells were daily checked for contamination and growth using an inverted microscope (Leica DMIL 090-135.001). 6 days after transfection, the medium was discarded and cells in each well were softly resuspended in 0,5 ml of PBS (137 mM NaCl, 2,7 mM KCl, Na_2HPO_4, KH_2PO_4). Transfection efficiency was evaluated by YFP fluorescence. If transfection efficiency was reaching 70%, the V_0 virus would be left for amplification. 25 mL of Sf21 cells (cell density $0,5x10^6$ cells/ml) were infected with 3 ml of V_0 virus, passed through a 0,22 μm filter. Cell density and YFP expression were checked 24 h after infection with the cell counter with arrest of proliferation in case of successful infection. 24 h later the cells were centrifuged at 800 rpm for 5 min. The supernatant was stored at 4°C protected from light as a stock of an amplified virus V_1. The cell pellet was resuspended in 25 ml of fresh medium in a 125 ml flask and the cells were incubated on a shaker at 27°C, 100 rpm. Protein expression was evaluated by SDS-PAGE on small samples that were collected every 12 h. Upon determining the optimal infection conditions, the cells were infected with the V_1 virus and after overexpression, cells were collected by centrifugation at 800 g for 15 min at 4°C. Cell pellets were snap-frozen in liquid nitrogen and stored at -80°C. Before centrifuging and freezing, small samples were collected for final validation of protein expression by SDS-PAGE. All the insect cell overexpressions were performed by Maria Gili.

2.2.3. Purification of Kinesin motors

Before thawing the cells, 50 ml of Lysis solution was prepared (~40 ml per 5g of cell pellet), supplementing 50 ml of the lysis buffer (0,31% $NaHPO_4$, 1,54% Na_2PO_4, 200 mM KCl, 5 mM $MgCl_2$, 2,5 mM EDTA, 0,1 mm ATP, 0,001% Brij-35, 2,5 mM DTT, pH 7,2) with 1 cOmplete ULTRA tablet (Roche) and a small spatula of DNAse A. The Lysis solution was added to the frozen cell pellet and it was thawed in a RT water bath. Cells were mixed with a pipette boy and carefully lysed on ice with a Dounce homogeniser (SigmaAldrich), 60 cycles. The lysate was ultracentrifuged for 45 min at 50'000 RPM (70Ti rotor, Beckman) at 4°C. Supernatant was applied to a 5 ml Streptavidin column (GE Healthcare), washed with 70 ml of GF (gel filtration) buffer (0,31% $NaHPO_4$, 1,54% Na_2PO_4, 200 mM KCl, 5 mM $MgCl_2$, 0,1 mm ATP, 0,001% Brij-35, pH 7,2) and eluted with 30 mM Desthiobiotin (Sigma), dissolved in GF buffer. The protein was cleaved with His-3C or His-3C/His-TEV proteases O/N at 4°C, the quality of the cleavage was checked with SDS-PAGE gel the next day. In order to fish out the proteases, solution was passed through 1 ml His FF column (GE Healthcare). 3C-cleaved protein was labelled with desirable SNAP-Cell® dyes (New England Biolabs) at a dye/protein molar ratio of 2:1, for 70 min at 15°C protected from light. Unbound dye was removed by passing the solution through a Zeba® Spin 7K MWCO (ThermoFischer) desalting column. Both, 3C- and 3C/TEV-cleaved versions were concentrated with Amicon® Ultra filter units (Merck Millipore), ultracentrifuged at 80'000 RPM (TLA120.2 rotor, Beckman) for 10 min, 4°C in a TableTop Ultracentrifuge (Beckman). Supernatants were gel-filtrated on a Superdex 200 10/300 GL column (SigmaAldrich), using an Äkta Purifier system (GE Healthcare). The eluate was collected with a 2 ml deep 9-well plate and correct fractions were pulled, based on an SDS-PAGE gel analysis. Pulled fractions were concentrated as before, aliquoted into PCR tubes and snap-frozen I liquid nitrogen.

All the solutions were prepared one day in advance and filtered with 0,22 um filters. ATP and DTT were added on the day of purification. Throughout the purification, small samples were collected for SDS-PAGE analysis. Kinesins, expressed in bacteria were lysed, passing 2x through ice-cold Avestin Emulsiflex® homogeniser.

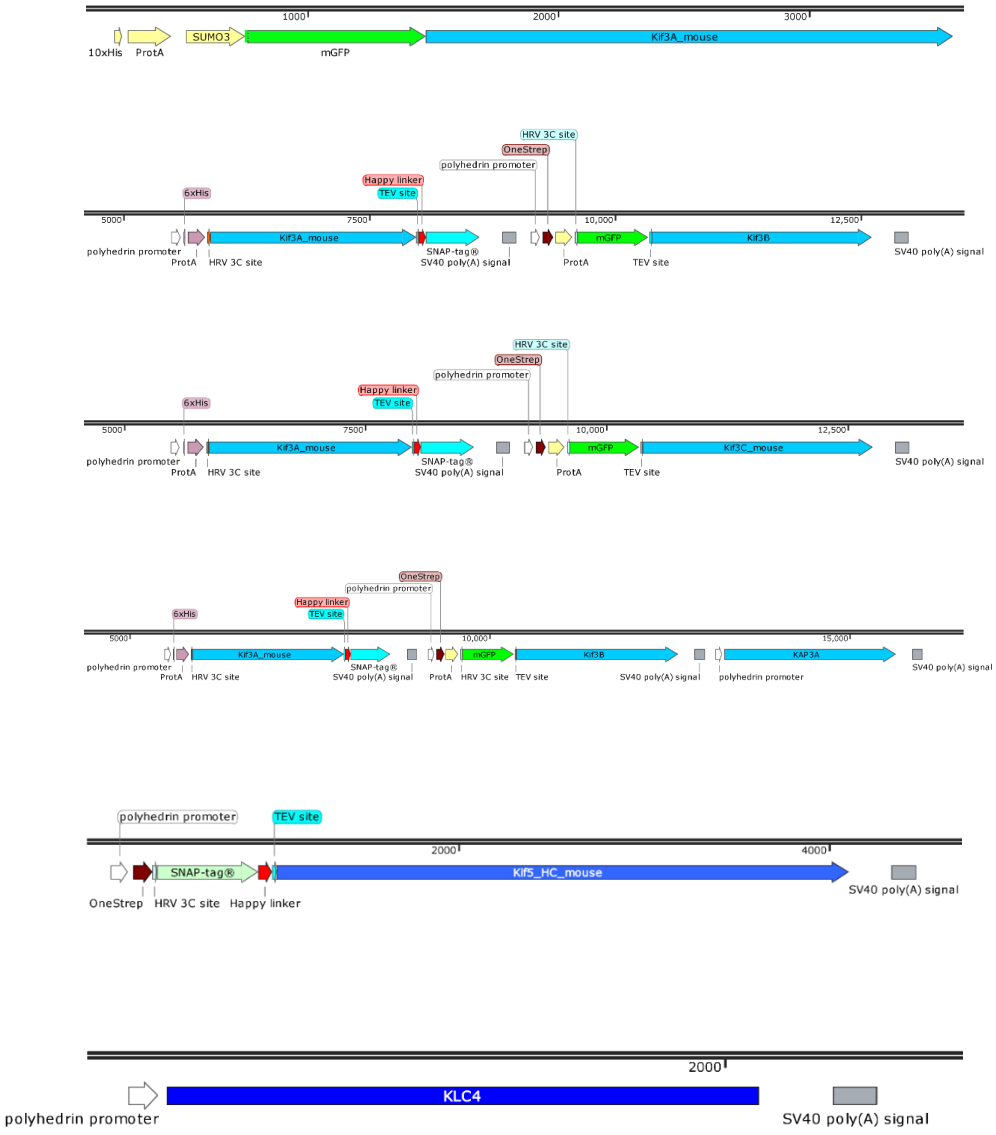

Fig. M.2. Kinesin expression plasmids.

The upper most plasmid was overexpressed in *E. coli*; the construct is based on the commercial pACE1 plasmid. The rest of the plasmids were expressed in Sf21 insect cells. Kinesin-1 and Kinesin-2 expressing constructs were based on pLIB and pBIG commercial plasmids correspondently.

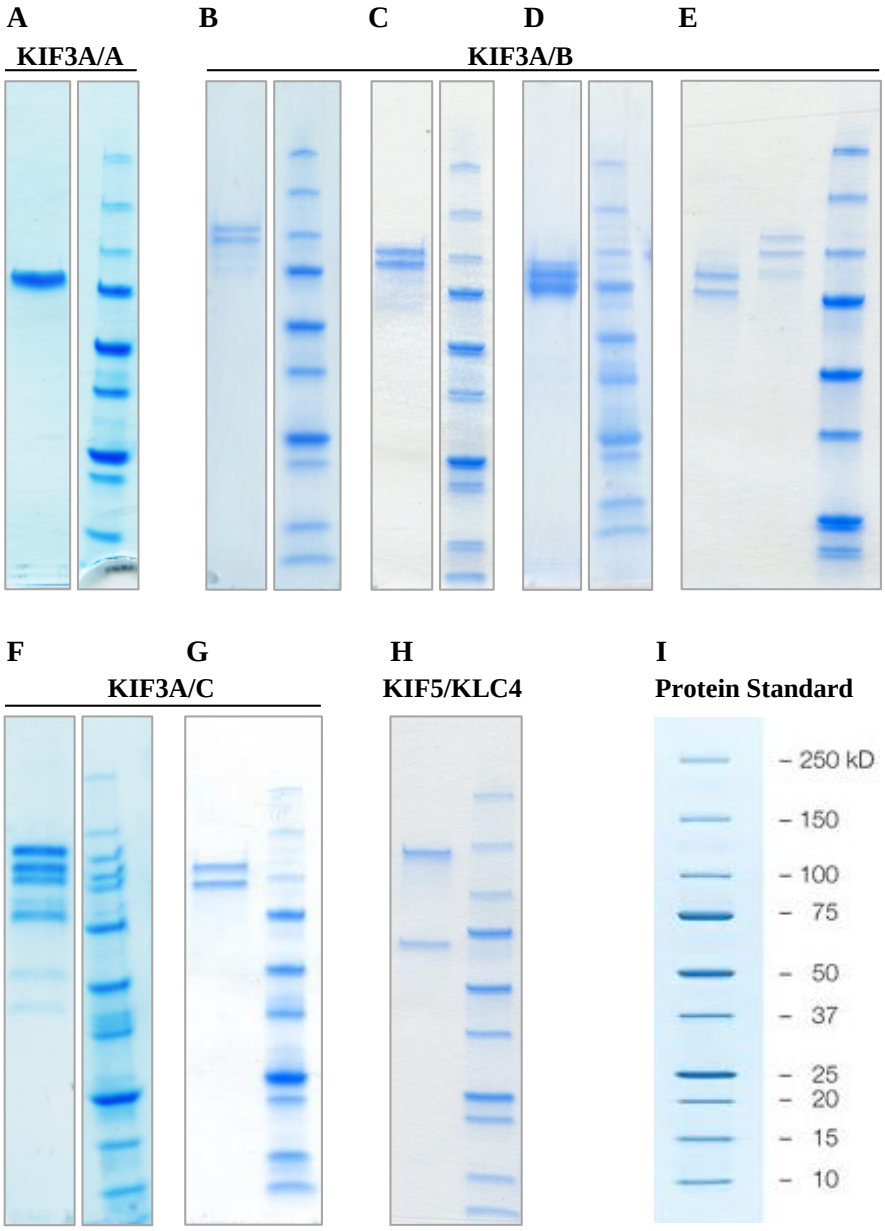

Fig. M.3. Some of the purified Kinesin motors.

A. Bacterial GFP-KIF3A/A, used on Fig. R.2., H. **B.** Insect AF488-KIF3A/B, used on Fig. R.2, A, G. **C.** Insect AF488-KIF3A/B, used on Fig. R.3, C, G. **D.** Insect KIF3A/B 3C/TEV cleaved, used on Fig. R.5, A, B. **E.** Insect 3C/TEV cleaved KIF3A/B/KAP3, used on Fig. R.5., D, E (left lane) and AF488-KIF3A/B/KAP3, used on Fig. R.5, F (middle lane). **F.** Insect GFP-KIF3A/C, used on Fig. R.2, C, D, F. **G.** Insect GFP-KIF3A/C, used on Fig. R.6, A-E, G-H, J-M. **H.** Insect AF647-KIF5/KLC4. **I.** Precision Plus Protein™ Standards, BioRad.

2.2.4. Purification of FMRP and FXR2

Throughout my PhD studies, I have done around 17 FMRP purifications. For convenience, I am providing here the last version of FMRP purification protocol, based on the results of few rounds of buffer optimisation attempts.

One day in advance, there was prepared 1L of 9E buffer (50 mM HEPES, 500 mM KCl, 50 mM arginine, 50 mM glutamate, 250 mM glucose, 5 mM $MgCl_2$, 0,001% Brij-35, pH 8,0). 9E buffer was divided into three further buffers: 100 ml of 9E-A (further supplemented additionally with 1 mM EDTA, 10 mM ATP, 2,5 mM DTT), 100 ml of 9E-B (further supplemented additionally with 10 mM ATP and 1 mM DTT) and 800 ml of 9E-C (further supplemented additionally with 1 mM DTT). 9E-A serves for cell lysis, as it contains EDTA that helps inhibit proteases, ATP to increase stability of FMRP and DTT to prevent protein oxidation. Buffer 9E-B was designed to allow fishing out the His-3C and His-TEV proteases that in my hands worked best, comparing to the GST versions. 9E-C buffer was used for gel filtration, equilibration of glassware and all the columns; absence of ATP reduces great costs that would otherwise apply. ATP and DTT were added on the day of purification, pH was adjusted at RT. All solutions were filtered with 0,22 um filter.

To prepare Lysis buffer, 70 ml of 9E-A buffer was supplemented with 1 cOmplete ULTRA tablet (Roche) and a small spatula of DNAse A. The Lysis buffer was added to the frozen cell pellet and it was thawed in a RT water bath. Cells were mixed with a pipette boy and carefully lysed with a Dounce homogeniser (SigmaAldrich), RT, 60 cycles. The lysate was ultracentrifuged for 45 min at 50'000 RPM (70Ti rotor, Beckman) at RT. The supernatant was filtered with 0,45 um filters and applied to a 5 ml Streptavidin column (GE Healthcare), washed with 50 ml of 9E-C buffer and eluted with 30 mM Desthiobiotin (Sigma), dissolved in 9E-B buffer. In the case of precipitation, the eluate was diluted with the rest of 9E-B buffer. The protein was cleaved with 2x concentrated from recommended by manufacturer His-3C or His-3C/His-TEV proteases at 20^{o}C for 1h. In order to fish out the proteases, solutions were passed through 1 ml His FF column (GE Healthcare) and the quality of cleavage was checked with SDS-PAGE gel. In case of incomplete cleavage, the procedure was repeated. If the volume of the 3C-cleaved protein was exceeding 4 ml, it was concentrated with Amicon® Ultra filter units (Merck Millipore). Next, the protein was labelled with TMR-Star SNAP-Cell® dye (New England Biolabs) at a dye/protein molar ratio of 2:1, for 75 min at 20^{o}C protected from light. Unbound dye was removed by passing the solution through a Zeba® Spin 7K MWCO (ThermoFischer) desalting column. Both, 3C- and 3C/TEV-cleaved versions were concentrated until the first signs of precipitation,

using Amicon® Ultra filter units (Merck Millipore) in 10 min steps, mixing in between. Concentrated protein was ultracentrifuged at 80'000 RPM (TLA120.2 rotor, Beckman) for 10 min, 20ºC in a TableTop Ultracentrifuge (Beckman). Supernatants were gel-filtrated on a Superdex 200 10/300 GL column (SigmaAldrich), equilibrated with 9E-C buffer, using an Äkta Purifier system (GE Healthcare). The eluate was collected with a 2 ml deep 96-well plate and correct fractions were pulled, based on an SDS-PAGE gel analysis. Pulled fractions were concentrated as before, aliquoted into PCR tubes and snap-frozen in liquid nitrogen. Protein concentrations were measured post-freezing.

All the procedures were undertaken at RT. All the glassware and plasticware was equilibrated with 9E-C buffer before it had any contact with the protein solution to prevent protein adsorption on the surfaces.

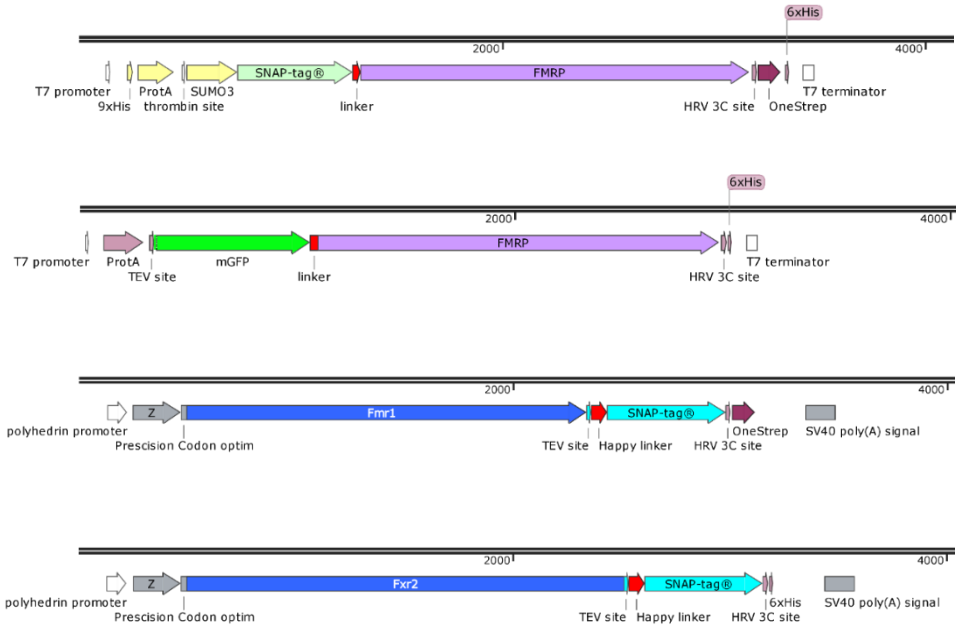

Fig. M.4. FMRP / FXR2 expression plasmids.

The two upper plasmids were overexpressed in *E. coli*; based on commercial construct pCoofy17. The rest were expressed in the Sf21 insect cells; based on commercial pLIB constructs.

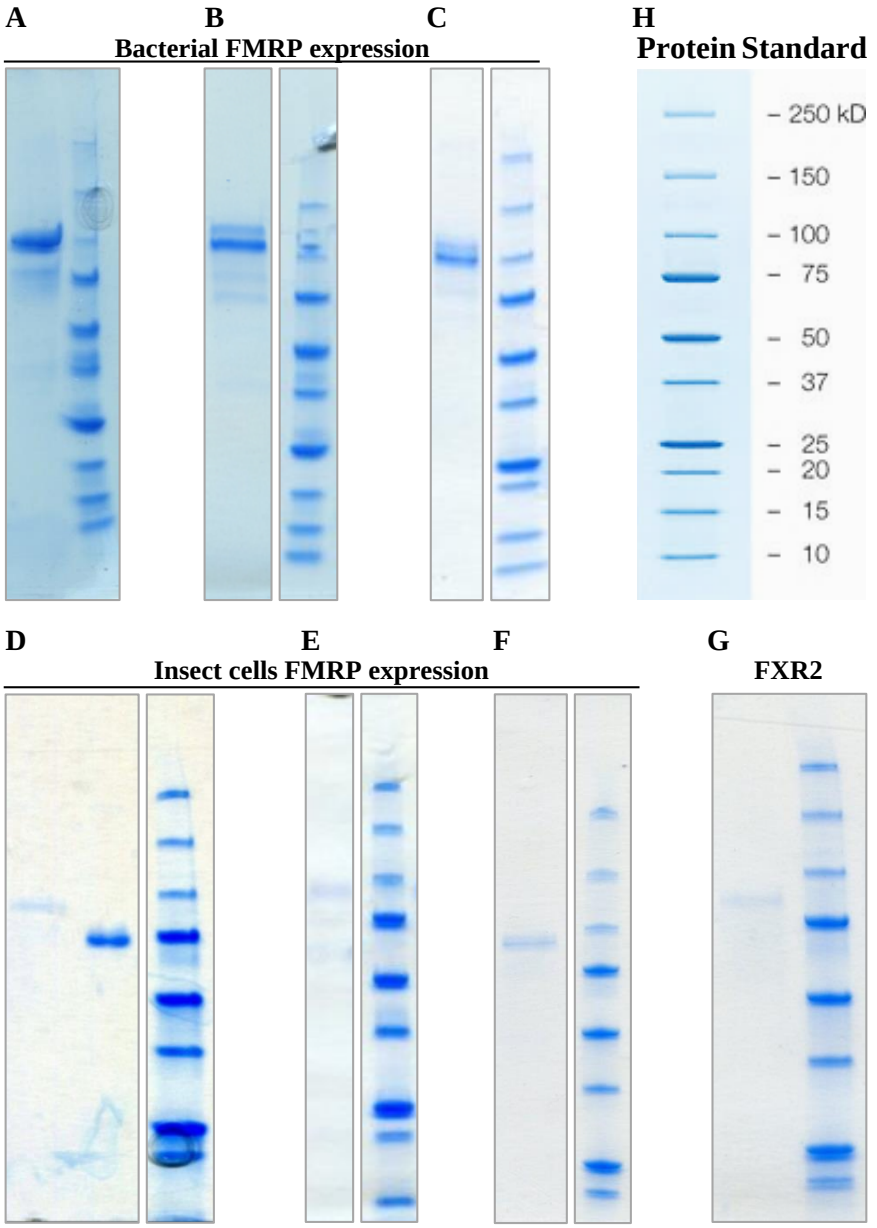

Fig. M.5. FMRP and FXR2 preps, used in this work

A. TMR-FMRP, used on Fig. R.2, B, E-H. **B.** GFP-FMRP, used on Fig. R.3, A. **C.** GFP-FMRP, used on Fig. R.3, B. **D.** TMR-FMRP, used on Fig. R.3, C, F-G, Fig. R.8, D-F for experiments with KIF5 motor. **E.** TMR-FMRP, used on Fig. R.5, A, D, Fig. R.7, A-C. Fig. R.8, D-F for experiments with KIF/KLC4 motor. **F.** TMR-FMRP, used on Fig. R.6, B-C, F, H, Fig. R.8, D-F for experiments with KIF5/KLC2 motor, Fig. R.9, C. **G.** Insect TMR-FXR2, used for Fig. R.10, B-C. **H.** Standard protein ladder.

2.3. RNA production

All the DNA constructs used to *in vitro* transcribed mRNA, contained a NotI or SwaI cleavage site at the end of the sequence of interest. Purified DNA plasmids were cleaved with SwaI (for *β2b-tubulin* mRNA) or NotI (the rest mRNAs) nucleases, ran on a 1% agarose gel in TE buffer and fully cleaved bands were excised from the gel and purified, using QIA® Quick Gel Extraction Kit (QIAGEN). mRNAs were transcribed *in vitro*, using Transcript Aid T7 High Yield kit (ThermoFischer). For transcription reaction, 1 ug of cleaved clean plasmid was added to the reaction mix, prepared according to the manufacturer's instructions. mRNAs were co-transcriptionally labelled with Cy-5 UTP (Perkin-Elmer). Cy5-UTP was added to the reaction mix additionally to UTP provided by the kit. In order to obtain mRNAs with ~1 fluorophore per mRNA molecule, the UTP/Cy-5 UTP ratios were determined empirically for each of the transcripts.

Transcription mix was incubated for 3h for long mRNAs (like *camkIIα* 3'-UTR) or for 6h for short mRNAs (*β2b-tubulin* and G-quadruplex mRNAs). Reaction was stopped with adding 1 ul of DNAse and 2,2 ul of EDTA, provided with the kit. Transcripts were purified with 1 column of the RNA Clean-up and Concentration Micro-Elute Kit (NORGEN) or with 2 columns of RNeasy® Mini Kit (QIAGEN). In the case of two columns, transcript was purified two times one after another to ensure removal of not incorporated Cy5-UTP. RNA quality was verified with agarose gels, using a Typhoon Trio fluorescence reader (GE Healthcare) for Cy5 incorporation assessment and the ChemiDoc reader (BioRAD) for SybrGOLD staining detection.

Commercial fluorescently labelled mRNA was ordered from IBA.

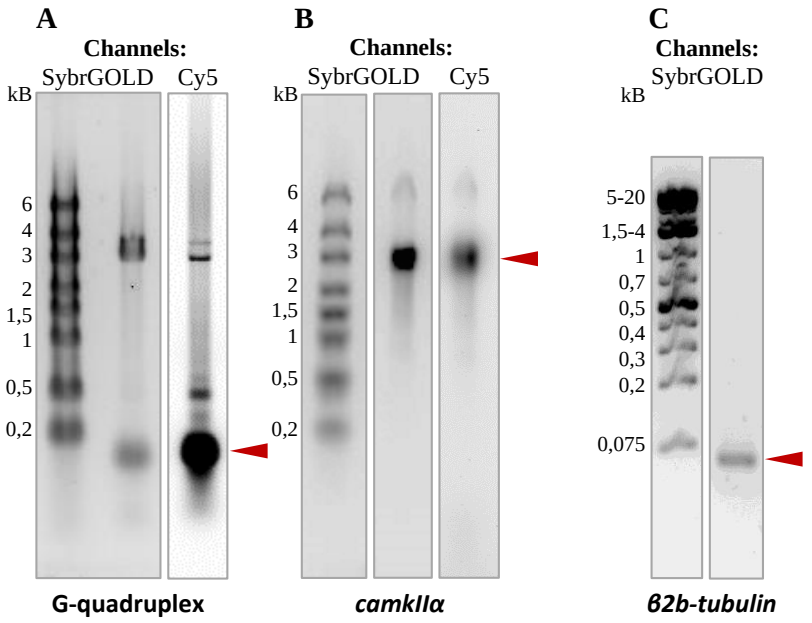

Fig. M.6. mRNA transcripts

All mRNAs were labelled co-transcriptionally with Cy5-UTP and purified with commercial RNA purification columns. **A.** G-quadruplex mRNA. **B.** *camkIIα* 3'-UTR. **C.** *β2b-tubulin* mRNA. Since RNA ladder was over at the moment of mRNA production, a DNA ladder was used, which can explain why 90-nt long mRNA ran lower than 75 bp lane. Correct mRNA bands are indicated with arrows.

Transcript	Length, nt	Sequence	Fluorophore	LR
G4x RNA	97	GAACTTGAATGACCACTGCTCAAACTT TCTGCTACTGGGGGGGTGGGGGAGGGG AGAAGAGATGTCTGGTTTATTCTTGGC GTTTTCAGTGAGAGCT	Cy5	1,3
β2b-tubulin	92	GGTTCCCCAGGCCAAGCAGGTTAGGGA AAGCTGAGATGAAAGGAGGGGGTGGG GGGGCTTAATCTGTGAAAATACCTTGG CAGTTGAAATTT	Cy5	1,8
camkIIα 3'-UTR	3405	GAGGACCAGGCCAGGGTCCCTGCGTCC TTGCTTCGCAGAGATCCGCTCTTTGTCC GTGGAATGTGGCTGCTGGTTCTCCTTTG GATTTTGCTGGAATTCTCCCTGTCAGAT CACCCTACCATTGCCACCTATGTACTCG CGTCACGAAAACCTGCTTGTTCACAGA AGTCGCCACGACATCACAGTGAACAGC CAGCTCTCCCCAGCTCCGTTGCCCAAG CTCTTCCTGCCAGTGGGGACCTTCTTCC GGCTTAAGTACCCAGGGTGCTGGCCCC AGGAACCCCCACCCCCTACCCACTGTT GTTGGCCTAGCCTAGCTTTAGCTATAG ATGGGGCCTCAGCTGTGCAATTGGCAG GAAGTGAGGAAGAGGCAGGCAAGCTG TGTTGAGGGCACCTCTCATCGATTCCTT CTTTCCTGGGGTTCCCCGGGGAAGCTC ACACGAGGCCCTCAGTCTCCAAGCCAA CCCCTTATGAGGGAGAGTGAGAGAGG AGCCAACGCCAGTGAGCCAGGAACTGC TGCTCTCATCTGCTCTCCTCTGTGTTGG CCTTGCCTTTGACCAGACCATCCGCTAC GAGGGGTGGGCTCTACCGCCCAGGTGC CCCACTCACTCTGCCTCAGTCCTCCTGT GAAGTTTGCCTCCAGTGTTGACCCACC CACCCTGCCCTTCAACGTCCTTGGAGA ATTCCAGCTTCATCTGTCTGAGAGGAG ATTGGAAGGTGTTTCAGGGGCAAAGCA AGCAACATTTAGGTATCACTTCTACTTG GACGCATGCCTTTTTACAGCCAAACTT CCGTGTATTTCGTAAATGGATTTTGCGT TAACGGACATCTATGTGATAACTAGAC CTCTCAAGTTTACTGTAAAGAAGAGTC GGATGGGTTGGGAAGTGGGTGGGAAG AGGAGTGAGAGGAAGTTTTAACCCCAT TCCAGAGGGTCTTTTTTTTGGGGGGTGT CCCTTCTGGGGGAGGGTGCTTTCTGAG GTGGCCTCACCCCCCAGGGAGCATGGT TTCCTTCCATTATGGTCCCCAAAGTCAG CTGACAAGATTTCTTCCAGAGCCAGCA TGACTAACACACAGTGAGTCAGGTCAG GGGAGGCTATCAGGAAGGGGTTATCTA GACTTGGCATCTCTGGAACTGGAGACC TCACTACCCTACTTCCCAGGAAATCTTT CCCGTATCCTTGTGCTATCTCTCCTCAG CCCAGCCCCCACTCACCACCTTCTAGG CACATTATTCTCATCACCTCTCTCAACT TGGCCAAGCAAGAGTGCCAGAAACTTA TTTTCCTACTTCATGCTGAACTTGGCCT GGTGTGCGCTCTATTGTGCTTGCCTGCC TCCCTGGCCTTCCTCGACTCCCCTGCCC CGACATACACACACACACACACACACA CACACACACGCACACGCACACGCGCGC ACACACACACATGCACACGCACATGCA CACACTCACACCACTTCCTTCCACCACT TCCTTCCTCCCCCCTCTCCCTCCCTTTCT CTTTCTCTTCTCTCCCTCTTCCTGGGTTT GGCTCTTGTATGGAATGCTGTATCTCAT TCACGGGGATCTCCTGTCTGCACTGTTT TCTTTGCATGACTTTATATGCAGTAAGT ATGTTGAAAAACAAACAAAAAACAAA AAAGGAGAAAAACACTCAACAAAATC AAACGACACGTTTTTTTTTGGACAAAA AATAATAACATTCAAGGTAATAGTCTC AGTGTCCAACTTGGACTTACGTTGCTG CCTCTCCGTGCTTTTGGTCTCTCTGTGG CTATGTTTTGCCAGCATGAGACCCTGTT CCCTCTGGAAGTTGCTAGGGGAGGAAG AGCCATGCGTCCAGGGGTTTGGAGACA GCTTTATCCTCTCGGCTTTTCTGAGGGT CGATGGGAGCAGAAGTGGAAGGGATG TTTAATCCAGAACTTTCTGGTATTCCCC TTTCGCCTACATGTGAGCTATATCCCGG	Cy5	1,23

		GCTCTTCTCTCAAATCCTGCTGCCCAGG GACAAGTACAGGGTAGAAGAGTGGCT CTCTTGTCTAAGCCGCTCCACTGTAGCC TCTGCCCTTGGTAGAGACACTGCTACC CAGGCCCAAGAATGGGCCCTTGTCCTG CCCCAGAACCAGGCTTCTTCATAAGGC TCAGCAAACCCATTGTCCCCAGCCACT CCCCAGATAAAGGTAAAGGAGGGTGT GGCCTTTACCAGGGGACACTGCAATCT CCATGCAGGATCTACAATCCCTTCTTCA AGCCTCAGTTTCTCCATCAATGTTCCTA CCCAGACTGATGGAGGGTCAGAGTAAA AGATGTCACAAGCACCCACCACCTCTG AGAGCTTGTTGGGTTTGTCACTGGCTG GCCCTCTTATGCACCAGGTCTGGCCAA CCCCCACCCTTTCCTCTGTGTGCCCCTC ATTTTACTATTTGGTGCCAGTCCGTTGA TGACCAGCAATGGACTGCAGGGGAAA GAAGTGTTTGGGGGCTCTGATCCCGGG TTCTGACCAGATCCGGGTTTTGTGTAGC TTTGGGTAAATCCTTTGCCCTCTTCAGG CTTTAGTTTCGCCAACCAGAAGATGCC TATGCCCTGCCTTCCGTTGGCTAACATG CCCCTGTCCACTATGTGCTTGTTCACGT GTGGGAGAAGTGGAGGCAAGTCCCTGC CCCAGTCTGAGACGGCCCCCTCTGCAG AGGCCGCTCCTGTGGGTGGGCAGCCAA CTAATGAAGACCTTGGGACACTACGAT GGCCCCAAGGTGACAGGCAGGGGAAC AGGCAGAAAAACTGTCCAGAGCCCACC CTCATCTGACAAGCTCCATGCTCCGTCC AAATACCCTCCAGATGAAAAAAAAAA GAGAGAGAGAGAGAAAGAAACAAAGA GTCAAATCACATTTATAGGAAAAGCGT CTCCAGCTCTATGCACCATAGCTCAAA TCCTGCCCCATGGCTTCCCCACCCCCCT TCAAAGGGAGAGCCTTGGGGGAATGC GTTTGCCAGGCCCCGTGCTGGCTTCTTT GTTACTATTTGTTTAGGGTTTTGTTCTA GTTCTCTCTCTCTCTCTCTCTCTCTCTCT CTCTCTCTCTCTCTCTCTCTTTCTTTT TTAATCTGTGGCTGTGAACTTGAATGA CCACTGCTCAAACTTTCTGCTACTGGG GGGGTGGGGGAGGGGAGAAGAGATGT CTGGTTTATTCTTGGCGTTTTCAGTGGA ATAAATAGCTACAAATTTATGTGAGTC CGTGTCTTCCTGAATTGGTCAAGGCAC AGAGCCCCAGGAACTGGCATTTTGCTT TGGCTTGTTTTTTGGGTTTTTTGTTTGTT TGTTTGTTTTTGTTTGTTTCAAATCTCCC CTGTTGCAAAATAAAAGTCCTGGTCCT ATGGATTGGAAAAAAAAAAAAAAAGCT CGATACGTCGAAAATGC		
CL G4x RNA	90	TGCTCAAACTTTCTGCTACTGGGGGGG TGGGTGGGGGAGGGGAGAAGAGACGT CTGTTTTATTCTTGGTGTTTTCAGTGGA ATAAATAGC	3’-AF647	1
CL no G4x RNA (*β2b-tubulin* mutant)	87	GUUCCCCAGGCCAAGCAGGUUAGGGA AAGCUGAGAUGAGUACGUCCUUGGCU AGAGAUAGACCUGUGAAAAUACCUUG GCAGUUGAA	5’-AF647	1

Table 1. Used in the study mRNAs.

The first 3 mRNAs were made in house, the latter two were produced commercially (CL). The G-quadruplex sequences are marked in red. *camkIIα* 3’-UTR has two G-quadruplex structures. Since the second one was also confirmed in the literature[175], this fragment was chosen for the short G4x mRNA synthesis, see top-1 sequence.

2.4. TIRF assay

2.4.1. Production of taxol-stabilised microtubules

To prepare taxol-stabilized microtubules, the final concentrations of 32,5 µM tubulin, 10 µM biotin-tubulin, 14 µM ATTO 390-tubulin and 4 mM GTP were slowly and thoroughly mixed by pipetting in BRB80 buffer (80 mM PIPES pH 6,8, 2 mM MgCl2, 1 mM EGTA, KOH) in a final volume of 25 µl. The mixture was incubated for 25 min at 37°C at 300 rpm (Eppendorf Thermo-Mixer® C). Next, 200 µl of BRB80 buffer, containing 20 µM taxol, was added, gently mixed and the solution was further incubated for 90 min at 37°C at 300 rpm. MTs were pelleted by centrifuging at 14'000 rpm for 5 min at RT (Eppendorf 5424 tabletop centrifuge). Supernatant was discarded and the MT pellet was gently resuspended in 50 µl of pre-warmed to 37°C BRB80/taxol. If stored at 37°C, the taxol-stabilized MTs were stable and functional up to two days. During all the steps MTs were handled protected from direct light.

2.4.2. Preparation of the flow chambers

Microscopy slides (Menzel Gläser) were cleaned by intense rubbing by KIMTECH™ wipes (Kimberly-Clark), soaked in ACS-clean ethanol. In order to remove remaining fibers, dry slides were cleaned with clean KIMTECH™ wipes. Two pieces (~12x5 mm) of double-sided tape (TESA®) were cut and attached in parallel to each glass slide, forming the base for coverslip attachment and limit the borders of the future chamber. The area between the two pieces of tape was coated with 4 µl PLL-PEG (SuSoS) dissolved in PBS (137 mM NaCl, 2,7 mM KCl, Na_2HPO_4, KH_2PO_4), the slides were left to dry for 15 min at RT. Unbound PLL-PEG was extensively washed off with MilliQ H2O and the slides were incubated at 37°C until dry (~1 h). Biotinylated coverslips (MicroSurfaces Inc.), stored at -80°C, were kept in a vacuum-sealed packaging at RT for at least 1 h before usage. Each coverslip was cut to 6-8 pieces with a diamond-tipped glasscutter. Each coverslip fragment was attached to the sticky tape pieces of the dried microscopy slides, creating a flow chamber. The coverslip sides, attached to the tape, were sealed with transparent nail polish and left to dry. The flow chambers were kept at 4°C in a vacuum bag in the presence of silica beads and were used within one week.

2.4.3. Motility assays

A general protocol

One microscopy slide was used for each experiment. The slide was placed onto an ice-cold metal block, 100 µl of Blocking solution (5% m/v pluronic, 0,1 mg/ml of κ-casein (SIGMA) in 1x AB) was flowed into the chamber, the slide was left for 5 min incubation. Next, the chamber was flushed with 50 µl of 1x AB, supplied with 2,5 ug of Neutravidin (dissolved in BRB80 with 20% glycerol), immediately followed by a washing step with 100 ul of 1x AB. The slide was moved to a RT metal block and incubated for 2 min. Taxol-stabilised MTs were diluted 1:10-1:15 in 50 µl of 1x AB, supplemented with 8 um taxol, gently mixed and flowed into the chamber. The slide was incubated for 3 min at RT. 50 µl of the Assay mix containing the protein(s) of interest were flushed into the chamber, which was then sealed on both sides with transparent nail polish and shortly air-dried before the imaging.

The Assay Buffer
Assay buffer, AB (90 mM HEPES, 10 mM PIPES, 1,5 mM EGTA, 1,5 mM $MgCl_2$, KOH, pH 6,9), was prepared with Molecular Biology grade water (SIGMA) in a 2x concentration at RT, filtered with 0,22 um filters (Millipore Express® PLUS PES) and stored at 4°C for up to 3 weeks.

The assay mix
The Assay mix was prepared for each experiment fresh, while the chamber was incubated for 5 min with the Blocking solution. First, the elementary components were mixed (1x AB, 100 um glucose, 0,12% methyl cellulose and H_2O), followed by macromolecules (0,64 uM glucose oxidase (Serva), 0,55 uM catalase (SIGMA), 50 uM β-casein (SIGMA) and 1 U of SUPERase-In RNAse inhibitor mix (Invitrogen) for experiments with RNA). The Assay mix was incubated on ice before being moved to RT during 3 min of incubation of the chambers with MTs. During this time, 2,5 mM ATP was added, followed by protein pre-mix solution. The oxygen scavengers and caseins were prepared the same day in cold BRB80 solution, dissolved and centrifuged for 80'000 RPM for 10 min at 4°C. The supernatants were used for microscopy.

Protein and RNA dilutions
Protein aliquots, were removed from the liquid nitrogen immediately before the experiment, placed on ice-cold metal block, protected from light. Each aliquot was used for 1-2 experiments. Proteins and the RNA were pre-diluted in 10 ul of a pre-mix solution, supplied with 1x AB, 2,5 mM ATP and 0,1 U of RNase inhibitor. The pre-mix was incubated on ice for 15 min

before being added to the Assay mix. In cases when some of the components needed additional dilution steps, the dilution scheme was prioritising incubation of all the components at the highest possible concentration in order to favour intermolecular interactions.

Imaging
Microscopy data were acquired with a custom-built total internal reflection fluorescence (TIRF) microscope, using a 100x 1,49 N.A. objective lens (Olympus). For double and triple colour imaging, up to three channels were recorded in an alternating manner, at 150 or 250 ms exposure per channel. Laser used: 488 nm, 561 nm and 639 nm. ATTO 390-microtubules were recorded with a single snapshot after time-lapse movies at 800 ms exposure. Acquisition settings were kept constant for all the experiments to allow comparisons between different conditions. For channel alignments, 100 μm Tetra Speck™ fluorescent microspheres (ThermoFisher) were photographed in all three channels before each experimental session.

2.5. Data analysis

Time-lapse movies and images were acquired, using the FEI Life Acquisition program and analysed with the Fiji software[176]. The channels were aligned using images with TetraSpeck™ fluorescent microspheres (ThermoFisher) as a reference. Kymographs were generated from individual MTs over the time-stack of the images, using the Multi Kymograph plugin (https://www.embl.de/eamnet/html/kymograph.html). Kymographs were used for qualitative assessment of particles motility (static/diffusive or processive).

Data on the speeds of the motor particles as well as on particles' intensities and the numbers of tracks were obtained from analysis with the Trackmate plugin[177]. LoG detector was used to mark he particles with diameter of 1,3 um, while the chosen threshold depended on the fluorophores used, and varied between 4 and 10, but remained constant for comparison of the same molecules over experimental replicates. Next, the Quality and Signal/Noise ratio filters were used to select only processively moving particles. For trajectory analysis, I used Simple LAP tracker with the Linking max distance of 1 um, Gap-closing max distance of 1 to 2 um depending on fluorophore quality, Gap-closing max frame gap of 5. Track displacement filter was used to remove diffusive and leave only processive run events for analysis. A minimum of 3 separate experiments were performed for each condition. Data were processed and statistical analysis was performed with the Microsoft Excel software. Data distributions were plotted showing the standard error of the mean (SEM).

2.6. Materials

Table 2. Commercial proteins and enzymes

Product	Manufacturer	Catalogue number
b-Casein from bovine milk	Sigma	C6905-250MG
Bovine serum albumine (BSA)	Sigma	A4503-100G
Catalase from bovine liver	Sigma	C40-100MG
DNase I	Roche	10104159001
Glucose oxidase from *Aspergillus niger*	Sigma	G7141-10KU
k-Caseine	Sigma	C0406-100MG
Neutravidin	Invitrogen	A-2666

Table 3. Commercial kits and Consumables

Product	Manufacturer	Catalogue number
1000 ul FILTERED TIP	LABCLINICS	LAB1000ULF
20 ul FILTERED TIP	LABCLINICS	LAB20ULF
200 ul FILTERED TIP	LABCLINICS	LAB200ULF
4-15% Mini-PROTEAN TGX Precast Gels, 10-well, 30 µl	Bio-Rad	456-1083
96 well plates	Greiner Bio-One	655101
Amicon Ultra-4 centrifugal filter unit MWCO 100 kDa	Merck Millipore	UFC810024
Biotinylated coverslip	Microsurfaces Inc	Bio_01(2007134-01)
Corning® syringe filters 0,45	Sigma	CLS431220-50EA
Double-sided tape	Amazon	B0007OEBDQ
Eppendorff tubes	Eppenforf	FUTUB82-1X1000U
Falcon tubes 50 ml	BDFalcon	FUTUB71-1X500U
Falcon tubs 15 ml	BDFalcon	FUTUB401-1x500U
HiTrapTM Chelating HP affinity columns 5x5 ml	GE Healthcare	17-0409-03
Kimtech paper wipes 11x21	VWR	KIMB7552
Microscope Cover Slips 25x60 mm glass, Thickness Nr.1,	Menzel-Glaser	BB025060A1
MinElute PCR Purification Kit	Qiagen	28004
Mini-PROTEAN TGX Gels (4-15%) 10-well comb 10 precast gels	Bio-Rad	456-1083
Mini-PROTEAN TGX Gels (4-15%) 12-well comb 10 precast gels	Bio-Rad	456-1085
Mini-PROTEAN TGX Gels (4-15%) 15-well comb 10 precast gels	Bio-Rad	456-1086

Mini-PROTEAN TGX Gels (4-15%) 12-well comb 10 precast gels	Bio-Rad	456-1085
Mini-PROTEAN TGX Gels (4-15%) 15-well comb 10 precast gels	Bio-Rad	456-1086
PD-10 desalting columns	GE Healthcare	17-0851-01
QIAprep Spin Miniprep Kit	QIAGEN	27106
QIAquick Gel Extraction Kit	QIAGEN	28704
QIAquick PCR Purification Kit	QIAGEN	28106
RNA Clean-Up and Concentration Micro-Elute Kit	Norgen Biotech	61000
RNeasy MinElute Cleanup Kit	QIAGEN	74204
Steritop-GP filterig units 0,22 µm PES 1000ml	Millipore	S2GPT10RE
Steritop-GP filterig units 0,22 µm PES 500ml	Millipore	S2GPT05RE
TetraSpeckTM fluorescent microspheres	ThermoFisher	T-7284
Transcript Aid T7 High Yield Transcription Kit	ThermoFisher	K0441
ZebaTM Spin Desalting Column 7K MWCO 5 ml	ThermoFisher	89893

Table 4. Chemicals

Product	Manufacturer	Catalogue number
1,4-Piperazinediethanesulfonic acid (PIPES)	Sigma	P6757-1KG
2-Mercaptoethanol	Sigma	M6250-10ML
4-(2-hydroxyethyl)-1-piperazineethanesulfonic acid (HEPES)	Sigma	H3375
Adenosine triphosphate (ATP)	Sigma	2383-10G
ATTO 390 NHS-ester	Sigma	89204-1MG-F
BlueSafe	Nzytech	MB15201
Bradford reagent	Sigma	B6916-500ML
Brij-35 10%	ThermoFisher	28316
Cobalt chloride (CoCl2)	Sigma	255599-100G
cOmpleteTM EDTA-free protease inhibitor tablet	Sigma	5056489001
cOmpleteTM ULTRA EDTA-free protease inhibitor tablet	Sigma	5892953001
Cyanine 5-UTP, 100 nmol	Perkin Elmer	NEL583001EA
D-glucose	Sigma	G7021-1KG
Dimethyl sulfoxide (DMSO)	ThermoFisher	D12345
Disodium hydrogen phosphate (Na2HPO4)	Sigma	S9390-500G
Dithiothreitol (DTT)	Sigma	D0632-10G
Ethanol	Merck	64-17-5
Ethylene glycol-bis(β-aminoethyl ether)-N,N,N′,N′-tetraacetic acid (EGTA)	Sigma	E3889-100G

Ethylenediaminetetraacetic acid (EDTA)	Sigma	EDS-500G
Glycerol	Sigma	G5516-500ML
Guanosine triphosphate (GTP)	Sigma	G8877-1G
Imidazole	Sigma	I2399-500G
Isopropyl b-D-1-thiogalactopyranoside (IPTG)	ThermoFisher	R0392
Kanamycin (KAN)	Sigma	K4000-5G
L-Arabinose	Sigma	A3256-500G
L-arginine (ARG)	Sigma	A5006-100G
Magnesium chloride (MgCl2)	Sigma	M8266-100G
Methylcellulose	Sigma	M0512-100G
Monosodium phosphate (Na2HPO4)	Sigma	S3139-1KG
Nickel(II) sulfate hexahydrate	Sigma	467901-50G-D
Nuclease-Free Water	ThermoFisher (Ambion)	AM9937
Paclitaxel (taxol)	Sigma	T7191
PLL(20)-g[3.5]- PEG(2)	SuSoS	PLL(20)-g[3.5]- PEG(2)
Pluronic	Sigma	P2443-250G
Polyethylene glycol 3350	Sigma	1546547-1G
Potassium chloride (KCl)	Sigma	P9541-1kg
SNAP-Cell TMR-Star	NEB	NEB S9105S
SNAP-Surface Alexa Fluor 647	NEB	S9136S
SNAP-Surface® Alexa Fluor 488	NEB	S9129S
Sodium chloride (NaCl)	Sigma	S3014-5KG
Sodium hydroxide (NaOH)	Sigma	S8045-500G
Sucrose	Sigma	84097-1KG
SYBR® Gold Nucleic Acid Gel Stain (10,000X Concentrate in DMSO)	ThermoFisher	S11494
Triton X-100	Sigma	T8787-250
Ultrapure agarose	Invitrogen	15510-027

Chapter 3

3. RECONSTITUTION OF FMRP-MEDIATED mRNA TRANSPORT

3.1. Optimisation of purification protocol for FMRP

FMRP is a protein that is hard to purify due to its intense aggregation and precipitation (Fig. R.1, A). Its N-terminus is prone to protofibril formation[178], while the C-terminus is unstructured and can phase-separate[179]. Before I have joined the lab, Sebastian Baumann managed to purify FMRP using a buffer with 500 mM arginine (Fig. R.1, B). Arginine is used to sustain poorly soluble proteins in solution and inhibit protein aggregation[180].

Using this protocol, I have purified GFP-FMRP, but I could not see any transport with labelled and unlabelled versions of the KIF3A/A motor. Since arginine is thought to function by covering hydrophobic protein surfaces and could therefore potentially unfold protein domains that rely on hydrophobic interactions[180], arginine could be the reason why I could not detect FMRP transport in my early *in vitro* assays. Due to this concern, I have worked on optimisation of the purification buffer, aiming to decrease maximally arginine content.

Searching in the literature, I have found articles that used 250 mM arginine[179] or urea[181] in the purification buffer, which were the compounds we would like to avoid for correct protein conformation concerns. The other studies had very similar conditions to the ones that failed to work in my hands[182,183]. The most of these buffers contained 10-40 mM imidazole; from my experience, upon removal of imidazole, FMRP was readily precipitating. Therefore, I made an effort to optimise our FMRP purification protocol.

Using the buffer with arginine, reduced down to 50 mM, with addition of 50 mM glutamate, led to FMRP precipitation inside the streptavidin column. Addition of various detergents (Tween-20, Triton™ X-100, CHAPS), chaotropes (urea) and protein stabilisers[184,185] (glycerol[186], sucrose, glycine) did not help to reverse FMRP precipitation (data not shown). In contrast, purification of FMRP at the room temperature (RT), as it was suggested in the literature on phase-separating proteins[187], led to very promising results. Reduced precipitation rate let me obtain FMRP in suitable for molecular assays concentrations (Fig. R.1, C). Next, I could switch to insect-produced FMRP that can possess post-translational

modifications, valuable for its functions. RT purification protocol allowed for FMRP purification, yet its yield was still very low due to precipitation.

Next, I have performed a systematic study to improve FMRP solubility, aiming to prevent its precipitation. In order to set up a protocol for quantitative comparison of FMRP solubility in tested buffers, I expressed FMRP in bacteria, because of low cost, quick and unlimited production. The protocol was based on repetitive ultracentrifugation steps and concentration of each supernatant fraction (SN) (Fig. R.1, D), with a probe collected for each step and fraction. The probes were then loaded into an SDS-PAGE gel, stained with the BlueSafe® dye, and band intensities were measured with ImageJ software. To make the probes compatible, always the same volume fractions (1/500) were loaded into the gel on every step, while the pellets were resuspended in the same volume as the initial volume of the solution.

In the first test, I aimed at comparing buffers (HEPES vs Tris vs Phosphate) as well as three classes of molecules, reported to improve solubility of aggregating proteins: salts (KCl), polyols (glucose) and non-ionic detergents (Brij-35). Addition of 200 mM glucose, 0,01% Brij-35 and usage of Tris buffer turned out to be the most efficient additives (Fig. R.1, E). At the same time, I have encountered an intriguing study demonstrating that at millimolar concentrations, ATP/Mg^{2+} can serve as a chaotrope, helping to maintain poorly soluble proteins in solution[188]. Next, I have repeated my previous test with more complex combinations of additives (Fig. R.1, F). Although buffer 6 (HEPES-based with 0,01% Brij-35) appeared to be more efficient (quantifying SN2 relatively to the sum of SN1 and P1) than buffer 9 (Tris-based with 250 mM glucose, 10 mM $MgCl_2$ and ATP, 0,01% Brij-35), buffer 9 remained clear through all the assay steps with no signs of precipitation whatsoever. During the next FMRP purification, it appeared that Prescission (3C) protease did not tolerate high glycerol (10%) and/or Brij-35 (0,01%) content. Doing research on this issue, I found supporting evidence in the literature[189,190].

Buffer 9 has undergone further optimisations, therefore here I would like to present you the last version of the buffer (Fig. R.1, G) that I used for FXR2 purification (Fig. R.1, H) and Silvia Speroni used to purify the dRGG mutant of FMRP for my project. For the experiments described below, I have used FMRP from different purifications, since this work was done in parallel throughout the last three years of my PhD studies.

A

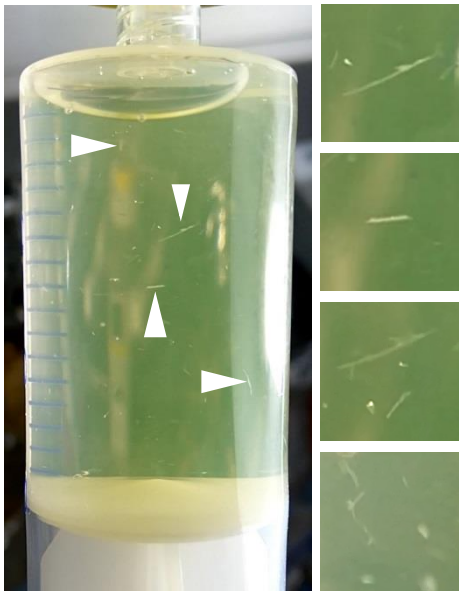

C

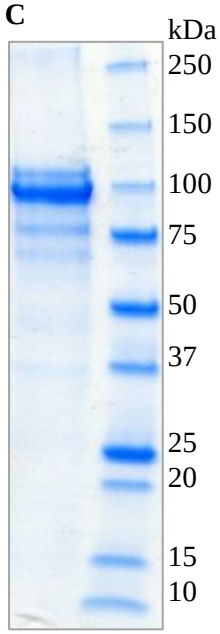

B

LEG buffer		**pH 7,6**
Component	Final concentration	Units
HEPES	50	mM
KCl	400	mM
$MgCl_2$	2	mM
Glycerole	5	%
L-Arginine	500	mM
β-ME	0,75	mM

Fig. R.1 Optimisation of FMRP purification protocol

A. FMRP precipitates after the lysis of the cells. Some of the fibril-shaped precipitate fragments are magnified on the right. **B.** The composition of the FMRP lysis buffer, developed by Sebastian Baumann. **C.** Room temperature purification of FMRP for the first time gives promising results. **D.** A general scheme of the protocol used to quantitatively compare the effect of tested buffer compositions on FMRP recovery rate. **E.** and **F.** Results of the first and second rounds of buffer optimisation, correspondently. Compared components are indicated above: Ph, Tr and Hs – phosphate, Tris and HEPES buffers, Glc – glucose, KCl – potassium chloride, Bj – Brij-35, A/M – ATP/$MgCl_2$. P and SN refer to the Pellet and Supernatant fractions; the number indicates the centrifugation round. **G.** The last version of FMRP lysis buffer. **H.** FXR2 purification: 3C-cleaved TMR-FXR2 (left lane), 3C+TEV-cleaved FXR2 (right lane). Arrows indicate protein bands.

D

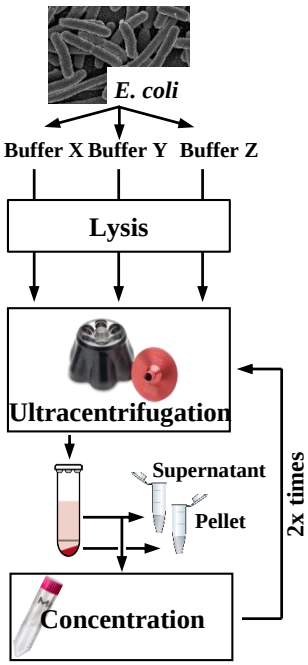

E

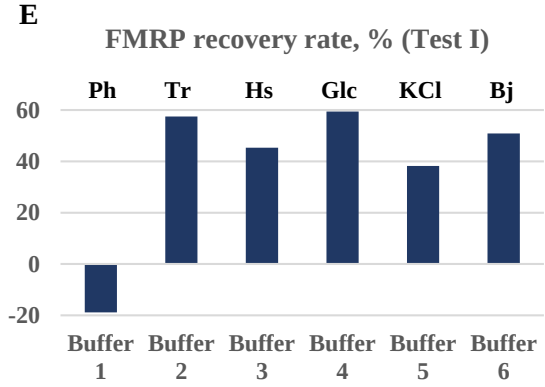

F

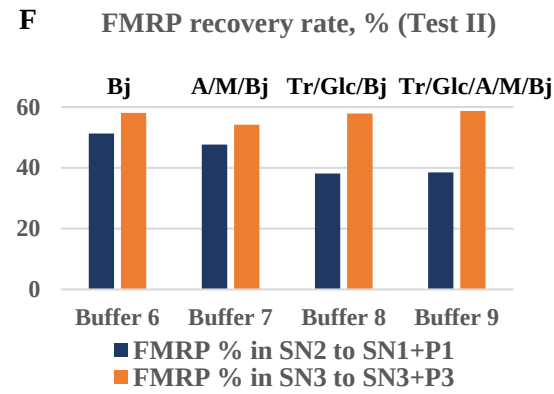

G

LEG buffer		**pH 8,0**
Component	Final concentration	Units
HEPES	50	mM
KCl	500	mM
L-Arginine	50	mM
L-Glutamate	50	mM
Glucose	250	mM
ATP	10	mM
$MgCl_2$	5	mM
Brij-35	0,001	%
DTT	1	mM

H

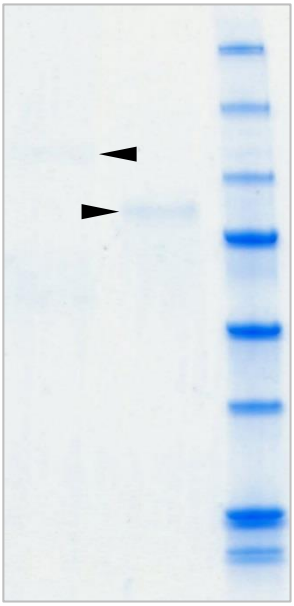

3.2. FMRP is transported by Kinesin-2 motors

I have started validating FMRP-motor interactions with KIF3A/C motor, since these data was based on the yeast-2-hybrid (Y2H) screen[150]. GFP-KIF3A/C alone has demonstrated perfect motility (Fig. R.2, A), with median run speed of 490±180 nm/s (Fig. R.2, C), which is faster compared to previous studies (169 nm/s)[65]. The particle brightness distribution showed a clear prevalence of particles with median intensity of 770±85,9 a.u. (Fig. R.2., D). Importantly, the smallest intensity value detected equalled to 615 a.u., probably corresponding to a single GFP molecule fused to the GFP-KIF3A/C heterodimer. If so, the smallest aggregate of two motor dimers would correspond to an intensity of ~1230 a.u. Since the vast majority of particles (96,6%) falls into the 615-999 a.u. brightness bin, we can assume that almost all of the motor particles are single heterodimers.

TMR-FMRP alone had bidirectional diffusive behaviour along the microtubules (Fig. R.2, B), which coincides with the earlier observations on tau protein in the 2-10 nM range[191], PABP-mRNA complex[192] and even on positively charged nanoparticles[193]. These unidimensional movements are mediated by charge, since removal of a negatively charged C-terminal peptide of tubulin by subtilisin was shown to decrease diffusion of tau by up to 70%. Moreover, diffusion along MT lattice was shown to be ionic strength- and pH-dependent[191]. Since our PostDoc, Sebastian Baumann, observed similar behaviour of another RBP, APC, on the microtubule lattice[43], we considered such behaviour as a proxy for appropriate assay conditions.

Upon addition of GFP-KIF3A/C, TMR-FMRP was processively transported by kinesin along the MTs, while free unbound TMR-FMRP molecules conserved their diffusive behaviour (Fig. R.2, F). Next, I aimed to test, which of the FMRP domains were responsible for FMRP's interaction with the motor.

To devise FMRP domains relevant for interaction with the motor, I performed a classical domain exclusion analysis. As mentioned in the introduction, the N-terminal third of FMRP sequence is responsible for multiple protein-protein interactions. The middle third (M-part) houses two KH domains, potentially responsible for less specific mRNA recognition and binding. The C-terminal part accommodates the well-studied RGG box, surrounded by putative unstructured regions. This part could therefore potentially harbour Kinesin-2 interaction moieties. I have generated three FMRP clones missing either of three domains. To my surprise, TIRF microscopy demonstrated a massive loss of transportability for all the three FMRP mutants (Fig. R.2, E), suggesting that the whole FMRP protein

sequence is participating in formation and maintenance of correct 3D-fold, relevant for FMRP functioning. While planning and engineering FMRP constructs with more subtle point mutations, I have purified another Kinesin-2 motor, known to exist in living cells, AF488-KIF3A/B.

Intriguingly, AF488-KIF3A/B was also able to transport FMRP along the microtubules (Fig. R.2, G). Since both GFP-KIF3A/C and AF488-KIF3A/B motors had only KIF3A in common, I have expressed and purified GFP-KIF3A/A homodimer too, although it had not been reported to exist in animal tissues. GFP-KIF3A/A homodimer turned out to be enough to transport FMRP along the microtubules (Fig. R.2, H).

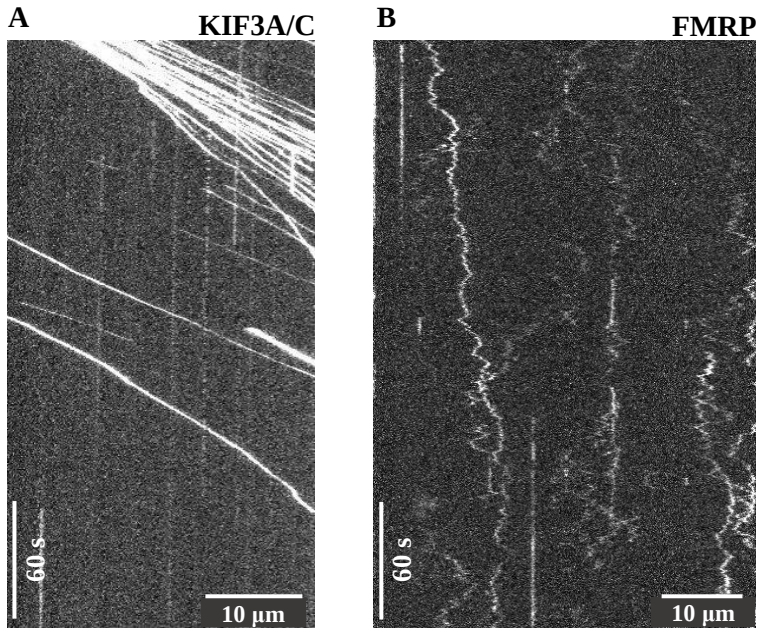

Fig. R.2. FMRP is transported by Kinesin-2 motors.

A. A kymograph of GFP-KIF3A/C motor (100 pM), moving processively along the microtubule lattice. A kymograph is a 2D-plot of brightness along the line of interest, in this case a microtubule (X-axis, distance) changing over time (Y-axis, time). **B.** TMR-FMRP (100 pM) is freely diffusing along the microtubules. **C.** Distribution of median speeds of GFP-KIF3A/C tracks. **D.** Distribution of GFP-KIF3A/C particles' brightness. The data for C and D was collected from 4 movies generated in 3 independent experiments. **E.** Comparative analysis of transport efficiencies of three TMR-FMRP mutants, compared to WT protein. NC mutant is lacking middle part, MC is missing N-terminus, while NM is lacking its C-terminus. N, number of movies. **F.** Overlaid kymographs of GFP-KIF3A/C (100 pM, green) transporting TMR-FMRP (50 pM, red). In contrast to B, in the presence of GFP-KIF3A/C, TMR-FMRP displayed processive runs. **G** and **H**, TMR-FMRP (1,3 nM or 150 pM, red) is transported by AF488-KIF3A/B (100 pM) and GFP-KIF3A/A (400 pM) motors respectively (green).

C

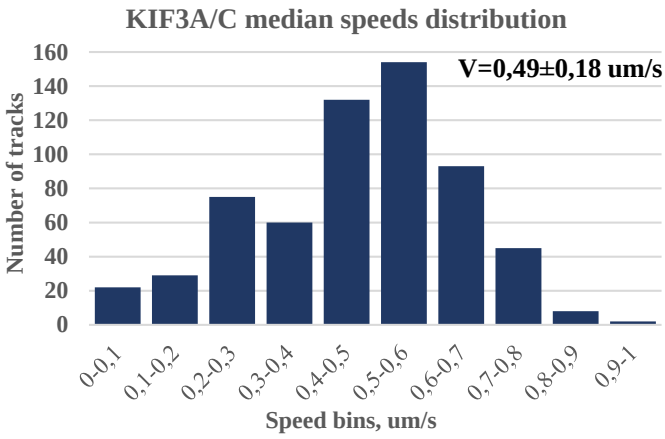
KIF3A/C median speeds distribution
V=0,49±0,18 um/s
Number of tracks
160
140
120
100
80
60
40
20
0
0-0,1
0,1-0,2
0,2-0,3
0,3-0,4
0,4-0,5
0,5-0,6
0,6-0,7
0,7-0,8
0,8-0,9
0,9-1
Speed bins, um/s

D

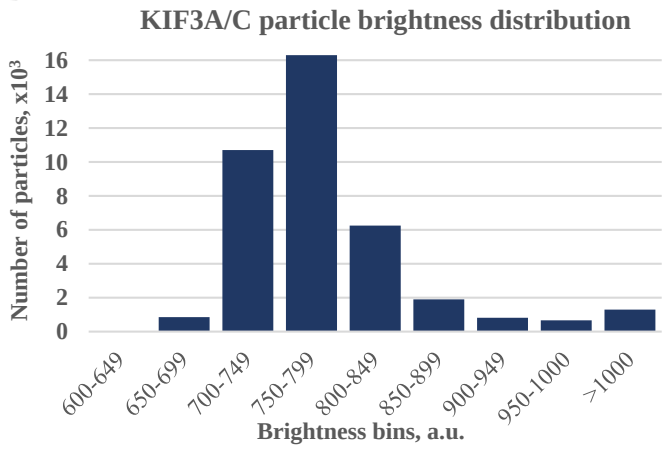
KIF3A/C particle brightness distribution
Number of particles, x10³
16
14
12
10
8
6
4
2
0
600-649
650-699
700-749
750-799
800-849
850-899
900-949
950-1000
>1000
Brightness bins, a.u.

E

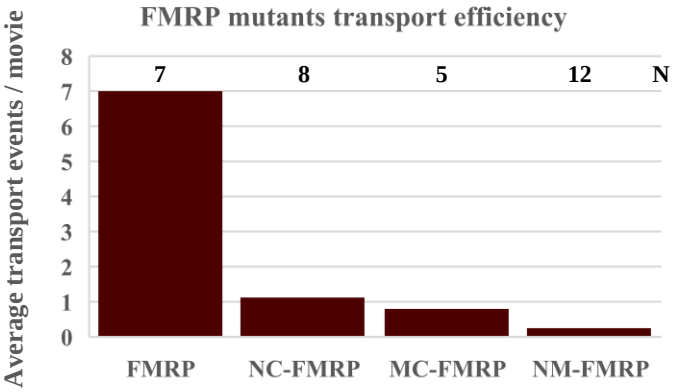
FMRP mutants transport efficiency
Average transport events / movie
8
7
6
5
4
3
2
1
0
7
8
5
12
N
FMRP
NC-FMRP
MC-FMRP
NM-FMRP

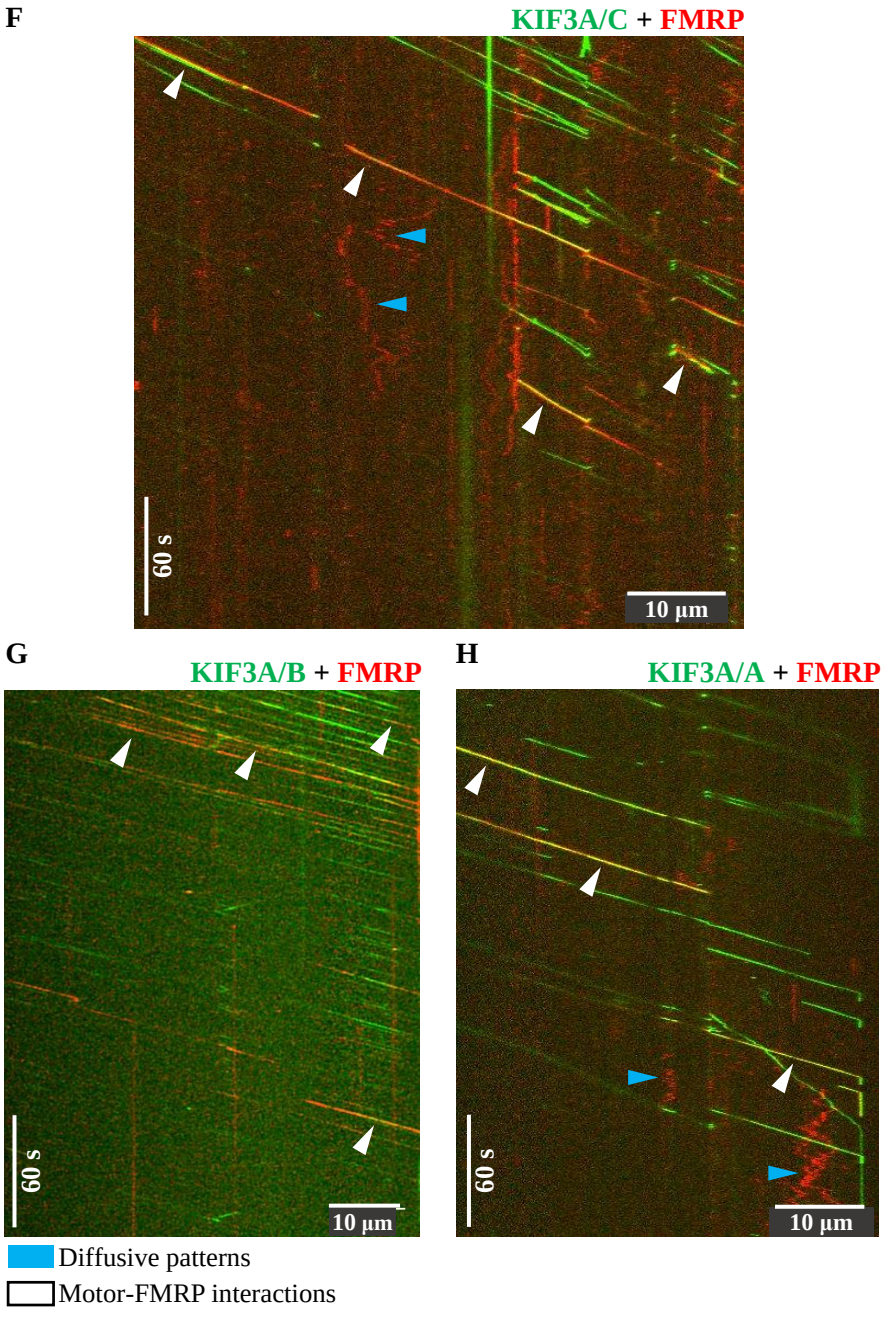
F
KIF3A/C + FMRP
60 s
10 µm
G
KIF3A/B + FMRP
60 s
10 µm
H
KIF3A/A + FMRP
60 s
10 µm
Diffusive patterns
Motor-FMRP interactions

3.3. FMRP-KIF3A/B complex transports short G-quadruplex mRNA

The next logical step was to test whether FMRP-motor complexes can transport target mRNA molecules. To test this, I have *in vitro* transcribed and co-transcriptionally labelled with Cy5 fluorescent dye, a 3'-UTR fragment of the *camkIIα* mRNA, a well studied FMRP target. Unexpectedly, both GFP-KIF3A/A and GFP-KIF3A/C motors were able to transport this mRNA in the absence of FMRP (data not shown). AF488-KIF3A/B motor did not transport *camkIIα* 3'-UTR on its own, yet I could not see mRNA transport in the presence of FMRP either. In order to test whether FMRP can bind mRNA on its own, I studied behaviour of these molecules after their pre-incubation in a common mix, using the TIRF microscope.

FMRP showed no co-diffusion with *camkIIα* 3'-UTR (Fig. R.3, A). To exclude a possibility that this mRNA was just too bulky (3,4 kB) to bind efficiently to FMRP, I have cloned and *in vitro* transcribed a 90-nt long fragment of *camkIIα* 3'-UTR, containing its second G-quadruplex sequence (G4x, see Table 1). This sequence corresponds to a fragment of homologues rat *camkIIα* that was shown to be bound by FMRP[175]. At the same time, I have purified FMRP, expressed in insect cells. This new FMRP protein, in combination with the short G4x mRNA fragment, showed much better co-diffusion (Fig. R.3, B), implying a direct interaction between FMRP and its target mRNA fragment. Next, I had to test formation of the whole complex. Unfortunately, AF488-KIF3A/B was binding the G4x fragment unspecifically and addition of various concentrations of Heparin, BSA or PEG did not help to resolve this problem in full (data not shown).

The problem was eliminated when we acquired a short, commercially produced G4x fragment from the rat *camkIIα* mRNA. This mRNA fragment was readily co-diffusing with FMRP and was not unspecifically transported by the motor. In result, TMR-FMRP was able to transport commercial G4x mRNA fragments in complex with AF488-KIF3A/B (Fig. R.3, C). Based on analysis of 11 movies from 3 experiments, 41% of motor particles were carrying FMRP, while only 3% of FMRP particles were transporting G4x mRNA (Fig. R.3, G). With the median brightness of 847 a.u. vs the smallest observed brightness value of 631 a.u., AF488-KIF3A/B motor was likely to be represented by single heterodimers (Fig. R.3, D). The median speed of AF488-KIF3A/B motor equalled 0,6 um/s (Fig. R.3, E), which fits with the previous studies *in vitro* (0,5 um/s[194], 0,59 um/s[60] and 0,57 um/s in our last study[43]) as well as of *β-actin* mRNA transport speed in neurons (0,6 um/s[195]). Since the median brightness of transported TMR-FMRP particles equalled 747 a.u., and the smallest observed brightness was 573 a.u. high

TMR-FMRP was transported chiefly in the form of monomers. It should be mentioned that this method of evaluation is not precise, since it is based on the minimal observed brightness that could be represented by protein oligomers in case of intense oligomerisation, or could be limited by sensitivity of the microscope's light detector matrix or the level of background noise.

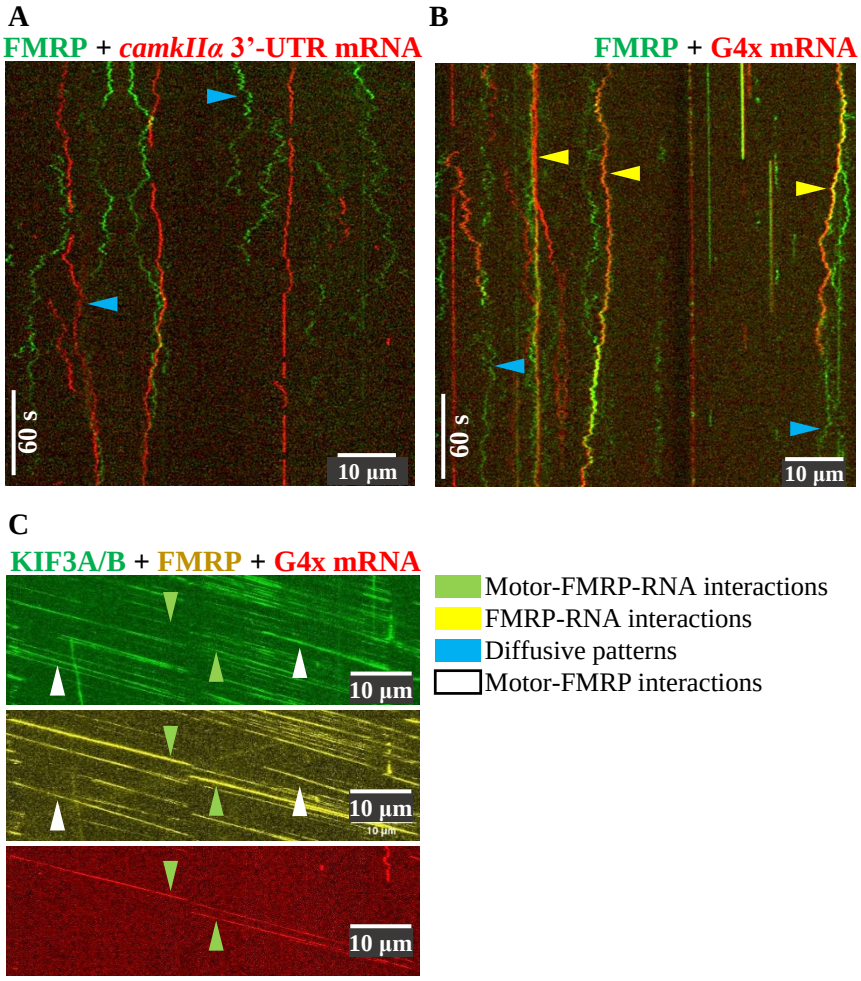

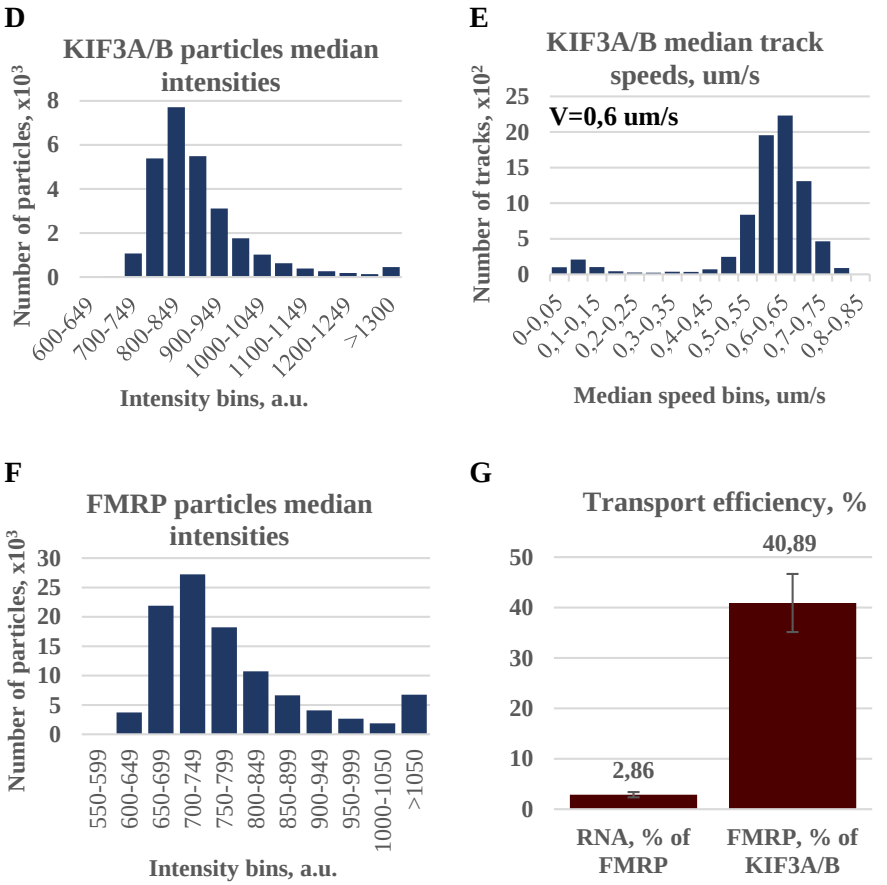

Fig. R.3. FMRP-KIF3A/B complex transports short G-quadruplex mRNA

A. GFP-FMRP and *camkIIα* 3'-UTR RNA fragment diffuse individually on the MT lattice. **B.** GFP-FMRP co-diffuses with a 90 bases-short G-quadruplex containing fragment of *camkIIα* 3'-UTR mRNA. **C.** Rat G4x from *camkIIα* mRNA (red) is transported by FMRP (yellow) in complex with KIF3A/B motor (green). **D.** An intensity distribution of KIF3A/B particles. **E.** Distribution of KIF3A/B median track speeds. **F.** Intensity distribution of transported FMRP particles. **G**. FMRP transport efficiencies; error bars represent SEM. Data for **D-G** was collected from 11 movies of 3 independent experiments.

3.4. HEPES matters

Throughout my studies, I had been facing a drastic variation between the experiments. In most of the cases, the problem was manifested on a basic level, alternating between motor proteins processively running on the microtubules and just sticking to them, sometimes with slight diffusion. After making tests for dozens of components that our *in vitro* assay consists of, I decided to account for possible differences between the two magnesium chloride and the two HEPES bottles that were simultaneously used by all the lab members, in an arbitrary order. To do so, I have labelled them as A and B, both for magnesium and HEPES, and made corresponding assay buffers. While there was no difference between magnesium bottles, in the buffer made from the "HEPES A", AF488-KIF3A/B remained attached to the MTs, rarely diffusing along the MT lattice. I was observing rare 1-3 motile particles per movie (Fig. R.4, A). Buffer made from the "HEPES B" bottle, however, led to excellent AF488-KIF3A/B motility (Fig. R.4, B). HEPES from a brand new bottle had a similar effect to the "HEPES A".

The problem would had been considered as solved if not another observation, coming from Sebastian Baumann, who was working with the same KIF3A/B motor, but co-expressed and co-purified with its adaptor protein, KAP3. In his hands, AF488-KIF3A/B/KAP3 motor was sticking to the microtubules with rare diffusion and processive run events, which was very similar to my observations on AF488-KIF3A/B in the buffers, made with "HEPES A" or new HEPES salts. In his project, Sebastian was working on reconstitution of the KIF3A/B/KAP3-APC-mRNA complex, a work that was published recently[43], but was still under development when I was trying to interpret these results. Incubation of my AF488-KIF3A/B motor with the KAP3 protein, purified by Sebastian Maurer, did not suffice to activate the motor (Fig. R.4, C). The same motor with KAP3 protein demonstrated excellent motility in the "HEPES B" buffer (Fig. R.4, D). To exclude the possibility that the KAP3 adaptor protein, which was expressed and purified separately, was not binding to my AF488-KIF3A/B motor, I asked Sebastian for a few aliquots of his AF488-KIF3A/B/KAP3 complex, co-expressed and purified together. Sebastian's motor in his own buffer looked similar to my AF488-KIF3A/B motor (Fig. R.4, E) and coincided with his own observations, while in the "HEPES B" assay buffer it appeared to be motile (Fig. R.4, F). Sebastian's AF488-KIF3A/B/KAP3 motor complex could even transport TMR-FMRP in the "HEPES B" buffer (data not shown). To solve this conflict of observations, the following considerations were taken into account:

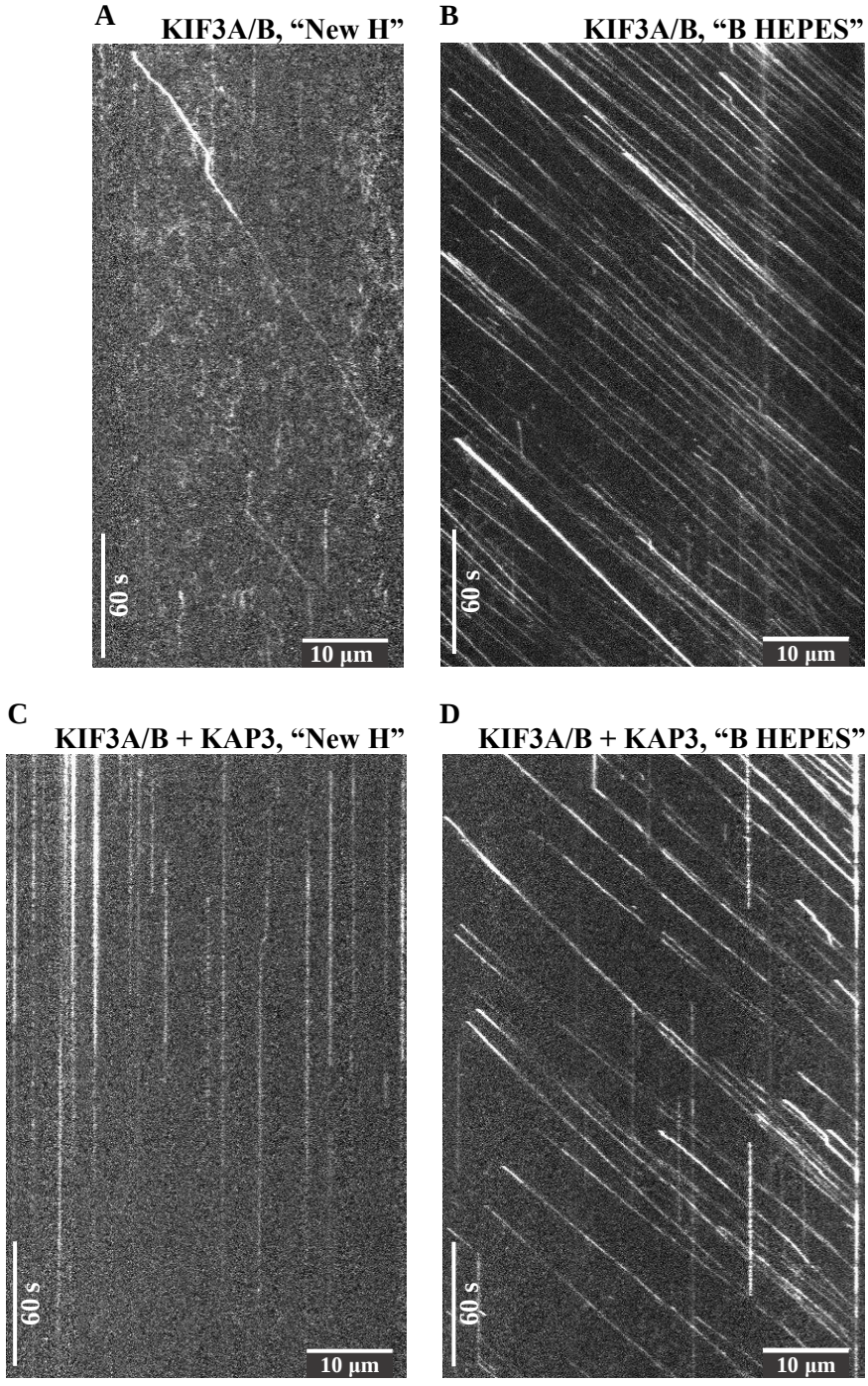
A
KIF3A/B, “New H”
60 s
10 µm
B
KIF3A/B, “B HEPES”
60 s
10 µm
C
KIF3A/B + KAP3, “New H”
60 s
10 µm
D
KIF3A/B + KAP3, “B HEPES”
60 s
10 µm

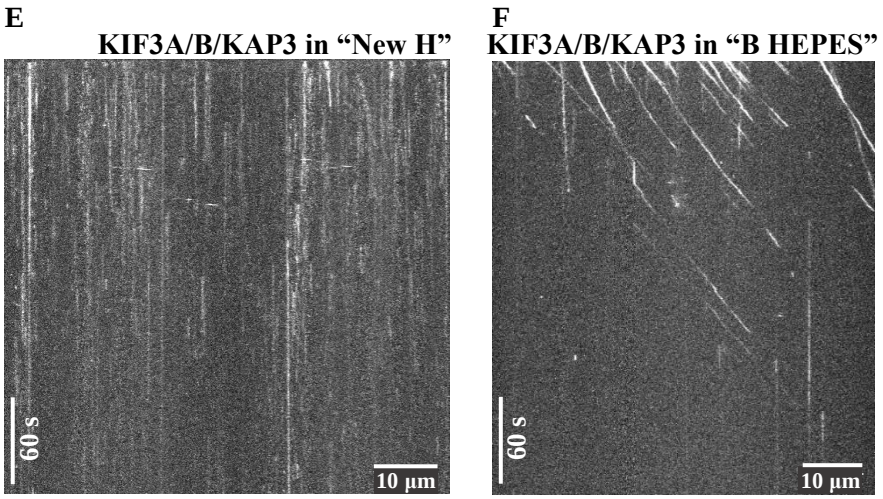

Fig. R.4. HEPES matters

A. AF488-KIF3A/B motor mostly diffuses in the buffer made from a new HEPES bottle. **B.** The same motor is very active in "HEPES B"-based buffer. **C.** Addition of KAP3 to the experiment from A seems to further stabilise the inhibited state of AF488-KIF3A/B. **D.** AF488-KIF3A/B with KAP3 demonstrated excellent motility in the "HEPES B" buffer. **E.** AF488-KIF3A/B/KAP3 motor, kindly provided by Sebastian Baumann, remained autoinhibited in his assay buffer. **F.** The same motor protein complex actively moves in the "HEPES B" buffer.

1. In the assay buffer, made from a brand-new, recently ordered HEPES bottle, AF488-KIF3A/B was behaving as in the buffer made from the "HEPES A" bottle or as in Sebastian's assay buffer. AF488-KIF3A/B remained active only in a buffer made from one single HEPES (B) bottle, thus predetermined to be irreproducible by any other laboratory, provided my results would be published;

2. Available literature states that Kinesin-2 motors can be auto-inhibited in the absence of cargo (please, refer to the Introduction section);

3. Potential publishing of these results would lead to contradictions with our leading study[40].

Therefore, I switched to the smallest HEPES bottles available from Sigma that were used individually and were purchased on a regular basis.

3.5. Outlook from Part I

Although very promising, the reconstituted Kinesin-2-based FMRP-mediated mRNA transport system was destined to be abandoned for objective and logical reasons. For my project, it left three possible ways of development:

a) Test, whether FMRP is able to activate Kinesin-2 motor on its own and/or in complex with its target mRNA molecule(s);

b) If the first option fails, test, whether FMRP can be co-transported with Kinesin-2 motor, activated in the KAP3/APC/mRNA complex, as observed by Sebastian Baumann shortly before;

c) Test another FMRP interactors that could link it to the motor (like FXR2) or search for completely new interactions that could be tested with my assay.

The results from this order of experimental priorities will be demonstrated in the next Chapter.

Chapter 4

4. NEW HEPES BRINGS NEW CHALLENGES

4.1. FMRP does not activate KIF3A/B motor

Based on the data that APC binds and pulls down KAP3 protein[45], Sebastian Baumann had previously found that APC protein in complex with its target *β-actin* and *β2b-tubulin* mRNA molecules, can reactivate an auto-inhibited heterotrimeric KIF3A/B/KAP3 motor[43]. Although there is no evidence of FMRP-KAP3 interaction, it still could be possible that FMRP, as a cargo, could reactivate an autoinhibited Kinesin-2 directly without the aid of the KAP3 adaptor.

First, I studied whether FMRP can activate the auto-inhibited KIF3A/B motor by analogy with APC, whose presence is enough to enhance the number of active motor molecules, although much less than in the presence of mRNA[43]. TMR-FMRP was not enough to activate AF488-KIF3A/B (Fig. R.5, A). In this series of experiments, I used fully cleaved (by 3C and TEV proteases) motor to exclude a possibility that the interaction is not happening due to some sterical limitations. Moreover, a reversed experiment with the labelled motor and fully cleaved FMRP was not different (data not shown). The next test I made was in the presence of mRNA. Addition of commercial Cy5-G4x mRNA to the fully cleaved KIF3A/B and FMRP was not enough to activate the motor (Fig. R.5, B). Since it was still possible that KIF3A/B requires its adaptor, KAP3, for the cargo activation mechanism to be functional, I have tested the motor in the presence of KAP3 (Fig. R.5, C) and the whole KIF3A/B/KAP3 complex in the presence of G4x mRNA (Fig. R.5, D). Although I could observe some rare events of FMRP/mRNA co-transport (~1 event per 2-3 movies, Fig. R.5., D right), the vast majority of FMRP and RNA particles displayed short stochastic diffusive movements (Fig. R.5, D left). The rare transport events observed in the assay could be explained by the motor blobs that were scarce, yet the only motile molecules in this assay. Unfortunately, KIF3A/B motor remained autoinhibited and I could not reconstitute FMRP-mediated mRNA transport system in this manner.

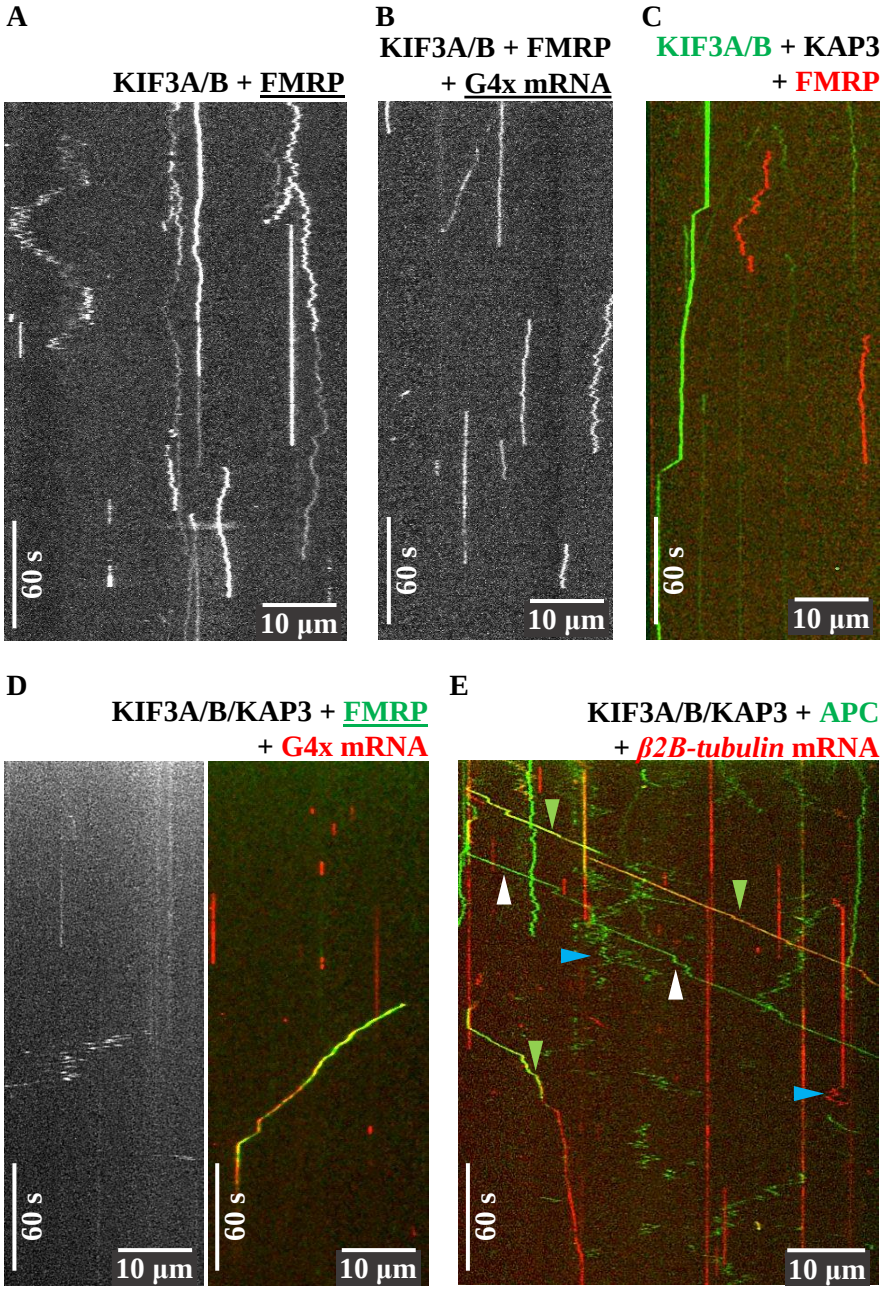
A
KIF3A/B + FMRP
60 s
10 µm
B
KIF3A/B + FMRP
+ G4x mRNA
60 s
10 µm
C
KIF3A/B + KAP3
+ FMRP
60 s
10 µm
D
KIF3A/B/KAP3 + FMRP
+ G4x mRNA
60 s
10 µm
60 s
10 µm
E
KIF3A/B/KAP3 + APC
+ β2B-tubulin mRNA
60 s
10 µm

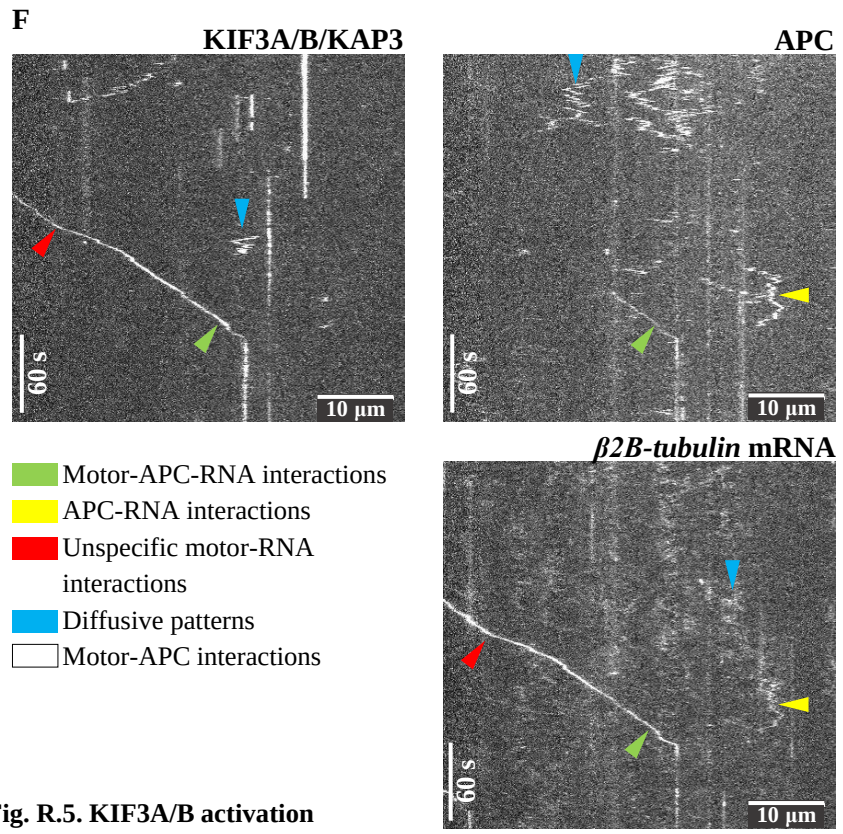

Fig. R.5. KIF3A/B activation

A. TMR-FMRP (230 pM) does not activate fully cleaved KIF3A/B (1,5 nM). **B.** Addition of commercial Cy5-G4x mRNA (4 nM) to fully cleaved FMRP (744 pM) and fully cleaved KIF3A/B motor (750 pM) did not activate the motor. **C.** TMR-FMRP (230 pM, red) does not activate AF488-KIF3A/B (0,5 nM, green), incubated with KAP3 (2 nM). **D.** Fully cleaved KIF3A/B/KAP3 (1,4 nM) did not release its autoinhibition in the presence of TMR-FMRP (230 pM, green) and commercial Cy5-G4x RNA (3,75 nM, red). Left: TMR-FMRP diffusion, a typical FMRP behaviour; right: rare FMRP/RNA transport events on the scarce, not autoinhibited motor particles. **E.** Commercial *Cy5-β2B-tubulin* mRNA (3,5 nM, red) in complex with TMR-APC (150 pM, green) activates fully cleaved KIF3A/B/KAP3 motor complex (1,4 nM), all components provided by Sebastian Baumann. **F.** APC/RNA-mediated activation of KIF3A/B/KAP3 with alternative components was much less efficient. Here you can see kymographs from three channels of the same movie. AF488-KIF3A/B/KAP3 (1,4 nM, left) remains mostly either immobile or shows diffusive patterns along the MTs. Particles that display processive runs are rare and tend to be agglomerates that unspecifically bind short Cy5-*β2B-tubulin* mRNA fragments (3,75 nM, right). The vast majority of mRNA molecules diffuse over short distances. TMR-APC (150 pM, middle) did not bind the motor, freely diffusing along the MTs. Motor-APC-RNA interactions are marked with green arrows, unspecific motor-RNA interactions with red, APC-RNA with yellow and plain diffusion patterns with blue.

4.2. Poor reconstitution of the KIF3A/B/KAP3/APC/*β2b-tubulin* complex

Since the AF488-KIF3A/B motor failed to be activated by TMR-FMRP and its corresponding mRNA, another strategy to test FMRP-KIF3A/B interaction was to activate the Kinesin-2 motor with APC-mRNA complex first, repeating Sebastian's findings[43], and then add FMRP.

Using components that Sebastian kindly provided me with, I could reach 28 APC and 48 *β2b-tubulin* mRNA transport events per movie (I had materials for one experiment only, Fig. R.5, E). In order to reproduce his experiment and in a case of success involve FMRP, I have purified the whole KIF3A/B/KAP3 motor complex and transcribed *in vitro* a 90 nt short target mRNA of the APC, *β2b-tubulin*. Due to the limited amount of available insect pellets, expressing APC, and their indispensability for ongoing Sebastian's project, I was offered APC, treated with protein kinase A for another project. Combining fully cleaved motor complex and Cy5-*β2b-tubulin* mRNA with TMR-APC, provided by Sebastian, I managed to obtain only ~5 APC and ~11 RNA transport events per movie (Fig. R.5, F). Firstly, it was much less than in Sebastian's experiments (~418 processive mRNA transport events per movie) and secondly, the assay showed unspecific motor-mRNA interaction. With such a low motor activation efficiency and a tight limitation on the resources, there was no reason to continue experiments with FMRP.

4.3. KIF3A/C efficiently transports FMRP

Since GFP-KIF3A/C remained active and not autoinhibited in the "new HEPES" buffer (Fig. R.6, A), we decided to return to this motor to study FMRP transport mechanisms. New experimental conditions required new motor characterisation. The median speed of the recorded motor tracks equalled 314±100 nm/s, which is near twice as high as indicated in some of the *in vitro* studies (168,8±5,6 nm/s[65] and 182,1±5,4 nm/s[196]). More intriguingly, it was 1,6 times slower than I observed initially in my first assays, made in the "HEPES B" buffer (Fig. R.2., C). The minimal brightness observed reached 755 a.u., the intensity distribution formed a single and clean bell-shaped distribution peak with the median motor particle brightness value of 1201 a.u., located in the middle of distribution. Assuming that 755 a.u. corresponded to a GFP-KIF3A/C dimer, we could expect the dimmest tetramers would start from intensity of ~1500 a.u., suggesting that the majority of observed particles were single heterodimers (Fig. R.6, E).

GFP-KIF3A/C was efficiently transporting TMR-FMRP molecules (Fig. R.6, B). TMR-FMRP had a single peak on the brightness distribution plot (Fig. R.6, F), however significantly shifted to the right, compared to Fig. R.3, F. The least value observed was 861 a.u. (vs 573 a.u. before), preserving the single peak of the brightness distribution between this and its doubled value, ~1700 a.u. This difference to the previous studies could be explained by three factors. First, the last experiments were performed on the TIRF microscope, kindly provided by Prof. Dr. Thomas Surrey, while ours was being repaired. Slightly different laser intensities or any minor differences in the optics could be the cause of the issue. Second, I had been using different FMRP preps that can differ in their solubility and agglomeration state. Third, due to the ongoing process of optimisation of FMRP purification protocol, I used different purification buffers that could influence the labelling efficiency of the SNAP tag. Although the most of the FMRP particles seem to be monomers, large motile TMR-FMRP aggregates with intensity values of up to ~7300 a.u. were rarely detected. Around 25% of the motile motor particles were transporting FMRP (Fig. R.6, G, left). Importantly, after decreasing the motor concentration 2,7 times, FMRP transporting efficiency dropped only by ~20% (Fig. R.6, G, centre), implying this interaction to be specific and not linearly concentration-dependent. Since the coarse truncation analysis of FMRP failed (Fig. R.2, E), I have generated mutants with two point mutations that were shown to destroy the KH1 and KH2 domains[135] (I241N and I304N correspondently) or the RGG box deletion, dRGG FMRP. Silvia Speroni kindly helped by purifying the latter mutant. Deletion of the RGG box did not influence ability of FMRP to be transported by the motor, as we

expected (Fig. R.6, G, right). The test of the KH1,2 mut FMRP will be performed after the submission of this Thesis.

KIF3A/C-FMRP complex was also able to transport commercially produced short G4x fragments of the rat *camkIIα* mRNA (Fig. R.6, C). Unfortunately, a significant portion of the transported mRNA molecules was bound to GFP-KIF3A/C in the absence of TMR-FMRP. Indeed, RNA transport efficiency reached 45%, superseding FMRP's by almost two times (Fig. R.6, H, right). Importantly, FMRP and mRNA transport was not mutually exclusive, as I could observe co-transport events (Fig. R.6, C). Surprisingly, addition of RNA led to a significant ($p<0,02$) double decrease of FMRP transport efficiency (Fig. R.6, H, left). This result indicated that either there was a competition between FMRP and its target mRNA for the motor binding, or RNA binding by FMRP inhibited interaction between FMRP and the motor. Judging by the mRNA particles' intensity distribution (Fig. R.6, I), mRNA seemed to be monomeric (min intensity observed 551 a.u., median 642 a.u., with the peak ending around 750 a.u., a way earlier than the doubled minimal intensity threshold of ~1100 a.u.).

Next, I have tested the hypothesis of unspecific motor-RNA interaction. GFP-KIF3A/C was able to transport commercial G-quadruplex mRNA in the absence of FMRP (Fig. R.6, J) as well as the *in vitro* transcribed short *β2b-tubulin* mRNA that also has a G-quadruplex sequence (Fig. R.6, K). Since both of these mRNAs contain a G-rich motif, I have tested a short commercially produced *β2b-tubulin* mRNA with removed G-quadruplex (Fig. R.6, L). A very coarse set of experiments (1 experiment per mRNA molecule type) implied that the transport efficiency of the G-quadruplex-less mRNA was similar to commercial mRNA containing a G-quadruplex (Fig. R.6, M). This preliminary result indicates that KIF3A/C tends to transport mRNAs unspecifically, which could lead to an artificially generated competition between FMRP and mRNA for motor binding. To conclusively confirm or deny this possibility, more experimental work is needed, aiming to achieve conditions when this unspecific transport is minimised or eliminated, as well as to gain enough data for more systematic and objective analysis.

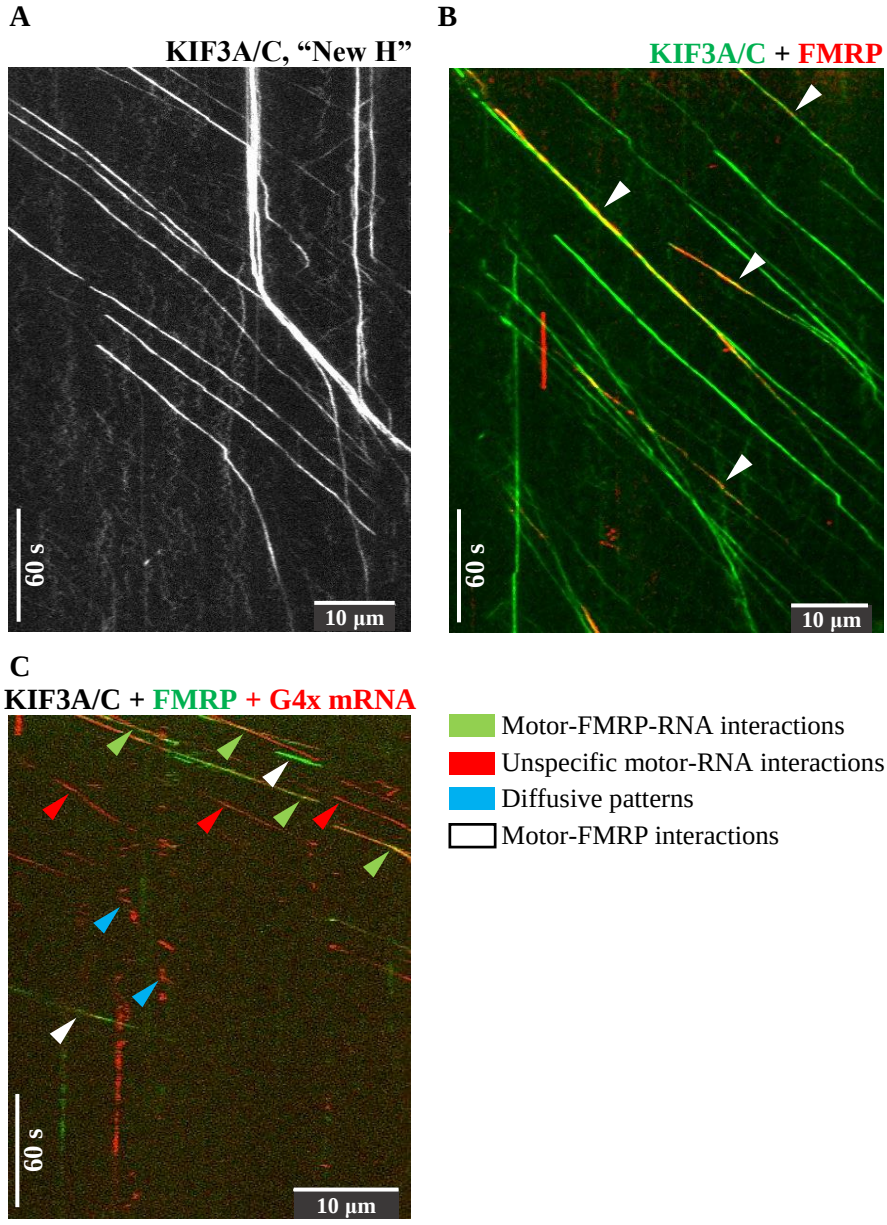
A
KIF3A/C, "New H"
60 s
10 µm
B
KIF3A/C + FMRP
60 s
10 µm
C
KIF3A/C + FMRP + G4x mRNA
60 s
10 µm
Motor-FMRP-RNA interactions
Unspecific motor-RNA interactions
Diffusive patterns
Motor-FMRP interactions

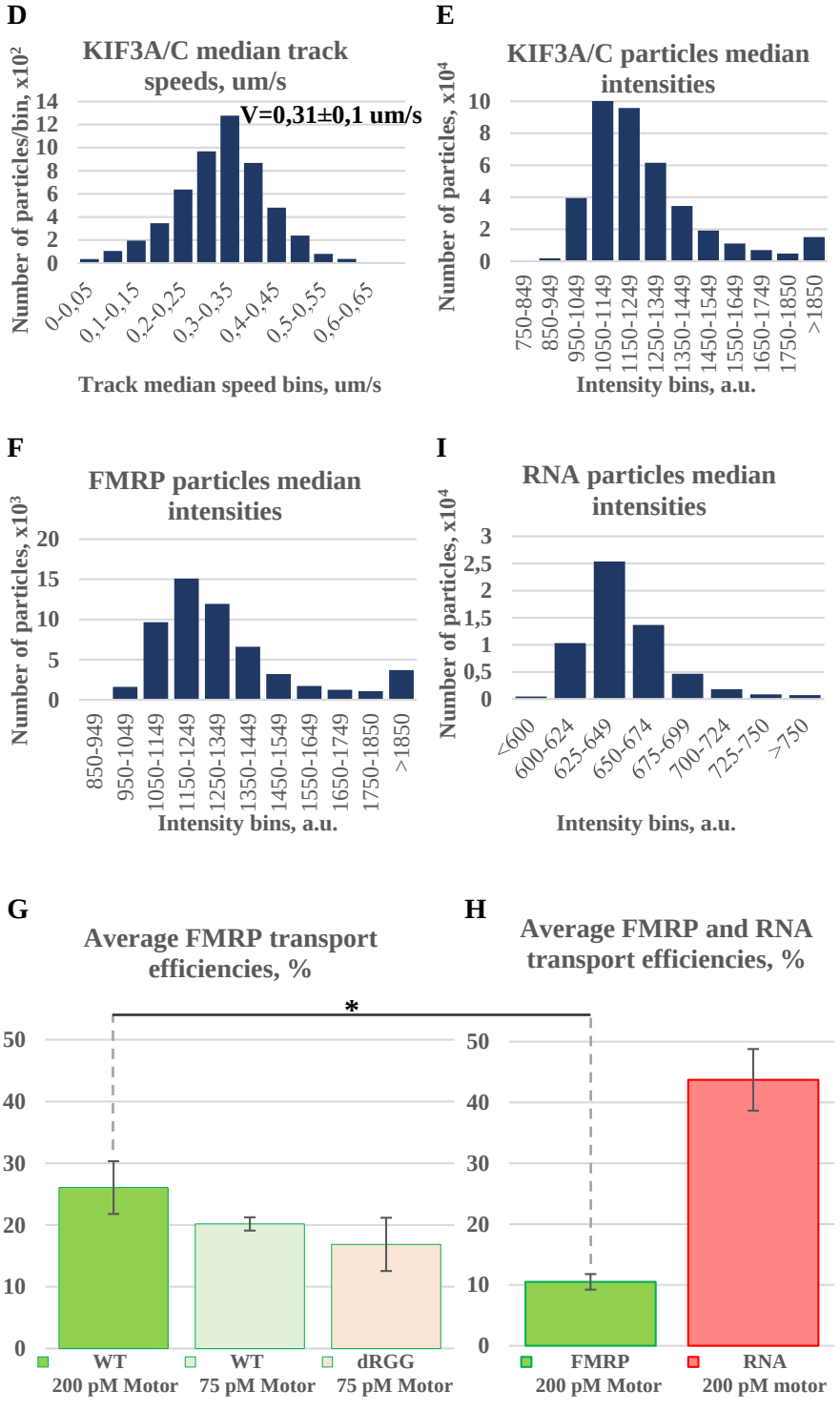
D
KIF3A/C median track speeds, um/s
V=0,31±0,1 um/s
Number of particles/bin, x10²
14
12
10
8
6
4
2
0
0-0,05
0,1-0,15
0,2-0,25
0,3-0,35
0,4-0,45
0,5-0,55
0,6-0,65
Track median speed bins, um/s
E
KIF3A/C particles median intensities
Number of particles, x10⁴
10
8
6
4
2
0
750-849
850-949
950-1049
1050-1149
1150-1249
1250-1349
1350-1449
1450-1549
1550-1649
1650-1749
1750-1850
>1850
Intensity bins, a.u.
F
FMRP particles median intensities
Number of particles, x10³
20
15
10
5
0
850-949
950-1049
1050-1149
1150-1249
1250-1349
1350-1449
1450-1549
1550-1649
1650-1749
1750-1850
>1850
Intensity bins, a.u.
I
RNA particles median intensities
Number of particles, x10⁴
3
2,5
2
1,5
1
0,5
0
<600
600-624
625-649
650-674
675-699
700-724
725-750
>750
Intensity bins, a.u.
G
Average FMRP transport efficiencies, %
*
50
40
30
20
10
0
WT
200 pM Motor
WT
75 pM Motor
dRGG
75 pM Motor
H
Average FMRP and RNA transport efficiencies, %
50
40
30
20
10
0
FMRP
200 pM Motor
RNA
200 pM motor

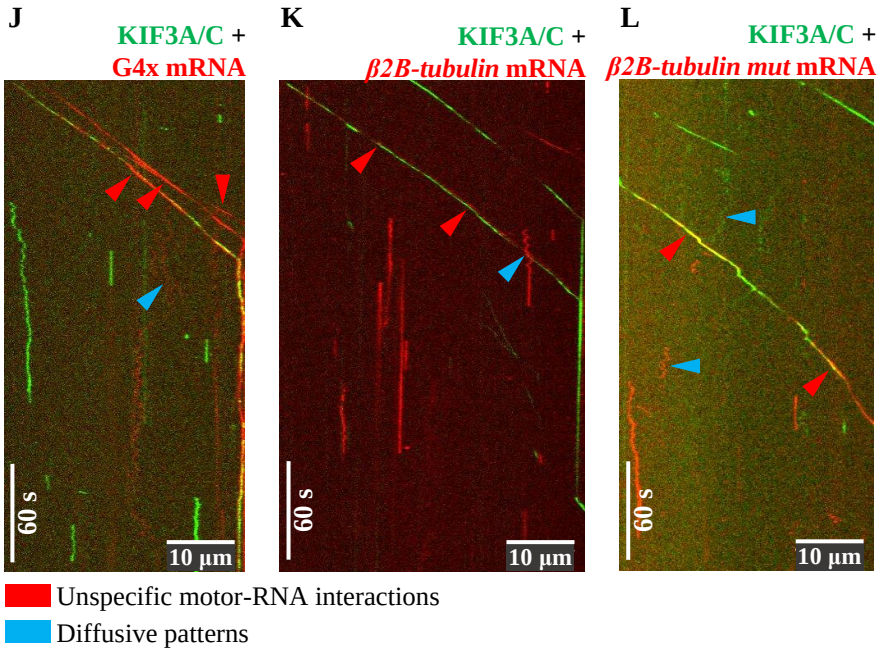
J
KIF3A/C +
G4x mRNA
K
KIF3A/C +
β2B-tubulin mRNA
L
KIF3A/C +
β2B-tubulin mut mRNA
60 s
10 µm
60 s
10 µm
60 s
10 µm
Unspecific motor-RNA interactions
Diffusive patterns

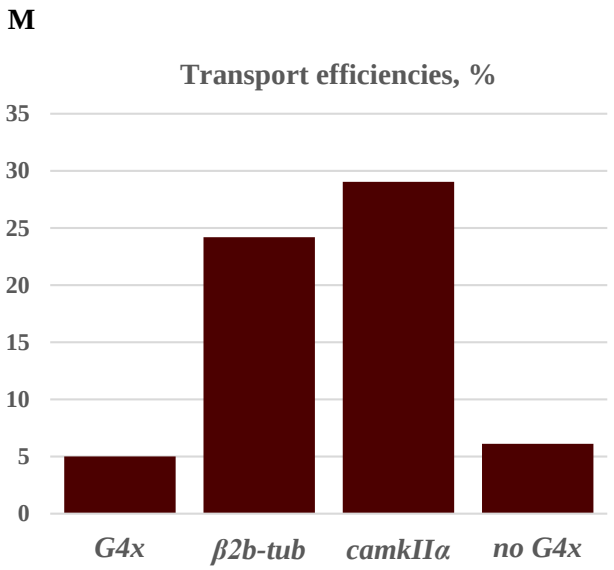
M
Transport efficiencies, %
35
30
25
20
15
10
5
0
G4x
β2b-tub
camkIIα
no G4x

Fig. R.6. KIF3A/C efficiently transports FMRP

A. GFP-KIF3A/C motor (200 pM) remains active in the "new HEPES" buffer. **B.** TMR-FMRP (230 pM, red) is efficiently transported by the GFP-KIF3A/C motor (200 pM, green), white arrows. **C.** Commercial Cy5-G4x mRNA (3,75 nM, red) is transported alone (red arrows) at least as much as within the complex of TMR-FMRP (230 pM, green) and GFP-KIF3A/C (200 pM, not shown), green arrows. **D.** GFP-KIF3A/C median track speeds distribution. **E.** Distribution of the GFP-KIF3A/C particles' median intensities. **F.** Distribution of median intensities of mobile TMR-FMRP particles. **D-F.** Data was obtained from 14 movies from 9 independent experiments, performed on two different days. **G.** Averaged between the movies' transport efficiencies (TE) of TMR-FMRP particles, transported by GFP-KIF3A/C motor at different concentrations. TEs were calculated as a percentage of transported TMR-FMRP particles relative to the total number of processive motor run events for every movie. **H.** Averaged between the movies' TMR-FMRP or G4x mRNA transport efficiencies, relative to the total number of the motor run events. **G, H.** For the analysis were used 4-5 movies, obtained from 3 independent experiments. An asterisk indicates $p<0,02$, according to the paired two-tailed t-test. Error bars represent SEM. **I.** Intensity distribution of transported commercial G4x mRNA molecules, based on 5 movies from 3 independent experiments. **J., K.** and **L.** Commercial Cy5-G4x, *in vitro* transcribed short *Cy5-β2b-tubulin* and commercial G4x-less *Cy5-β2b-tubulin* mRNAs correspondently (3,75 nM, red) are transported by GFP-KIF3A/C (75 pM, green) in the absence of FMRP, red arrows. **M.** Transport efficiencies of 4 tested mRNAs indicate unspecific binding by the GFP-KIF3A/C motor. TEs were calculated as the percentage of motor molecules carrying mRNA.

4.4. FMRP does not bind its target mRNA

There could be two possible explanations for the two-fold drop of FMRP transport efficiency upon addition of mRNA (Fig. R.6, G-H). The first is that mRNA competes with FMRP for motor binding, and the second, that motor and the mRNA compete for FMRP binding. In the second case, addition of mRNA could knock FMRP off the motor, decreasing FMRP transport efficiency.

To discriminate between these two possibilities, I conducted two basic tests to check FMRP-RNA interaction. If the two molecules interact, I would expect FMRP to diffuse along the microtubules in co-localisation with the G4x mRNA molecules. A basic co-diffusion experiment has demonstrated no binding whatsoever (Fig. R.7 A). This experiment was repeated with 4 different FMRP concentrations (150, 230, 700 and 1000 pM), yet only rare co-diffusion events were observed even at the highest FMRP concentration (Fig. 7, B).

However, it could be still possible that mRNA binds FMRP in the region, responsible for its charge-mediated interaction with the microtubules. If true, mRNA binding would lead to dissociation of the FMRP-RNA complex from the microtubule lattice. To test for this possibility, I have done a titration experiment, where I pre-incubated TMR-FMRP and commercial G4x mRNA at different concentrations and measured changes in the TMR-FMRP microtubule occupancy. If the mRNA is capable to knock FMRP off the microtubules upon binding, I would expect to observe a decrease of number of FMRP diffusion events with increase of mRNA concentration. Based on the results from 4 experiments (1 exp / condition), I am reporting an absence of any decrease of FMRP diffusion activity along the microtubules with an increase of RNA concentration (Fig. R.7, C).

Both of these results imply that FMRP does not bind commercially produced G-quadruplex fragment of the rat *camkIIα* mRNA with detectable by microscopy affinities and/or in these experimental conditions. Therefore, we can refer to a competition between mRNA and FMRP for motor binding.

Fig. R.7. FMRP does not bind its target mRNA

A and **B.** TMR-FMRP (150 pM in **A** and 1 nM in **B**, green) does not co-diffuse with its target commercial G-quadruplex mRNA fragment (3,75 nM, red), blue arrows, in exception of one to two co-diffusion events per movie, yellow arrow. **C.** RNA titration experiment discards the hypothesis of RNA-induced detachment of FMRP from the microtubules.

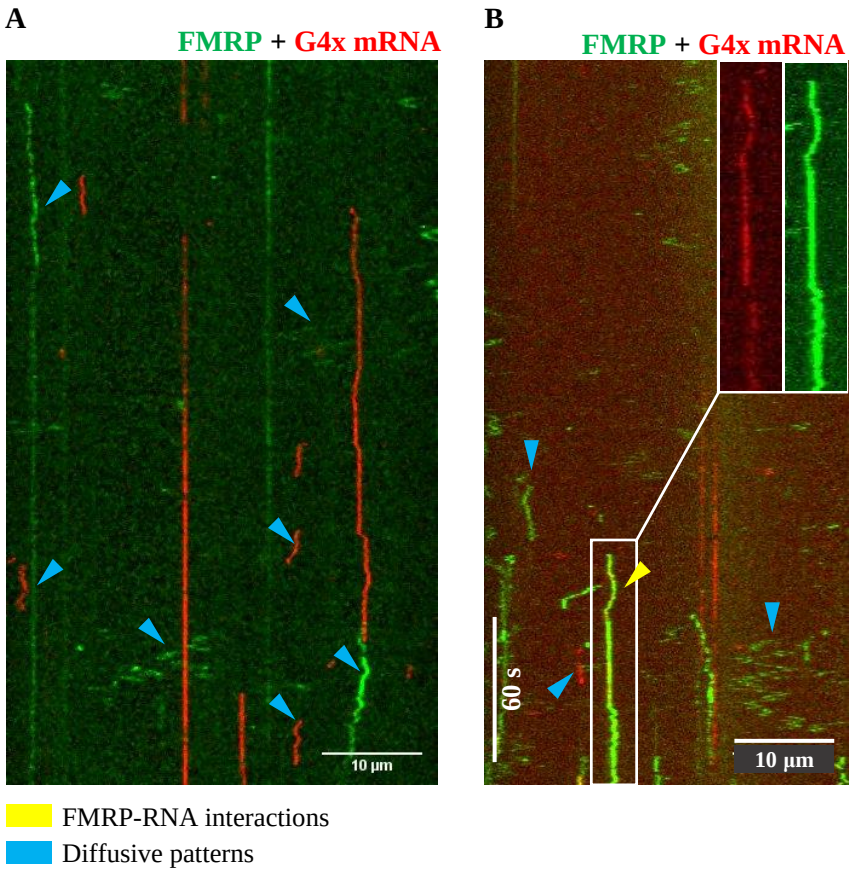
A
FMRP + G4x mRNA
10 µm
B
FMRP + G4x mRNA
60 s
10 µm
FMRP-RNA interactions
Diffusive patterns

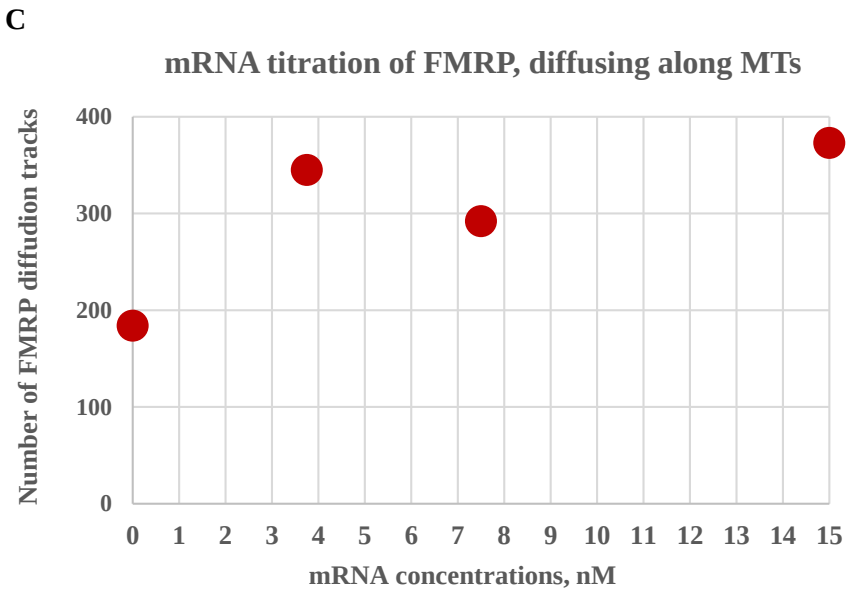
C
mRNA titration of FMRP, diffusing along MTs
Number of FMRP diffudion tracks
400
300
200
100
0
0 1 2 3 4 5 6 7 8 9 10 11 12 13 14 15
mRNA concentrations, nM

4.5. FMRP is not transported by Kinesin-1 motors

Next, I tested Kinesin-1 motor, reported to bind FMRP[39]. Although I have already done these experiments before in the "HEPES B" buffer (data not shown), I repeated them in the "new HEPES" buffer to make the results comparable with the Kinesin-2 studies. All the three versions of Kinesin-1 motor we had, AF647-KIF5, AF647-KIF5/KLC2 and AF647-KIF5/KLC4, remained processive and not auto-inhibited. Fig. R.8, A demonstrates motility of AF647-KIF5, which is representative for all the three versions of the motor.

All the three versions demonstrated a single peak on the particle intensity distribution plot (Fig. R.8, B), implying homogeneity of the particles' multimerisation states. The dimmest motile AF647-KIF5 particle detected had an intensity of 519 a.u., which in case of a homodimer would imply that tetramer would have an intensity in the range of 1038 a.u. or more. The vast majority of the motile particles (94%) lay in the range of 595±78 a.u., suggesting their dimeric state, although there were detected some blobs with intensity up to 2378 a.u. Kinesin-1 motors with the light chains had similarly sharp bell-shaped intensity profiles, however shifted by 25 a.u. to the right. Interesting is that all the versions of Kinesin-1 showed two populations of particles by speed, one centring around 100 nm/s and another around 300-450 nm/s (Fig. R.8, C). In the literature, human KIF5B was shown to have a speed of 305 nm/s *in vitro*[65], which nicely fits with the second peak of the speed distribution. In order to test, whether two speed populations of the motor correlate with the multimerisation state of the molecules, I have performed a correlation analysis. The correlation analysis between tracks' median speeds and median intensities gave the R^2 value of $1{,}4 \times 10^{-5}$, clearly indicating absence of any correlation (Fig. R.8, F).

All the three motors transported TMR-FMRP very poorly (Fig. R.8, E). FMRP was showing clear diffusion patterns with very rare transport events with on average 0,6, 3,2 and 1,3 events/movie for AF647-KIF5, AF647-KIF5/KLC2 and AF647-KIF5/KLC4 correspondently. Unfortunately, due to a low number of transported FMRP particles, I could not build clear FMRP speed distribution histograms. Nevertheless, FMRP transport speeds were falling into both of the motor speed peaks, suggesting that FMRP had no preference to any of the motor particles' populations (data not shown). All the motors had also very low TMR-FMRP transport efficiencies (Fig. R.8, D), which let me conclude that Kinesin-1 motors do not transport FMRP. Subsequently, presence of two speed populations of motors could not be explained by a conformational switch upon FMRP binding.

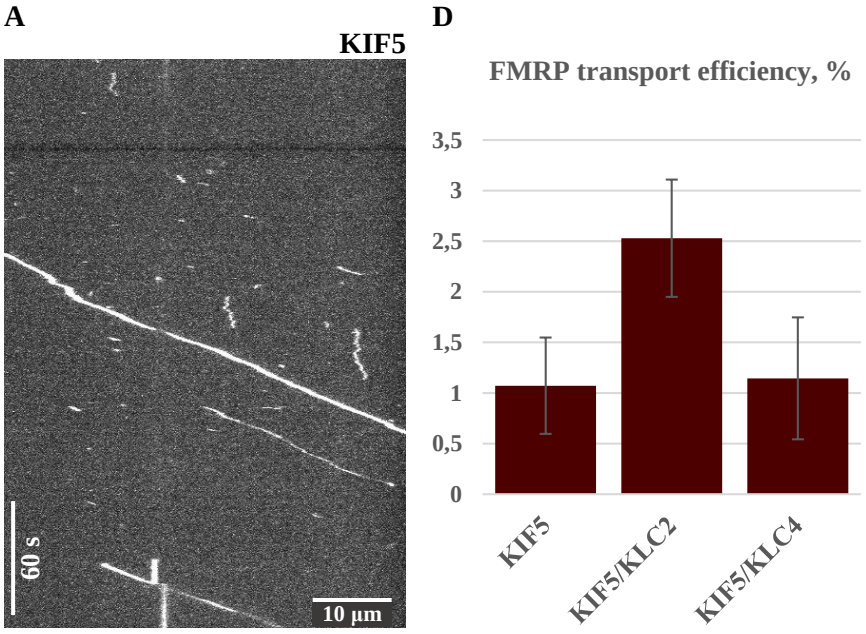

Fig. R.8. FMRP is not transported by Kinesin-1 motors

A. AF647-KIF5 motor (0,5 nM) remains processive and not auto-inhibited despite the evidence from the literature. **B.** Median intensities' distributions of running particles of the three Kinesin-1 motors. **C.** Median track speeds distributions for the same motors. **D.** TMR-FMRP transport efficiencies are represented by averaged over all the analysed movies' percentages of the motor particles that transport TMR-FMRP. The data was collected from 5 movies from 3 independent experiments (AF647-KIF5 and AF647-KIF5/KLC2), 10 movies from 4 independent experiments (AF647-KIF5/KLC4). Error bars represent SEM. **E.** AF647-KIF5 barely transports TMR-FMRP. TMR-FMRP (230 pM, red) shows diffusive patterns in the presence of the motor (left and middle, blue arrow) and is rarely transported (right, white arrow). AF647-KIF5 (0,5 nM, green) moves processively. A representative figure for all three Kinesin-1 versions tested. **F.** There is no correlation between intensity and running speed of the AF647-KIF5 particles. Every point represents a median speed and intensity values for each single motor particle track, detected by software in 3 independent experiments, one movie for each.

B

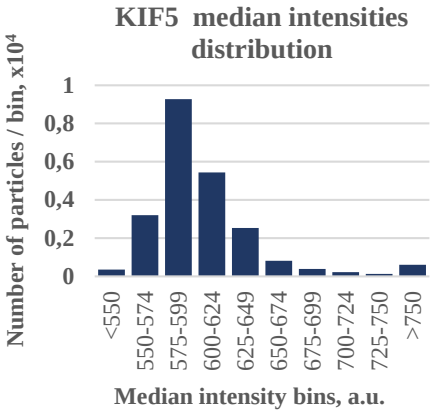
KIF5 median intensities distribution
Number of particles / bin, x10⁴
1
0,8
0,6
0,4
0,2
0
<550
550-574
575-599
600-624
625-649
650-674
675-699
700-724
725-750
>750
Median intensity bins, a.u.

C

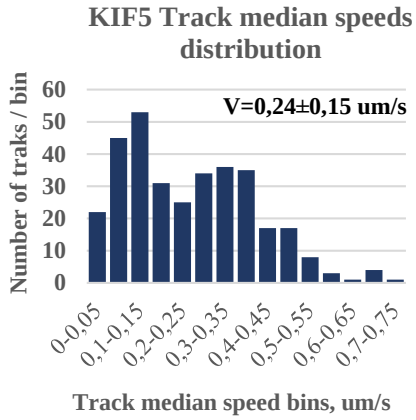
KIF5 Track median speeds distribution
V=0,24±0,15 um/s
Number of traks / bin
60
50
40
30
20
10
0
0-0,05
0,1-0,15
0,2-0,25
0,3-0,35
0,4-0,45
0,5-0,55
0,6-0,65
0,7-0,75
Track median speed bins, um/s

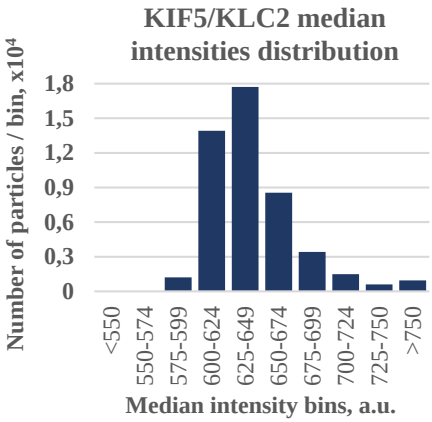
KIF5/KLC2 median intensities distribution
Number of particles / bin, x10⁴
1,8
1,5
1,2
0,9
0,6
0,3
0
<550
550-574
575-599
600-624
625-649
650-674
675-699
700-724
725-750
>750
Median intensity bins, a.u.

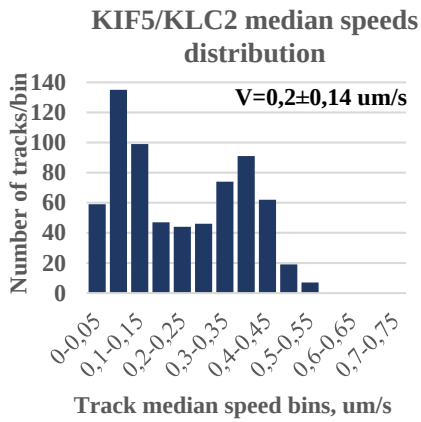
KIF5/KLC2 median speeds distribution
V=0,2±0,14 um/s
Number of tracks/bin
140
120
100
80
60
40
20
0
0-0,05
0,1-0,15
0,2-0,25
0,3-0,35
0,4-0,45
0,5-0,55
0,6-0,65
0,7-0,75
Track median speed bins, um/s

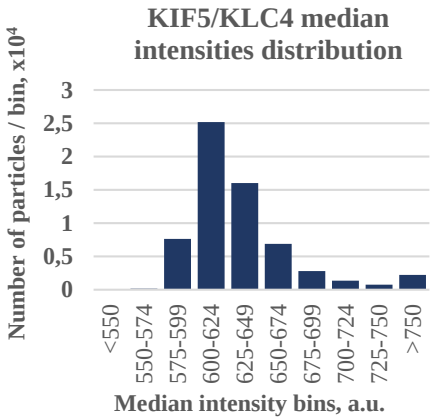
KIF5/KLC4 median intensities distribution
Number of particles / bin, x10⁴
3
2,5
2
1,5
1
0,5
0
<550
550-574
575-599
600-624
625-649
650-674
675-699
700-724
725-750
>750
Median intensity bins, a.u.

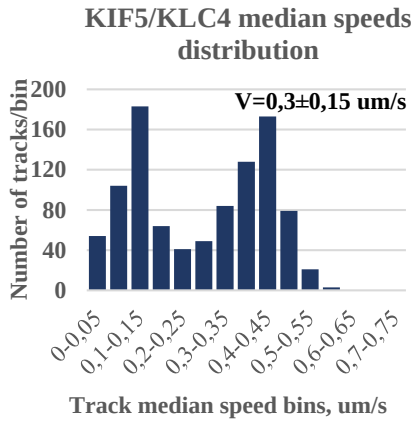
KIF5/KLC4 median speeds distribution
V=0,3±0,15 um/s
Number of tracks/bin
200
160
120
80
40
0
0-0,05
0,1-0,15
0,2-0,25
0,3-0,35
0,4-0,45
0,5-0,55
0,6-0,65
0,7-0,75
Track median speed bins, um/s

E

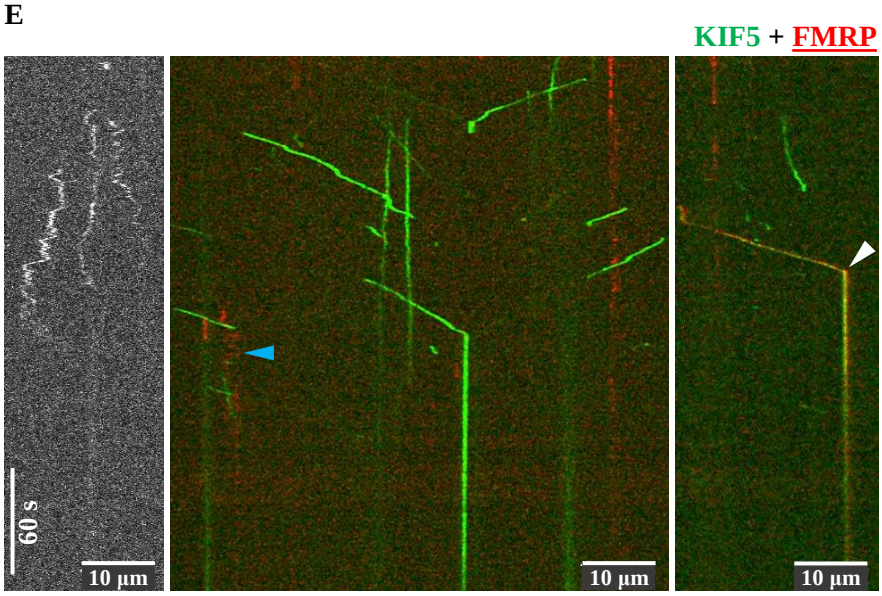
KIF5 + FMRP
60 s
10 µm
10 µm
10 µm

F

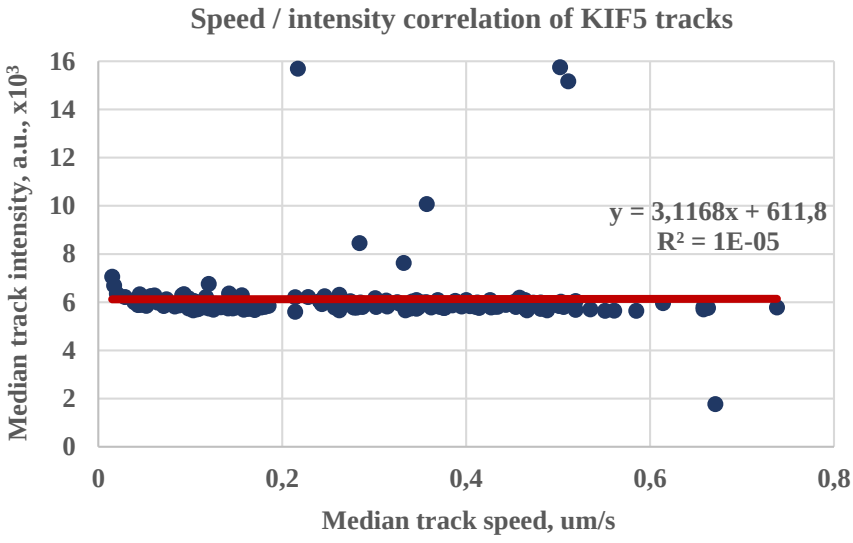
Speed / intensity correlation of KIF5 tracks
Median track intensity, a.u., x10³
16
14
12
10
8
6
4
2
0
0
0,2
0,4
0,6
0,8
Median track speed, um/s
y = 3,1168x + 611,8
R² = 1E-05

4.6. FMRP is not transported by KIF1Bβ

Finally, to test the data of the Charalambous paper[95] *in vitro*, I have tested GFP-KIF1Bβ motor, purified by another PhD student, Andrea Tassinari. This motor has demonstrated a very special track speed distribution pattern, forming a clean peak centred around the median speed value of 570 nm/s, followed by a long tail of rare particles with extremely high motility rates (Fig. R.9, A). Notably, these individual molecules were very clearly visible in the raw data as very dim and fast-moving points. One can see a variety of motor running speeds on Fig. R.9, C. In order to record these fast run events, I have decreased the imaging framerate from 250 to 150 ms per channel. Similarly to the other motors, GFP-KIF1Bβ had a single peak in the particle intensity distribution histogram, with the minimal intensity observed equal to 677 a.u. and the median of 820 a.u. (Fig. R.9, B). Based on this distribution, I am speculating that GFP-KIF1Bβ is represented by mostly monomeric molecules.

The transport efficiency of TMR-FMRP by GFP-KIF1Bβ was extremely low, ranging between 1-2 transport events per movie. Therefore, I am reporting that in my assay conditions GFP-KIF1Bβ failed to transport TMR-FMRP efficiently.

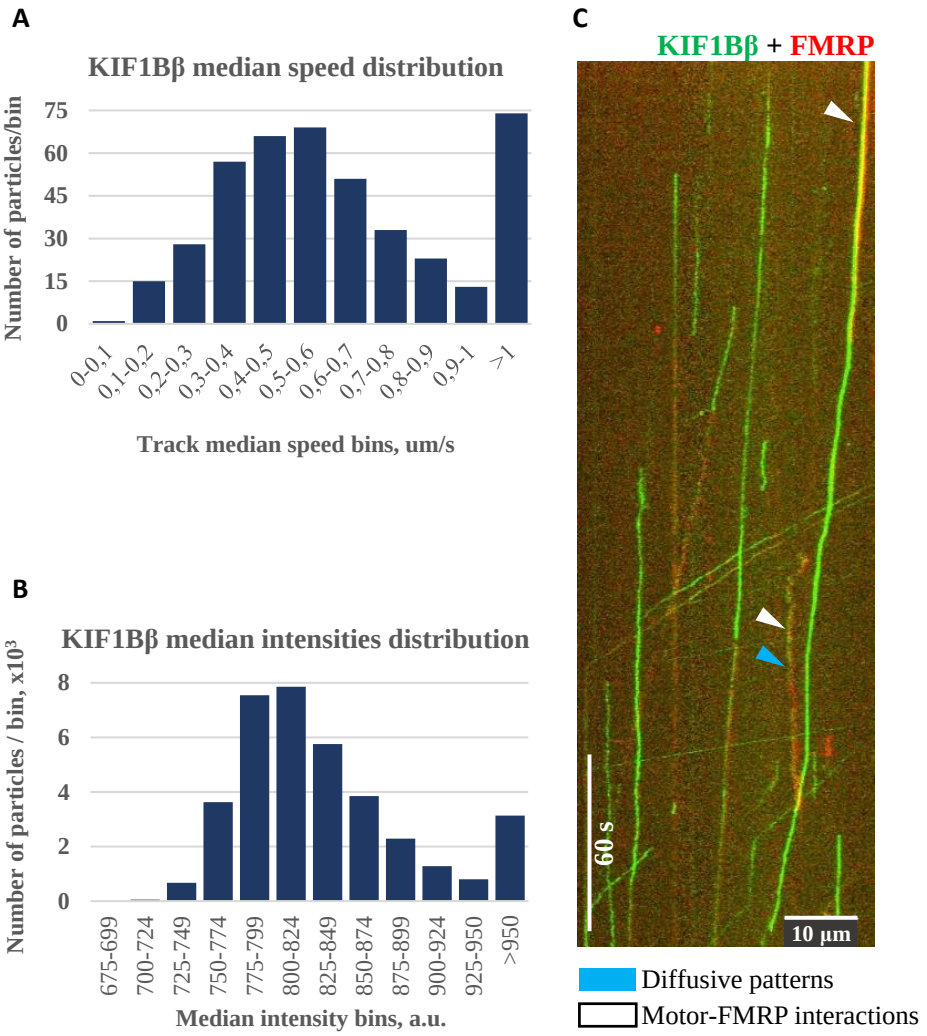

Fig. R.9. FMRP is not transported by KIF1Bβ

Median track speed (**A**) and median particles intensity (**B**) distributions of GFP-KIF1Bβ**.** Obtained data was based on 6 movies, recorded from 3 independent experiments (1 nM GFP-KIF1Bβ, 230 pM TMR-FMRP). **C.** GFP-KIF1Bβ (1 nM, green) does not efficiently transport TMR-FMRP (230 pM, red).

4.7. FXR2 is not transported by Kinesin-1 and 2

Since FMRP failed to transport mRNA, I aimed at testing another possible interaction that we have discovered in our yeast-two-hybrid screen, based on the library of RBPs, MAPs, some splicing factors and motor adaptors[197]. The screen was performed by Mireia Garriga and Silvia Speroni. Through these studies, we have identified exciting novel interactions between FXR2, an FMRP homologue, and KLC4, Kinesin-1 adaptor (Fig. R.10, A). As FXR2 is widely known to heterodimerise with FMRP[129] as well as bind mRNA[116], we have considered this protein to be very promising for FMRP-mediated mRNA transport reconstitution. I have purified FXR2 protein, cloned by Julia Grawenhoff and overexpressed by Maria Gili.

The TMR-FXR2 particles demonstrated a single peak on the brightness distribution histogram (Fig. R.10, B). The minimal brightness value observed equalled 857 a.u., while the median laid just at 1068 a.u., implying that the distribution was most probably represented by single monomers. In my experimental conditions, TMR-FXR2 demonstrated a very low (2%) transport efficiency with the GFP-KIF3A/C motor and almost zero with AF647-KIF5/KLC4 (Fig. R.10, C).

Although our Y2H screen contained a line of various controls with a stringent cut-off, some of the interactions were additionally validated with the NanoBRET assay. NanoBRET has confirmed another interesting interaction – a CGI-99 protein that binds to both FMRP and KLC4 (Fig. R.10, A). CGI-99 could be therefore a missing link between FXR2 and KLC4. Thanks to our collaborator, Prof. Martin Jinek, who kindly provided us with some CGI-99 protein, I could test, whether CGI-99 can promote FXR2 transport by KIF5/KLC4. Unfortunately, pre-incubation of TMR-FXR2 with CGI-99 at various concentrations did not result in TMR-FXR2 transport by AF647-KIF5/KLC4 (Data not shown).

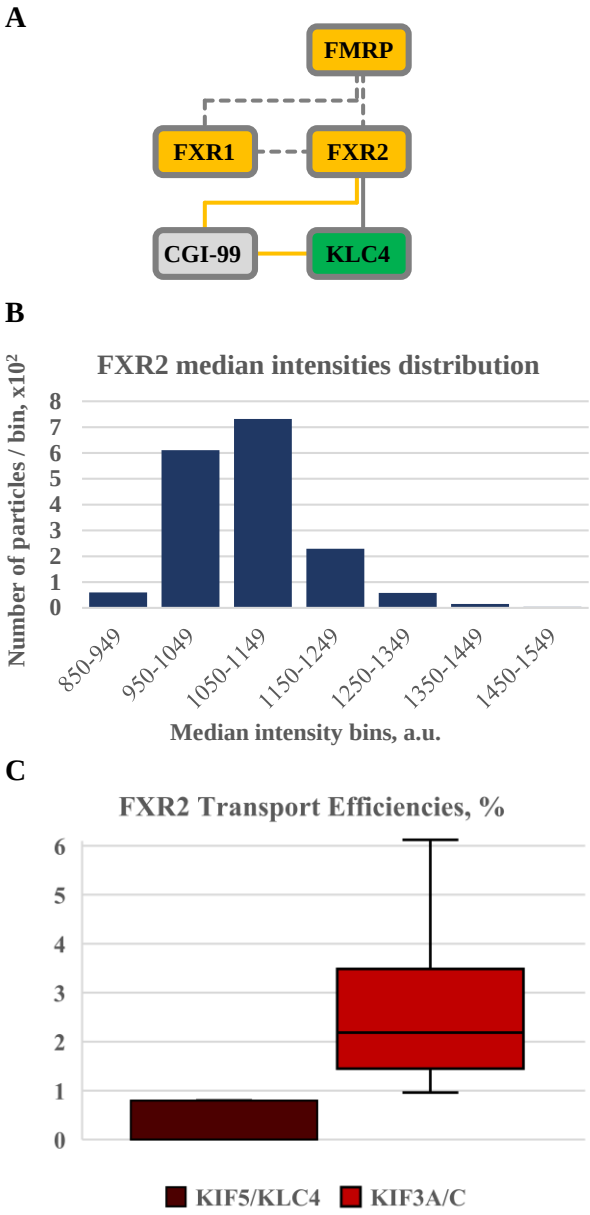

Fig. R.10. FXR2 is not transported by Kinesin-1 or 2

A. A fragment of the interaction screen results. Dashed lines represent interactions, confirmed only by the BioGRID Database; solid lines represent highly confident interactions from the Y2H screen, among which golden lines represent interactions, confirmed as positive in the NanoBRET assay; solid grey lines were not tested with the NanoBRET assay. **B.** Distribution of median intensities of the transported TMR-FXR2 particles. **C.** Transport efficiencies of TMR-FXR2 (230 pM) on AF647-KIF5/KLC4 (250 pM) or GFP-KIF3A/C (200 pM) motors. **B** and **C**, results were obtained from 6 movies, generated in 3 independent experiments.

4.8. Outlook from Part II

The *in vitro* reconstitution assay proved itself to be a powerful tool to study FMRP transport. Using this technique, I could demonstrate that FMRP can be efficiently transported with Kinesin-2 only, namely KIF3A/C motor, independently from its adaptor protein, KAP3. Kinesin-1 and Kinesin-3 motors failed to transport FMRP. Unfortunately, I could not release the autoinhibition of the KIF3A/B motor in order to test it for FMRP transport. The last remaining barrier for the full FMRP transport complex reconstitution is to find the conditions that would favour binding of the target mRNA by FMRP, while avoiding unspecific motor-RNA interactions. I am planning to study this question after submission of this thesis.

Despite the evidence from our Y2H screen and the NanoBRET assays, FXR2 was not transported by KIF5/KLC4 in the presence or absence of CGI-99.

Chapter 5

5. DISCUSSION

5.1. Buffer quality and differences between similar reagents can be decisive for success of an *in vitro* assay

There had been multiple obstacles on the way of making the assays work. First of all, the pipetting. It turned out that FMRP can tolerate only exceptionally slow pipetting, also limited by the number of pipetting steps. A special attention must be payed to the bubble-less pipetting. It has been known before that the proteins may lose their activities when exposed to the air bubbles, due to surface denaturation[198] and aggregation[199]. In sensitive *in vitro* assays, these effects can be more explicit. Choice of the labelling dyes is an additional factor that can greatly influence unspecific sticking to the glass surface[200] as well as protein aggregation and solubility[201].

My discovery that HEPES was the main source of my assays' poor reproducibility, as well as that "HEPES B" alone can remove an auto-inhibition of the KIF3A/B motor with or without its adaptor, KAP3, or cargo, was an absolute paradigm-changer. It turned the reconstituted FMRP-based mRNA transport system from a great success to merely a technical artefact.

Besides troubleshooting purposes, the question of what was the difference between the "B" HEPES bottle from the others, is extremely interesting from the biological perspective, since the content of that bottle could release KIF3A/B autoinhibition. To look into this question, I have outlined a few possible factors: age, accumulated exposure to light, degradation and synthesis by-products that could have been (badly) removed in this specific batch by the manufacturer.

Since the pH of both buffers was almost identical down to the second sign after the comma, I moved on to test the other hypotheses. Sigma Aldrich has kindly provided me with a lot-specific quality control dates, which were 17.02.2016 for SLBQ6703V ("HEPES A") and 14.07.2017 for SLBV3740 ("HEPES B"). Surprisingly, the "HEPES B" turned out to be almost 1,5 years younger than the "HEPES A". On the other hand, the literature contains evidence that HEPES has cytotoxicity effects upon its exposure to light[202]. This effect was explained by HEPES-mediated hydrogen peroxide

formation in direct light[203]. Other studies report that HEPES can form free radicals when in complex with copper[204] or iron[205] ions. Unfortunately, Sigma could not provide me with information about the presence and concentrations of any by-products or trace elements. Yet, the certificates of analysis of HEPES products of different purity levels did mention possible presence of the following trace elements: Ag, As, Bi, Cd, Cu, Hg, Mo, Pb, Sb, Sn and Fe (<5 ppm). Since the buffers were always stored in the fridge darkness, it makes the radical formation hypothesis very questionable. On the other hand, it could be still possible that some of these trace elements release the autoinhibition of the motor directly. Unfortunately, too few of these elements' salts could be found at CRG to test. Besides that, we still cannot exclude formation of HEPES' degradation products that could influence enzyme behaviour. We still do not understand what makes "HEPES B" activate KIF3A/B motor. In the end, this example demonstrates the importance of using absolutely fresh components for *in vitro* assays, due to their exceptional sensitivity to various factors.

The origin of the reagents can also make a big difference for the assay outcome. For instance, using a short Cy5-labelled commercial G4x mRNA stretch from the rat *camkIIα* mRNA solved the problem of unspecific sticking to the KIF3A/B motor in the "HEPES B"-based assay buffer (subchapter 3.3). A similar problem could have been the reason the poor result in repeating Sebastian's KIF3A/B/KAP activation assay with APC/mRNA. Since I was provided with the original reagents for only one clean experiment, and the purchased commercial *β2b-tubulin* mRNA as well as the insect cell pellets, overexpressing APC, were reserved for Sebastian's ongoing project, I had to substitute his components with the ones I produced myself: an *in vitro* transcribed *Cy5-β2b-tubulin* mRNA and purified KIF3A/B/KAP3 motor. As a substitute for the original APC, I was using the PKA-treated APC, purified earlier for another research question. Although the assay worked *per se*, reaching ~5 APC transport events per movie, it was still much less than with the original components (~28 APC transport events). I have therefore concentrated my efforts on the KIF3A/C motor.

5.2. Motor speeds partially reflect data from the literature

The speed of KIF3A/C motor that I measured in my reconstitution assays, was almost twice as high as in some previous *in vitro* studies (314±100 nm/s against 168,8±5,6 nm/s[65] and 182,1±5,4 nm/s[196], Table 5). However, both of these papers come from the same lab and are based on an artificially designed KIF3A/C motor, consisting of the native motor domains, neck regions and the helices α7 of the stalk regions, fused to the EB1 dimerisation domain, followed by the TEV cleavage site and a strep or his tags, not cleaved. This construct is missing a substantial part of the stalk regions as well as its C-termini. We utilise a full-length protein with the tags cleaved off, not counting a GFP or SNAP entity. This difference could account for the speed discrepancy. The speeds of Kinesin-1 motors generally coincide with the literature. The median speed of the only Kinesin-3 motor I used, KIF1Bβ, is slower than in the literature, but lies in the range of 660±100 nm/s. Furthermore, the median speed distribution of its tracks (Fig. R.9, A) formed a long tail towards the higher speed range that would make sense with respect to the literature. The median speed of the KIF3A/B motor I obtained is harder to judge, since this motor remained autoinhibited in the "New HEPES" buffer, but the values, obtained in the "HEPES B" buffer, generally fit with the high-end speed values in the literature.

At the same time, the velocities of mRNA granules in dendrites and axons vary, depending on the system used: *rac* mRNPs in primary hippocampal neurons move with average speed of 1 um/s and this speed drops by 25% upon FMRP knock-down[94]. Motility speed of the GFP-fused C-terminus of FMRP in hippocampal neurons ranges between 1-1,5 um/s[119]. In the S2 cells, FMRP was shown to be transported at 0,2 um/s[39]. *β-actin* mRNA is transported in hippocampal neurons at the mean speed of 1,3 um/s[206], while in *Xenopus* RGC axons at only at 0,6 um/s[195]. DDX1/DDX3 granules in hippocampal neurons move at the speed of ~0,3 um/s[207]. This comparison of the motor speeds *in vivo* and *in vitro* demonstrates that we still do not understand the mechanics of neuronal mRNA transport. Different motor speeds *in vivo* might depend on the motors types, their multimerisation state, post-translational modifications of the motors and their cargoes, splice variants of the motor and adaptor proteins. *In vitro* systems tremendously simplify the cellular processes for research, yet generate the other sources of variability. As we can see from the Table 5, GFP-KIF3A/C can have quite different median run speeds in different buffers. Moreover, from my experience, I can declare that the motor velocity is sensitive to reactive oxygen species present in solution, which in turn depends on the oxygen scavengers' activity. Provided the used proteins are identical, such

factors like buffer composition, oxygen scavengers and even temperature[208], among others, can be the source of discrepancies between the motor velocities, measured between different research groups.

Another important aspect to discuss is the motor autoinhibition. Literature, mentioned in the Introduction section, demonstrates that kinesins from both subfamilies, Kinesin-1 and Kinesin-2, are normally autoinhibited. In our laboratory, only KIF3A/B motor was autoinhibited, and this inhibition could be raised by APC/mRNA cargo binding[43]. Studies on KIF17 motor, a member of the Kinesin-2 subfamily, demonstrate that fusion of bulky tags to either N- or C-terminus of the motor lead to removal of an autoinhibited state, and that it can be prevented by inserting long (~20 aa) spacers[66]. These data support the idea that Kinesin-2 and 1 might have similar autoinhibition mechanisms. Both of our KIF3A/B motors, with or without KAP3, contained between KIF3A and their C-terminal SNAP-tag a 25 aa long "happy linker" (see Fig. M.2.), successfully used previously for microtubule studies[209]. On the other hand, KIF3A/C construct had the same linker before its C-terminal fusion; N-terminal fusions of KIF5 motors contained the "happy linker" too, yet these motors remained active. The only explanation left is the multimerisation state of the motors. The only motile KIF3A/B particles I observed were clearly oligomerised (Fig. R.5, C), yet the brightness distributions of the motor particles had quite narrow peaks in the range of 1x-1,5x a.u. of the dimmest particles observed (Fig. R.6, E; Fig. R.8, B), pointing towards normal heterodimerised state of the motors.

In the majority of the *in vitro* studies, referenced in Table 5, the motors remained not autoinhibited. It demonstrates that the field needs to develop less invasive strategies for fluorescent protein labelling, or one has to limit *in vitro* studies to the fully cleaved motor proteins, whose activity could be read-out by motility of their fluorescently labelled cargoes.

Motors	**Speeds, nm/s**		
	Experimental		Literature (*in vitro*)
	HEPES B	New HEPES	
Kinesins-1	-	300-450	305[65]
			309[196]
			700[208]
			800[194]
KIF3A/B	600	-	207[196]
			224[65]
			300[61]
			500[194]
			570[43]
			590[60]
KIF3A/C	490	314	169[65]
			182[196]
KIF1Bβ	-	570	660[67]
			750[68]

Table 5. Comparison between the motor speeds measured in my PhD Thesis work and the speeds, obtained in various *in vitro* assays, published previously.

Green hue: Kinesin-1 motors, blue hue: Kinesin-2 motors, orange hue: Kinesin-3.

5.3. FMRP binds directly to and is transported by the KIF3A/C motor

FMRP has been linked in several studies to dendritic mRNA transport upon stimulus[86,119,210], although always indirectly. Multiple attempts to understand, which motor proteins are mediating FMRP transport in living cells, led to accumulation of versatile and sometimes mutually exclusive data. Davidovic et.al. have demonstrated with Y2H and IP a direct FMRP association with KIF3C motor[150]. Dictenberg et.al. reported that the C-terminus of FMRP associates with KLC of KIF5 motor; dendritic co-localisation between FMRP and Kinesin-2 particles, in contrast to Kinesin-1[119]. Ling et.al. showed by IP, microscopy and motor KDs in somatic *Drosophila* cells that dFMRP transport is based on FMRP-KHC (Kinesin-1) association, whereas KLC plays no role in FMRP transport[39]. Finally, Charalambous et.al. performed an IP of FMRP pulled by KIF1Bβ motor[95].

In this study, I have used *in vitro* reconstitution assays, coupled to TIRF microscopy in order to explore, which of these motors can bind FMRP directly and transport it along the microtubules. I am reporting here that FMRP directly binds to and is transported by KIF3A/C heterodimer motor, and not by KIF1Bβ or KIF5 with or without KLC2/4 adaptors. This result coincides with the Y2H screen, performed in the work of Davidovic et.al.[150]. Indeed, among all the other studies, only Y2H tends to detect direct protein interactions with relatively high probability. We still cannot exclude that FMRP can be transported by the other motors and their adaptors in a bigger complex with other, yet unknown factors that could mediate the motor-FMRP interaction. Nevertheless, thanks to this this study, we can state that FMRP interacts directly exclusively with Kinesin-2 motors, primarily KIF3A/C, which answers the first question stated among the Research Goals of the project.

5.4. Elusive FMRP domain organisation

There had been made attempts to identify, which domains or regions of FMRP are responsible for its transport. Dictenberg et al. have demonstrated that the C-terminus of FMRP is pulled down by KLC, although ~3 times less efficiently than the full length FMRP[119]. The authors also show that an overexpression of this C-terminal fragment leads to a 5-fold reduction of the endogenous full-length FMRP and *camkIIα* mRNA localisation in the dendrites. Since IP does not guarantee direct protein interactions and FMRP-KLC2/4 interaction was not confirmed in our *in vitro* studies, I conclude that this interaction is not direct.

Wang et.al., reported that introduction of the I304N mutation to FMRP, a mutation that ruins the functionality of its second KH domain (interaction with the polysomes)[135], does not affect FMRP association with the fibroblast microtubules[210]. It means that the region, responsible for motor binding, is located somewhere else. To find this out, I have conducted a domain exclusion studies of FMRP.

Unfortunately, all the three FMRP truncation mutants severely diminished its ability to be transported (Fig. R.2, E). Nevertheless, among these constructs, NC-FMRP and NM-FMRP showed a similar transportability, while the NM-FMRP mutant, missing the C-terminus, was barely ever transported. This result suggests that although FMRP-KIF3A/C interaction seems to depend chiefly on the overall fold of FMRP, its C-terminal region plays the most relevant role in motor binding. Based on the structural studies on the N-terminal domain of FMRP, Adinolfi et.al. speculate that FMRP takes the right (and stable in solution) conformation upon its homodimerisation, which depends on both, its N-terminus and the KH domains[211]. If this "right conformation" assumption were ever confirmed as true, it would explain the results of my domain deletion analysis.

My latest result, showing that deletion of the RGG box of FMRP has no influence on its ability to be transported (Fig. R.6, G), implies that mechanistically FMRP could still carry mRNA while being transported. It paves the road for further optimisation of my *in vitro* assay conditions for mRNA binding. Combined, these results partially answer the second and the third questions among the Research Goals of the project.

5.5. The missing puzzle in the FMRP transport complex: mRNA

It has been known before and was recently confirmed once more[140] that FMRP's RGG box region is necessary for correct dendritic localisation of its target mRNAs, enriched with G-quadruplex stretches. In this work, I am reporting that FMRP, missing an RGG box sequence, was still efficiently transported by the KIF3A/C motor (Fig. R.6, G). This result demonstrates that the concerns that FMRP might be not able to transport mRNA cargos while being bound to the motor, are not justified.

Unfortunately, my *in vitro* system was missing some conditions, necessary for this well-proven and very much expected interaction between FMRP and G-quadruplex mRNA (Fig. R.7). G-quadruplexes of various mRNA targets of FMRP do not consist of consensus sequences[175], but are based on rather complex 3D-folds they form in solution[212]. The real mRNAs' G4x structures were proposed to form two hairpins[175], which resemble the fold of the artificial RNA aptamers, generated to be recognised by the RGG stretch of FMRP[141,142] (Fig. I.8, B-D). Moreover, functionality of the G4x structures strictly depends on presence of the K^+ cations[140]. For various *in vitro* assays with real mRNAs or RNA aptamers, full-length FMRP or RGG box-containing fragments, different potassium concentrations have been successfully used: 25 mM[212], 50 mM[142] and 150 mM[140,175]. To adjust the pH of the assay buffer, I used KOH that equalled to 4,3 mM final concentration of K^+. I have tested addition of 100 mM KCl in the KIF3A/B activation assay, using unlabelled motor, FMRP and commercial Cy5-G4x mRNA, but it did not lead to any mRNA transport events. In the nearest future, I aim to test different KCl concentrations for FMRP-G4x binding. Another option that I would test next is mRNA refolding, achieved by incubation of RNA at 70°C for 10 min and passive cooling to the RT, in the presence of K^+ ions. With this step, one could exclude that FMRP could not bind the RNA due to its incorrect folding.

Another option that could explain why FMRP did not bind its target mRNA, is that after purification it remained occupied by some mRNA molecules of the insect cell origin. With the salt concentration of 750 mM KCl, mRNA binding should be strongly disfavoured. At the highest adsorption peak of the chosen FPLC fractions, the $A_{260/280}$ of the most used FMRP prep equalled 0,76, which is just slightly over the preferred ratio of 0,7. This indicates that although there might be slight nucleic acid contamination, it is not a major issue.

Since both, the RNA dilution buffer and the assay mix contained commercial RNAse inhibitors, I exclude the possibility of RNA degradation. *In vitro* studies on the G-quadruplex-containing *fmr1* mRNA fragment and full-length FMRP have demonstrated a binding K_d of 120±7 nM for the same FMRP isoform I was using in these studies, ISO1[212]. Another studies on a G4x region of *semaphorin 3f* mRNA, reported a K_d=104±11 nM[213]. Both of these results are very close, although they were generated in the presence of quite different potassium ions concentrations, 25 mM and 150 mM KCl correspondently. In both of the cases titration was performed over fixed mRNA concentration (150 nM), which is ~30 times higher than maximally acceptable for TIRF assays. Therefore, it would be extremely interesting to measure the K_d of my FMRP protein and the commercial G4x mRNA interaction, using alternative biophysical methods, like microscale thermophoresis (MST).

Another remaining problem is that G4x mRNA is transported by the KIF3A/C motor much more efficiently than FMRP (Fig. R.6, G-H). Since the control mRNA that does not contain G4x sequence was still transported by KIF3A/C (Fig. R.6, L), I can speculate that this mRNA transport is probably unspecific. Such behaviour is very common with aggregated motor particles (personal experience), but the particle brightness histogram implies that my KIF3A/C motor is mostly dimeric (Fig. R.6, E).

It was very unexpected to see the effect of competition for motor binding between FMRP and the G4x mRNA (Fig. R., G-H). KIF3A has a small stretch, enriched in positively charged amino acids on its C-terminus (Arg$_{910}$-Pro-Arg-Thr-Ser-Lys-Gly-Lys-Ala-Arg-Pro-Lys-Met-Gly-Arg-Arg-Lys-Arg$_{927}$) that might be responsible for charge-mediated unspecific mRNA binding. In the next experiments, it would make sense to increase salt concentrations, which might eliminate unspecific charged interactions with the motor. It is probable that addition of 25-100 mM KCl to the assay buffer could solve both problems at the same time, shifting mRNA binding affinity from the motor back to FMRP.

Lastly, just RGG box might be insufficient for recognition of specific mRNA targets. An older generation of FMRP research papers implies that FMRP might bind its target mRNAs through a short non-coding RNA *BC1* (known also as *BC200* for primates)[123]. *BC1* forms loops and hairpins that contain multiple sequence stretches, complementary to some of the well-known mRNA targets of FMRP, like *map1b*, *arc* and *camkIIα* mRNAs. *BC1* ncRNA binds strongly to FMRP and mediates pull-downs of these mRNA targets[124]. I did not work with *BC1/BC200* ncRNA, since it was associated with FMRP's mRNA translation regulatory function, while there are evidence that FMRP regulates transport and translation of two separate

pools of mRNAs[140]. If true, *BC1*-mediated FMRP-mRNA interactions would lie out of scope of my research focus.

5.6. Conclusions and Outlook

In this PhD thesis, I describe the results of my study on biochemical foundations of FMRP-dependent mRNA transport mechanisms. To do so, I utilised *in vitro* molecular reconstitution assays, coupled to total internal reflection microscopy (TIRF). First, I have performed an extensive work searching for optimal purification strategy for FMRP that resulted in purification of FMRP protein in a buffer with low arginine and detergent content. Next, I have purified the main candidate motors that were identified as potential FMRP binders in the literature.

With these i*n vitro* molecular reconstitution assays, I demonstrate for the first time that FMRP binds directly to Kinesin-2 motors, specifically to KIF3A/C heterodimer, and not to the representative Kinesin-1 and Kinesin-3 motors (Fig. D.1). Mutational analysis of FMRP has shown that FMRP-KIF3 interaction is preferentially based on the C-terminal fragment of FMRP, and is not dependent on the RGG box region.

My experimental conditions were not favourable for FMRP-mRNA interaction. FMRP did not co-diffuse and could not be displaced from the microtubules by increasing concentrations of a short G-quadruplex-containing fragment of rat *camkIIα* mRNA. On the other hand, KIF3A/C motor exhibited substantial binding to various mRNA species independently from the presence of the G-quadruplex sequence. Introduction of a G-quadruplex mRNA led to reduction of FMRP transport efficiency by the motor, pointing to a direct competition between FMRP and mRNA for the motor binding.

Future studies of the FMRP-mediated mRNA transport mechanisms should be focused on shifting binding affinity of the G-quadruplex mRNAs from motor to FMRP. Successful optimisation of the *in vitro* assay conditions, leading to molecular reconstitution of the KIF3-FMRP-mRNA transport complex, would be a big step towards understanding the mechanisms of synaptic plasticity. Reconstitution of FMRP-mediated mRNA transport complex could also shed light onto the biochemistry of the fragile X-associated spectrum of mental retardation disorders.

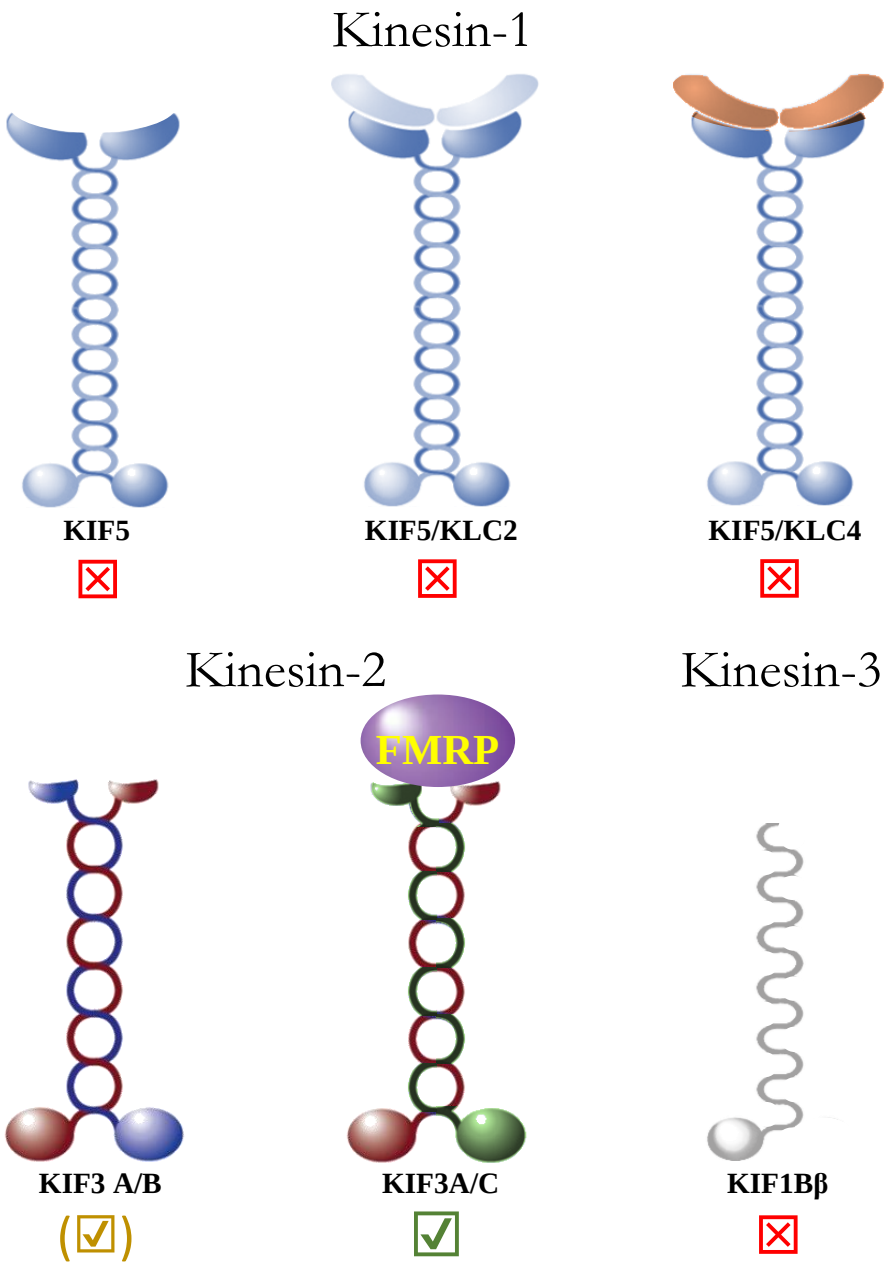

Fig. D.1. Conclusion: only Kinesin-2 directly binds and transports FMRP

Acknowledgements

Once, doing my EMBL internship during my Master's studies, I have invited myself to the microscopy room of my brilliant supervisor, Imre Gáspár, where Imre was performing TIRF microscopy on fruit fly egg extracts. When I realised that those slowly moving fluorescent dots were actually separate protein-RNA complexes, or granules, cutting through the living cytoplasm, I could hear some small toggle switching in my head. I wanted to work on mRNA transport, I had to do TIRF microscopy and study motility of molecules from our mammalian brains.

Eventually, this brought me to Barcelona. I had quite some time playing with TIRF, getting lost in the FPLC tubing, holding the breath when handling the RNA and drinking gallons of bitter coffee together with the other as happy, energetic and bravely looking into the future fellas. I want to thank **Sebastian Maurer** for giving me this opportunity to do the research I was the most excited about. I want to thank my TAC committee members, **Fatima Gebauer**, **Jens Lüders** and **Verena Ruprecht**, for fruitful discussions of my projects' progress and for valuable guidelines on where to focus next. This road was sometimes pebbly, winding, once upon a while it was changing its direction, yet if you keep going, you will end up more fit, endurable and confident, even if you fail to reach your original destination.

Looking back, I smile. I managed to extend my experiment bench beyond the revolving door of PRBB. For the first time, I have written a chapter of a new biology textbook for Ukrainian school pupils. I gave a science slam talk in a cosy bar in Poble Sec, thank you **Damjana Kastelic**. It was lots of fun to write my first article for a magazine, many thanks to **Maruxa Campos** from *"Ellipse"*. From the second attempt, I have conquered the Catalan mountain of the *"Tesi en 4 minuts"* competition. My gratitude to the **UPF** and **FCRI**. For me, this story will be a memorial of how to turn the bitterness of yesterday's loss into a triumph of tomorrow. Going home from the inline skating, I often tell to myself: "If you did not fall, then today you have not learned anything new".

Everybody has different values. For some it is the papers, for others it is the people. You choose. Here, I want to thank to the people without whom I could not imagine my daily life for the last four years. People that were always close to give a professional advice, pat on a back upon another failure and share a carajillo celebrating accomplishments of the others, together. People, whose presence or absence was making a difference. **Magüi**, **Andrea**, **Bogu**, from the very beginning, you have accepted me

with the open arms and so it stayed all this time. Thank you for your warmth, for being good friends. I will be missing our adventures. **Silvia**, **Elsa**, **Julia**, you have been ample islands of joy, relatedness and warm human touch. You made our work also our life. **Sebastian**, working next to you, I have learned a lot. You are an interesting person, and I wish I managed to reach more, peeping through the thick shell of a lab coat, by spending more time over a pint of beer. I have been very lucky with you all, guys! I could not have wished for better people.

Barcelona has also blessed me with friends. **Marcin**, the Spanish period of my life started with you. I am endlessly grateful for all our insane irresponsible adventures, they were the spice of our two (?) years and something I will think back about years and years after. **Tobias**, our full moon beers and full sun hikes were the needed gulps of calmness and wait-breathe-and-look-at-our-lives time. I will be missing it. Compactos! **Marcos**, **Silvia**, **Mar**, **Alejandra**, **Neus**, you were fantastic guides into the virtues and flavor of Spanish (and Catalan!) life. We have walked all Costa Brava along, checked all the Falles sculptures, counted countless estrellas across all the bars in Barcelona, now we could even write a whole dissertation on valencian paella. I am very happy we shared this time together.

I want to thank **my family** за постоянную поддержку. Хотя вы и далеко, все это время ощущалось, что вы близко. Вы сместе со мной расстравались, когда не получались эксперименты, и вместе со мной радовались, когда я чего-то добивался. Без вашей поддержки мне было бы намного тяжелее. Я вас люблю, спасибо, что вы у меня есть.

Mi kjæreste Мурчик, jeg kunne ikke forestille meg å dekke denne turen uten deg. Du har vært sjellevenn min, fyren, motivasjon for morgen og det viktigste at har passert til meg i løpet av disse årene. Takk at du har vært med meg hele denne tida. Elsker deg.

To make a full circle, let us come back to the CRG. Here I would love to express my gratitude to **Imma**, a person without whom our student life would be much more hard and foggy. She is a coordinator, psychologist and a friend. I want to thank **Montserrat Ruano**, who impressed me from the very beginning with her kindness and endless helpfulness in the wild jungle of Spanish bureaucracy. I want to thank the **UPF** for brilliant organisation and for their work providing with plenty of helpful online materials and guides in English. Last but not least, my gratefulness to the **La Caixa Foundation** for supporting the young fellows in their eager for science, ad for making my stay at CRG possible.

References

1. Zaccara, S., Ries, R. J. & Jaffrey, S. R. Reading, writing and erasing mRNA methylation. *Nat. Rev. Mol. Cell Biol.* **20**, 608–624 (2019).
2. Livneh, I., Moshitch-Moshkovitz, S., Amariglio, N., Rechavi, G. & Dominissini, D. The m6A epitranscriptome: transcriptome plasticity in brain development and function. *Nat. Rev. Neurosci.* (2019). doi:10.1038/s41583-019-0244-z
3. Decker, C. J. & Parker, R. mRNA decay enzymes: Decappers conserved between yeast and mammals. *Proc. Natl. Acad. Sci. U. S. A.* **99**, 12512–12514 (2002).
4. Koppers, M. *et al.* Receptor-specific interactome as a hub for rapid cue-induced selective translation in axons. *Elife* **8**, 1–27 (2019).
5. Nevo-Dinur, K., Nussbaum-Shochat, A., Ben-Yehuda, S. & Amster-Choder, O. Translation-independent localization of mRNA in E. coli. *Science (80-.).* **331**, 1081–1084 (2011).
6. Kannaiah, S. & Amster-Choder, O. Protein targeting via mRNA in bacteria. *Biochim. Biophys. Acta - Mol. Cell Res.* **1843**, 1457–1465 (2014).
7. Okita, T. W. & Choi, S. B. mRNA localization in plants: Targeting to the cell's cortical region and beyond. *Curr. Opin. Plant Biol.* **5**, 553–559 (2002).
8. Edelmann, F. T. *et al.* Molecular architecture and dynamics of ASH1 mRNA recognition by its mRNA-transport complex. *Nat. Struct. Mol. Biol.* **24**, 152–161 (2017).
9. Holt, C. E. & Bullock, S. L. Subcellular mRNA localization in animal cells and why it matters. *Science (80-.).* **326**, 1212–1216 (2009).
10. Niednery, A., Edelmanny, F. T. & Niessing, D. Of social molecules: The interactive assembly of ASH1 mRNA-transport complexes in yeast. *RNA Biol.* **11**, 998–1009

(2014).

11. Long, R. M. *et al.* Mating type switching in yeast controlled by asymmetric localization of ASH1 mRNA. *Science (80-.).* **277**, 383–387 (1997).

12. Gaspar, I., Sysoev, V., Komissarov, A. & Ephrussi, A. An RNA-binding tropomyosin recruits kinesin-1 dynamically to *oskar* mRNPs. *bioRxiv* 067876 (2016). doi:10.1101/067876

13. Weil, T. T. mRNA localization in the Drosophila germline. *RNA Biol.* **11**, 1010–1018 (2014).

14. Gautreau, D., Cote, C. A. & Mowry, K. L. Two copies of a subelement from the Vg1 RNA localization sequence are sufficient to direct vegetal localization in Xenopus oocytes. *Development* **124**, 5013–5020 (1997).

15. Thomsen, G. H. & Melton, D. A. Processed Vg1 protein is an axial mesoderm inducer in xenopus. *Cell* **74**, 433–441 (1993).

16. Mingle, L. A. *et al.* Localization of all seven messenger RNAs for the actin-polymerization nucleator Arp2/3 complex in the protrusions of fibroblasts. *J. Cell Sci.* **118**, 2425–2433 (2005).

17. Kislauskis, E. H., Zhu, X. C. & Singer, R. H. β-Actin messenger RNA localization and protein synthesis augment cell motility. *J. Cell Biol.* **136**, 1263–1270 (1997).

18. Miller, S. *et al.* Disruption of dendritic translation of CaMKIIalpha impairs stabilization of synaptic plasticity and memory consolidation. *Neuron* **36**, 507–519 (2002).

19. Medioni, C., Mowry, K. & Besse, F. Principles and roles of mRNA localization in animal development. *Development* **139**, 3263–3276 (2012).

20. Muddashetty, R. S., Kelić, S., Gross, C., Xu, M. & Bassell, G. J. Dysregulated metabotropic glutamate receptor-dependent translation of AMPA receptor and postsynaptic density-95 mRNAs at synapses in a mouse model of fragile X syndrome. *J. Neurosci.* **27**, 5338–5348

(2007).

21. Yoon, Y. J. *et al.* Glutamate-induced RNA localization and translation in neurons. *Proc. Natl. Acad. Sci.* 201614267 (2016). doi:10.1073/pnas.1614267113

22. Glock, C., Heumüller, M. & Schuman, E. M. mRNA transport & local translation in neurons. *Curr. Opin. Neurobiol.* **45**, 169–177 (2017).

23. John R.Giudicessi, BA.Michael J.Ackerman., 2013. Localization of all seven messenger RNAs for the actin-polymerization nucleator Arp2/3 complex in the protrusions of fibroblasts. *Bone* **23**, 1–7 (2008).

24. Hüttelmaier, S. *et al.* Spatial regulation of β-actin translation by Src-dependent phosphorylation of ZBP1. *Nature* **438**, 512–515 (2005).

25. Cohen, L. D. *et al.* Metabolic Turnover of Synaptic Proteins: Kinetics, Interdependencies and Implications for Synaptic Maintenance. *PLoS One* **8**, (2013).

26. Palacios, I. M. Hop-on hop-off: Polysomes take a tour of the cell on endosomes. *J. Cell Biol.* **204**, 287–289 (2014).

27. Jankowski, S. *et al.* The multi PAM 2 protein Upa2 functions as novel core component of endosomal mRNA transport. *EMBO Rep.* **20**, 1–15 (2019).

28. Olgeiser, L. *et al.* The key protein of endosomal mRNP transport Rrm4 binds translational landmark sites of cargo mRNAs. *EMBO Rep.* **20**, 1–17 (2019).

29. McCaffrey, M. W. & Lindsay, A. J. Roles for myosin Va in RNA transport and turnover. *Biochem. Soc. Trans.* **40**, 1416–20 (2012).

30. Shelke, A. R. , Roscoe, J. A. , Morrow, G. R. , Colman, L. K. , Banerjee, T. K. , & Kirshner, J. J. Myosin-Va Mediates RNA Distribution in Primary Fibroblasts From Multiple Organs. *Bone* **23**, 1–7 (2008).

31. Calliari, A. *et al.* Myosin Va associates with mRNA in ribonucleoprotein particles present in myelinated peripheral axons and in the central nervous system. *Dev.*

Neurobiol. **74**, 382–396 (2014).

32. Yoshimura, A. *et al.* Myosin-Va Facilitates the Accumulation of mRNA/Protein Complex in Dendritic Spines. *Curr. Biol.* **16**, 2345–2351 (2006).

33. Hammer, J. A. & Wagner, W. Functions of class v myosins in neurons. *J. Biol. Chem.* **288**, 28428–28434 (2013).

34. Lindsay, A. J. & Mccaffrey, M. W. Myosin Va is required for the transport of fragile X mental retardation protein (FMRP) granules. *Biol. Cell* **106**, 57–71 (2014).

35. Poirier, M. G., Eroglu, S. & Marko, J. F. Interactions of Elongation Factor 1 with F-Actin and ? ? -Actin mRNA: Implications for Anchoring mRNA in Cell Protrusions. *Mol. Biol. Cell* **13**, 2170–2179 (2002).

36. Rodriguez, A. J., Shenoy, S. M., Singer, R. H. & Condeelis, J. Visualization of mRNA translation in living cells. *J. Cell Biol.* **175**, 67–76 (2006).

37. Katz, Z. B. *et al.* β-actin mRNA compartmentalization enhances focal adhesion stability and directs cell migration. *Genes and Development* **26**, 1885–1890 (2012).

38. Kanai, Y., Dohmae, N. & Hirokawa, N. Kinesin transports RNA: Isolation and characterization of an RNA-transporting granule. *Neuron* **43**, 513–525 (2004).

39. Ling, S.-C., Fahrner, P. S., Greenough, W. T. & Gelfand, V. I. Transport of Drosophila fragile X rental retardation protein-containing ribonucleoprotein granules by kinesin-1 and cytoplasmic dynein. *Proc. Natl. Acad. Sci. U. S. A.* **101**, 17428–17433 (2004).

40. Delanoue, R. & Davis, I. Dynein anchors its mRNA cargo after apical transport in the Drosophila blastoderm embryo. *Cell* **122**, 97–106 (2005).

41. Tekotte, H. & Davis, I. Intracellular mRNA localization: Motors move messages. *Trends Genet.* **18**, 636–642 (2002).

42. Chaudhary, A. R. *et al.* MAP7 regulates organelle

transport by recruiting kinesin-1 to microtubules. *J. Biol. Chem.* **294**, 10160–10171 (2019).

43. Baumann, S. *et al.* A reconstituted mammalian APC-kinesin complex selectively transports defined packages of axonal mRNAs. *Sci. Adv.* **6**, eaaz1588 (2020).

44. Mcclintock, M. A. *et al.* RNA-directed activation of cytoplasmic dynein-1 in reconstituted transport RNPs. *Elife* 1–28 (2018). doi:10.7554/eLife.36312

45. Jimbo, T. *et al.* Identification of a link between the tumour suppressor APC and the kinesin superfamily. *Nat. Cell Biol.* **4**, 323–327 (2002).

46. Maurer, S. P. *et al.* EB1 accelerates two conformational transitions important for microtubule maturation and dynamics. *Curr. Biol.* **24**, 372–384 (2014).

47. Goodson, H. V & Jonasson, E. M. Microtubules and Microtubule-Associated Proteins. *Cold Spring Harb. Lab. Press* (2018). doi:10.1101/cshperspect.a022608

48. Löwe, J., Li, H., Downing, K. H. & Nogales, E. Refined structure of αβ-tubulin at 3.5 Å resolution. *Journal of Molecular Biology* **313**, 1045–1057 (2001).

49. Hirokawa, N., Noda, Y., Tanaka, Y. & Niwa, S. Kinesin superfamily motor proteins and intracellular transport. *Nat. Rev. Mol. Cell Biol.* **10**, 682–696 (2009).

50. Hirokawa, N. & Takemura, R. Molecular motors and mechanisms of directional transport in neurons. *Nat. Rev. Neurosci.* **6**, 201–214 (2005).

51. Hirokawa, N. Kinesin and dynein superfamily proteins and the mechanism of organelle transport. *Science (80-.).* **279**, 519–526 (1998).

52. Kanai, Y. *et al.* KIF5C, a Novel Neuronal Kinesin Enriched in Motor Neurons. *J. Neurosci.* **20**, 6374–6384 (2000).

53. Deboer, S. R. *et al.* Conventional Kinesin Holoenzymes Are Composed of Heavy and Light Chain Homodimers. **47**, 4535–4543 (2009).

54. Zhu, H. *et al.* Crystal structures of the tetratricopeptide repeat domains of Kinesin light chains: Insight into cargo recognition mechanisms. *PLoS One* **7**, 1–10 (2012).

55. Verhey, K. J. *et al.* Light chain-dependent regulation of kinesin's interaction with microtubules. *J. Cell Biol.* **143**, 1053–1066 (1998).

56. Kawano, T. *et al.* A Small Peptide Sequence is Sufficient for Initiating Kinesin-1 Activation Through Part of TPR Region of KLC1. *Traffic* **13**, 834–848 (2012).

57. Cai, D., Hoppe, A. D., Swanson, J. A. & Verhey, K. J. Kinesin-1 structural organization and conformational changes revealed by FRET stoichiometry in live cells. *J. Cell Biol.* **176**, 51–63 (2007).

58. Dietrich, K. A. *et al.* The kinesin-1 motor protein is regulated by a direct interaction of its head and tail. *Proc. Natl. Acad. Sci. U. S. A.* **105**, 8938–8943 (2008).

59. Yip, Y. Y. *et al.* The light chains of kinesin-1 are autoinhibited. *Proc. Natl. Acad. Sci.* **113**, 2418–2423 (2016).

60. Yamazaki, H., Nakata, T., Okada, Y. & Hirokawa, N. Cloning and characterization of KAP3: A novel kinesin superfamily-associated protein of KIF3A/3B. *Proc. Natl. Acad. Sci. U. S. A.* **93**, 8443–8448 (1996).

61. Yamazaki, H., Nakata, T., Okada, Y. & Hirokawa, N. KIF3A/B: A heterodimeric kinesin superfamily protein that works as a microtubule plus end-directed motor for membrane organelle transport. *J. Cell Biol.* **130**, 1387–1399 (1995).

62. Muresan, V. *et al.* KIF3C and KIF3A Form a Novel Neuronal Heteromeric Kinesin That Associates with Membrane Vesicles. *Mol. Biol. Cell* **9**, 637–652 (1998).

63. Yang, Z. & Goldstein, L. S. B. Characterization of the KIF3C neural kinesin-like motor from mouse. *Mol. Biol. Cell* **9**, 249–261 (1998).

64. Gilbert, S. P., Guzik-Lendrum, S. & Rayment, I. Kinesin-2 motors: Kinetics and biophysics. *J. Biol. Chem.* **293**,

4510–4518 (2018).

65. Guzik-Lendrum, S. *et al.* Kinesin-2 KIF3AC and KIF3AB can drive long-range transport along microtubules. *Biophys. J.* **109**, 1472–1482 (2015).

66. Hammond, J. W., Blasius, T. L., Soppina, V., Cai, D. & Verhey, K. J. Autoinhibition of the kinesin-2 motor KIF17 via dual intramolecular mechanisms. *J. Cell Biol.* **189**, 1013–1025 (2010).

67. Nangaku, M. *et al.* KIF1B, a novel microtubule plus end-directed monomeric motor protein for transport of mitochondria. *Cell* **79**, 1209–1220 (1994).

68. Matsushita, M., Yamamoto, R., Mitsui, K. & Kanazawa, H. Altered motor activity of alternative splice variants of the mammalian kinesin-3 protein KIF1B. *Traffic* **10**, 1647–1654 (2009).

69. Eom, T., Antar, L. N., Singer, R. H. & Bassell, G. J. Localization of a B-Actin Messenger Ribonucleoprotein Complex with Zipcode-Binding Protein Modulates the Density of Dendritic Filopodia and Filopodial Synapses. *J. Neurosci.* **23**, 10433–10444 (2003).

70. Fujii, R. & Takumi, T. TLS facilitates transport of mRNA encoding an actin-stabilizing protein to dendritic spines. *J. Cell Sci.* **118**, 5755–5765 (2005).

71. Chabanon, H., Mickleburgh, I. & Hesketh, J. Zipcodes and postage stamps: mRNA localisation signals and their trans-acting binding proteins. *Brief. Funct. Genomic. Proteomic.* **3**, 240–256 (2004).

72. Majumder, P., Chu, J. F., Chatterjee, B., Swamy, K. B. S. & Shen, C. K. J. Co-regulation of mRNA translation by TDP-43 and Fragile X Syndrome protein FMRP. *Acta Neuropathol.* **132**, 721–738 (2016).

73. Hentze, M. W., Castello, A., Schwarzl, T. & Preiss, T. A brave new world of RNA-binding proteins. *Nat. Rev. Mol. Cell Biol.* (2018). doi:10.1038/nrm.2017.130

74. Fu, Mi., Yu, X., Lu, J. & Zuo, Y. Repetitive motor learning induces coordinated formation of clustered dendritic

spines in vivo. **483**, 92–95 (2012).

75. Kastellakis, G., Denise, C. J., Sara, M. C., Silva, A. J. & Poirazi, P. Synaptic clustering within dendrites: an emerging theory of memory formation. 1922–2013 (2016). doi:10.1016/j.pneurobio.2014.12.002

76. Bennett, S. H., Kirby, A. J. & Finnerty, G. T. Rewiring the connectome: evidence and effects. *Neurosci. Biobehav. Rev.* (2018). doi:S0149763417304864

77. Sweatt, J. D. Neural plasticity and behavior – sixty years of conceptual advances. *J. Neurochem.* **139**, 179–199 (2016).

78. Bianchi, S. *et al.* Dendritic morphology of pyramidal neurons in the chimpanzee neocortex: Regional specializations and comparison to humans. *Cereb. Cortex* **23**, 2429–2436 (2013).

79. Hanus, C. & Schuman, E. M. Proteostasis in complex dendrites. *Nat. Rev. Neurosci.* **14**, 638–648 (2013).

80. Frotscher, M. *et al.* Fine structure of synapses on dendritic spines. *Front. Neuroanat.* **8**, 1–9 (2014).

81. Frey, U., Krug, M., Reymann, K. G. & Matthies, H. Anisomycin, an inhibitor of protein synthesis, blocks late phases of LTP phenomena in the hippocampal CA1 region in vitro. *Brain Res.* **452**, 57–65 (1988).

82. Bradshaw, K. D., Emptage, N. J. & Bliss, T. V. P. A role for dendritic protein synthesis in hippocampal late LTP. *Eur. J. Neurosci.* **18**, 3150–3152 (2003).

83. Sutton, M. A. & Schuman, E. M. Dendritic Protein Synthesis, Synaptic Plasticity, and Memory. *Cell* **127**, 49–58 (2006).

84. Cajigas, I. J. *et al.* The Local Transcriptome in the Synaptic Neuropil Revealed by Deep Sequencing and High-Resolution Imaging. *Neuron* **74**, 453–466 (2012).

85. Puthanveettil, S. V *et al.* A strategy to capture and characterize the synaptic transcriptome. *Proc. Natl. Acad. Sci. U. S. A.* **110**, 7464–9 (2013).

86. Pilaz, L. J., Lennox, A. L., Rouanet, J. P. & Silver, D. L. Dynamic mRNA Transport and Local Translation in Radial Glial Progenitors of the Developing Brain. *Curr. Biol.* **26**, 3383–3392 (2016).

87. Twiss, J. L. & Fainzilber, M. Ribosomes in axons - scrounging from the neighbors? *Trends Cell Biol.* **19**, 236–243 (2009).

88. Akins, M. R. *et al.* Axonal ribosomes and mRNAs associate with fragile X granules in adult rodent and human brains. *Hum. Mol. Genet.* **26**, 192–209 (2017).

89. Cioni, J. M. *et al.* Late Endosomes Act as mRNA Translation Platforms and Sustain Mitochondria in Axons. *Cell* **176**, 56-72.e15 (2019).

90. Das, S., Singer, R. H. & Yoon, Y. J. The travels of mRNAs in neurons: do they know where they are going? *Curr. Opin. Neurobiol.* **57**, 110–116 (2019).

91. Bressloff, P. C. & Earnshaw, B. A. Diffusion-trapping model of receptor trafficking in dendrites. *Phys. Rev. E - Stat. Nonlinear, Soft Matter Phys.* **75**, (2007).

92. Xu, K., Zhong, G. & Zhuang, X. Actin, spectrin, and associated proteins form a periodic cytoskeletal structure in axons. *Science (80-.).* **339**, 452–6 (2013).

93. Dent, E. W., Merriam, E. B. & Hu, X. The dynamic cytoskeleton: Backbone of dendritic spine plasticity. *Curr. Opin. Neurobiol.* **21**, 175–181 (2011).

94. Chu, J.-F., Majumder, P., Chatterjee, B., Huang, S.-L. & Shen, C.-K. J. TDP-43 Regulates Coupled Dendritic mRNA Transport-Translation Processes in Co-Operation with FMRP and Staufen1: A Mechanistic View. *SSRN Electron. J.* **29**, 3118-3133.e6 (2018).

95. Charalambous, D. C. *et al.* KIF1Bb transports dendritically localized mRNPs in neurons and is recruited to synapses in an activity-dependent manner. *Cell. Mol. Life Sci.* **70**, 335–356 (2013).

96. Mitsumori, K., Takei, Y. & Hirokawa, N. Components of RNA granules affect their localization and dynamics in

neuronal dendrites. *Mol. Biol. Cell* **28**, 1412–1417 (2017).

97. Arnold, D. B. & Gallo, G. Structure meets function: Actin filaments and myosin motors in the axon. *J. Neurochem.* **129**, 213–220 (2014).

98. Balasanyan, V. & Arnold, D. B. Actin and myosin-dependent localization of mRNA to dendrites. *PLoS One* **9**, (2014).

99. De Heredia, M. L. & Jansen, R. P. mRNA localization and the cytoskeleton. *Curr. Opin. Cell Biol.* **16**, 80–85 (2004).

100. Doyle, M. & Kiebler, M. A. Mechanisms of dendritic mRNA transport and its role in synaptic tagging. *EMBO J.* **30**, 3540–3552 (2011).

101. Fujii, R. *et al.* The RNA binding protein TLS is translocated to dendritic spines by mGluR5 activation and regulates spine morphology. *Curr. Biol.* **15**, 587–593 (2005).

102. Fritzsche, R. *et al.* Interactome of two diverse RNA granules links mRNA localization to translational repression in neurons. *Cell Rep.* **5**, 1749–1762 (2013).

103. Tolino, M., Köhrmann, M. & Kiebler, M. A. RNA-binding proteins involved in RNA localization and their implications in neuronal diseases. *Eur. J. Neurosci.* **35**, 1818–1836 (2012).

104. Eliscovich, C., Shenoy, S. M. & Singer, R. H. Imaging mRNA and protein interactions within neurons. *Proc. Natl. Acad. Sci.* 201621440 (2017). doi:10.1073/pnas.1621440114

105. Ohashi, S. *et al.* Identification of mRNA/protein (mRNP) complexes containing Pur??, mStaufen, Fragile X Protein, and myosin Va and their association with rough endoplasmic reticulum equipped with a kinesin motor. *J. Biol. Chem.* **277**, 37804–37810 (2002).

106. Dictenberg, J. B., Swanger, S. A., Antar, L. N., Singer, R. H. & Bassell, G. J. A Direct Role for FMRP in Activity-

Dependent Dendritic mRNA Transport Links Filopodial-Spine Morphogenesis to Fragile X Syndrome. *Dev. Cell* **14**, 926–939 (2008).

107. Darnell, J. C. *et al.* FMRP stalls ribosomal translocation on mRNAs linked to synaptic function and autism. *Cell* **146**, 247–261 (2011).

108. Narayanan, U. *et al.* S6K1 phosphorylates and regulates fragile X mental retardation protein (FMRP) with the neuronal protein synthesis-dependent mammalian target of rapamycin (mTOR) signaling cascade. *J. Biol. Chem.* **283**, 18478–18482 (2008).

109. Zhang, Y., Gaetano, C. M., Williams, K. R., Bassell, G. J. & Mihailescu, M. R. FMRP interacts with G-quadruplex structures in the 3 ′-UTR of its dendritic target shank1 mRNA. *RNA Biol.* **11**, 1364–1374 (2014).

110. Mazrou, R. *et al.* Fragile X Mental Retardation protein determinants required for its association with polyribosomal mRNPs. *Hum. Mol. Genet.* **12**, 3087–3096 (2003).

111. Jin, P. & Warren, S. T. Understanding the molecular basis of fragile X syndrome. *Hum. Mol. Genet.* **9**, 901–908 (2000).

112. Bagni, C., Tassone, F., Neri, G., Hagerman, R. Fragile X syndrome: causes, diagnosis, mechanisms, and therapeutics. *J. Clin. Invest.* **122**, 4314–4322 (2012).

113. Shah, S. *et al.* FMRP Control of Ribosome Translocation Promotes Chromatin Modifications and Alternative Splicing of Neuronal Genes Linked to Autism. *Cell Rep.* **30**, 4459-4472.e6 (2020).

114. Napoli, I. *et al.* The Fragile X Syndrome Protein Represses Activity-Dependent Translation through CYFIP1, a New 4E-BP. *Cell* **134**, 1042–1054 (2008).

115. Bechara, E. G. *et al.* A novel function for fragile X mental retardation protein in translational activation. *PLoS Biol.* **7**, (2009).

116. Fernández, E. *et al.* FXR2P Exerts a Positive

Translational Control and Is Required for the Activity-Dependent Increase of PSD95 Expression. *J. Neurosci.* **35**, 9402–8 (2015).

117. Hsu, P. J. *et al.* The RNA-binding protein FMRP facilitates the nuclear export of N 6 -methyladenosine–containing mRNAs. *J. Biol. Chem.* jbc.AC119.010078 (2019). doi:10.1074/jbc.AC119.010078

118. Zhang, F. *et al.* Fragile X mental retardation protein modulates the stability of its m6A-marked messenger RNA targets. *Hum. Mol. Genet.* **27**, 3936–3950 (2018).

119. Dictenberg, J. B., Swanger, S. A., Antar, L. N., Singer, R. H. & Bassell, G. J. A Direct Role for FMRP in Activity-Dependent Dendritic mRNA Transport Links Filopodial-Spine Morphogenesis to Fragile X Syndrome SUPP. *Dev. Cell* **14**, 926–939 (2008).

120. Eichler, E. E., Richards, S., Gibbs, R. A. & Nelson, D. L. Fine structure of the human FMR1 gene. *Hum. Mol. Genet.* **2**, 1147–1153 (1993).

121. Brackett, D. M. *et al.* Fmr1 Transcript Isoforms: Association with Polyribosomes; Regional and Developmental Expression in Mouse Brain. *PLoS One* **8**, 1–11 (2013).

122. Ramos, A. *et al.* The structure of the N-terminal domain of the fragile X mental retardation protein: A platform for protein-protein interaction. *Structure* **14**, 21–31 (2006).

123. Lacoux, C. *et al.* BC1-FMRP interaction is modulated by 2′-O-methylation: RNA-binding activity of the tudor domain and translational regulation at synapses. *Nucleic Acids Res.* **40**, 4086–4096 (2012).

124. Zalfa, F. *et al.* The Fragile X syndrome protein FMRP associates with BC1 RNA and regulates the translation of specific mRNAs at synapses. *Cell* **112**, 317–327 (2003).

125. Bardoni, B. *et al.* 82-FIP, a novel FMRP (Fragile X Mental Retardation Protein) interacting protein, shows a cell cycle-dependent intracellular localization. *Hum. Mol. Genet.* **12**, 1689–1698 (2003).

126. Bardoni, B., Schenck, A. & Mandel, J. L. A novel RNA-binding nuclear protein that interacts with the fragile X mental retardation (FMR1) protein. *Hum. Mol. Genet.* **8**, 2557–2566 (1999).

127. Schenck, A., Bardoni, B., Moro, A., Bagni, C. & Mandel, J. L. A highly conserved protein family interacting with the fragile X mental retardation protein (FMRP) and displaying selective interactions with FMRP-related proteins FXR1P and FXR2P. *Proc. Natl. Acad. Sci. U. S. A.* **98**, 8844–9 (2001).

128. Fernández, E., Rajan, N. & Bagni, C. The FMRP regulon: From targets to disease convergence. *Front. Neurosci.* **7**, 1–9 (2013).

129. Siomi, M. C., Zhang, Y., Siomi, H. & Dreyfuss, G. Specific sequences in the fragile X syndrome protein FMR1 and the FXR proteins mediate their binding to 60S ribosomal subunits and the interactions among them. *Mol. Cell. Biol.* **16**, 3825–3832 (1996).

130. Hu, Y. *et al.* The amino-terminal structure of human fragile X mental retardation protein obtained using precipitant-immobilized imprinted polymers. *Nat. Commun.* **6**, 1–11 (2015).

131. Valverde, R., Edwards, L. & Regan, L. Structure and function of KH domains. *FEBS J.* **275**, 2712–2726 (2008).

132. Jr, M. A. *et al.* FMR1 targets distinct mRNA sequence elements to regulate protein expression. **492**, 382–386 (2013).

133. Nicastro, E. *et al.* A point mutation in the FMR-1 gene associated with fragile X mental retardation. *Nat. Genet.* **3**, 73–96 (1993).

134. Zang, J. B. *et al.* A mouse model of the human fragile X syndrome I304N mutation. *PLoS Genet.* **5**, (2009).

135. Darnell, J. C., Mostovetsky, O. & Darnell, R. B. FMRP RNA targets: Identification and validation. *Genes, Brain Behav.* **4**, 341–349 (2005).

136. Siomi, H., Choi, M., Siomi, M. C., Nussbaum, R. L. & Dreyfuss, G. Essential role for KH domains in RNA binding: Impaired RNA binding by a mutation in the KH domain of FMR1 that causes fragile X syndrome. *Cell* **77**, 33–39 (1994).

137. Valverde, R., Pozdnyakova, I., Kajander, T., Venkatraman, J. & Regan, L. Fragile X Mental Retardation Syndrome: Structure of the KH1-KH2 Domains of Fragile X Mental Retardation Protein. *Structure* **15**, 1090–1098 (2007).

138. Menon, L. & Mihailescu, M. R. Interactions of the G quartet forming semaphorin 3F RNA with the RGG box domain of the fragile X protein family. *Nucleic Acids Res.* **35**, 5379–5392 (2007).

139. Menon, L., Mader, S. A. & Mihailescu, M. R. Fragile X mental retardation protein interactions with the microtubule associated protein 1B RNA. *Rna* **14**, 1644–1655 (2008).

140. Goering, R. *et al.* FMRP promotes RNA localization to neuronal projections through interactions between its RGG domain and G-quadruplex RNA sequences. (2019). doi:http://dx.doi.org/10.1101/784728

141. Phan, A. T. *et al.* Structure-function studies of FMRP RGG peptide recognition of an RNA duplex-quadruplex junction. **18**, 796–804 (2012).

142. Vasilyev, N. *et al.* Crystal structure reveals specific recognition of a G-quadruplex RNA by a β-turn in the RGG motif of FMRP. *Proc. Natl. Acad. Sci.* **112**, E5391–E5400 (2015).

143. Siomi, M. C., Higashijima, K., Ishizuka, A. & Siomi, H. Casein Kinase II Phosphorylates the Fragile X Mental Retardation Protein and Modulates Its Biological Properties. *Mol. Cell. Biol.* **22**, 8438–8447 (2002).

144. Brown, V. *et al.* Microarray identification of FMRP-associated brain mRNAs and altered mRNA translational profiles in fragile X syndrome. *Cell* **107**, 477–487 (2001).

145. Maurin, T. *et al.* HITS-CLIP in various brain areas reveals new targets and new modalities of RNA binding by fragile X mental retardation protein. *Nucleic Acids Res.* 1–12 (2018). doi:10.1093/nar/gky267

146. Chmielewska, J. J., Kuzniewska, B., Milek, J., Urbanska, K. & Dziembowska, M. Neuroligin 1, 2, and 3 Regulation at the Synapse: FMRP-Dependent Translation and Activity-Induced Proteolytic Cleavage. *Mol. Neurobiol.* **95**, 1–19 (2018).

147. Weiler, I. J. & Greenough, W. T. Synaptic synthesis of the fragile X protein: Possible involvement in synapse maturation and elimination. *Am. J. Med. Genet.* **83**, 248–252 (1999).

148. Huber, K. M., Gallagher, S. M., Warren, S. T. & Bear, M. F. Altered synaptic plasticity in a mouse model of fragile X mental retardation. *Proc. Natl. Acad. Sci.* **99**, 7746–7750 (2002).

149. Zalfa, F. & Bagni, C. Molecular insights into mental retardation: Multiple functions for the Fragile X mental retardation protein? *Curr. Issues Mol. Biol.* **6**, 73–88 (2004).

150. Davidovic, L. *et al.* The fragile X mental retardation protein is a molecular adaptor between the neurospecific KIF3C kinesin and dendritic RNA granules. *Hum. Mol. Genet.* **16**, 3047–3058 (2007).

151. Charalambous, D. C. *et al.* KIF1Bβ transports dendritically localized mRNPs in neurons and is recruited to synapses in an activity-dependent manner. *Cellular and Molecular Life Sciences* **70**, 335–356 (2013).

152. Siomi, M. C. *et al.* FXR1, an autosomal homolog of the fragile X mental retardation gene. *EMBO J.* **14**, 2401–2408 (1995).

153. Zhang, Y. *et al.* The fragile X mental retardation syndrome protein interacts with novel homologs FXR1 and FXR2. *EMBO J.* **14**, 5358–5366 (1995).

154. Adams-Cioaba, M. A. *et al.* Structural Studies of the

Tandem Tudor Domains of Fragile X Mental Retardation Related Proteins FXR1 and FXR2. *PLoS One* **5**, (2010).

155. Chyung, E., LeBlanc, H. F., Fallon, J. R. & Akins, M. R. Fragile X granules are a family of axonal ribonucleoprotein particles with circuit-dependent protein composition and mRNA cargos. *J. Comp. Neurol.* **526**, 96–108 (2018).

156. Darnell, J. C., Fraser, C. E., Mostovetsky, O. & Darnell, R. B. Discrimination of common and unique RNA-binding activities among Fragile X mental retardation protein paralogs. *Hum. Mol. Genet.* **18**, 3164–3177 (2009).

157. Bontekoe, C. J. M. *et al.* Knockout mouse model for Fxr2: a model for mental retardation. *Hum. Mol. Genet.* **11**, 487–498 (2002).

158. Cheng, J. Y., Zhang, T. & Ruangwattanapaisarn, N. Fragile X Proteins FMRP and FXR2P control synaptic GluA1 expression and neuronal maturation via distinct mechanisms. **42**, 407–420 (2016).

159. Tamanini, F. *et al.* Oligomerization properties of fragile-X mental-retardation protein (FMRP) and the fragile-X-related proteins FXR1P and FXR2P. *Biochem. J.* **343 Pt 3**, 517–523 (1999).

160. Nishimura, T. *et al.* Role of the PAR-3-KIF3 complex in the establishment of neuronal polarity. *Nat. Cell Biol.* **6**, 328–334 (2004).

161. Morfini, G., Schmidt, N., Weissmann, C., Pigino, G. & Kins, S. Conventional kinesin: Biochemical heterogeneity and functional implications in health and disease. *Brain Res. Bull.* **126**, 347–353 (2016).

162. Wang, X., Vukovic, L., Koh, H. R., Schulten, K. & Myong, S. Dynamic profiling of double-stranded RNA binding proteins. *Nucleic Acids Res.* **43**, 7566–7576 (2015).

163. Pestova, T. V. & Hellen, C. U. T. Reconstitution of eukaryotic translation elongation in vitro following initiation by internal ribosomal entry. *Methods* **36**, 261–269 (2005).

164. Alkalaeva, E. Z., Pisarev, A. V., Frolova, L. Y., Kisselev, L. L. & Pestova, T. V. In Vitro Reconstitution of Eukaryotic Translation Reveals Cooperativity between Release Factors eRF1 and eRF3. *Cell* **125**, 1125–1136 (2006).

165. Laan, L. *et al.* Cortical dynein controls microtubule dynamics to generate pulling forces that position microtubule asters. *Cell* **148**, 502–514 (2012).

166. Sladewski, T. E. & Trybus, K. M. A single molecule approach to mRNA transport by a class V myosin. *RNA Biol.* **11**, 986–91 (2014).

167. Amrute-Nayak, M. & Bullock, S. L. Single-molecule assays reveal that RNA localization signals regulate dynein-dynactin copy number on individual transcript cargoes. *Nat. Cell Biol.* **14**, 416–23 (2012).

168. Fish, K. N. Total Internal Reflection Fluorescence (TIRF) Microscopy. *Curr Protoc Cytom* 1–21 (2009). doi:10.1002/0471142956.cy1218s50.Total

169. Jain, A. *et al.* Probing cellular protein complexes using single-molecule pull-down. *Nature* **473**, 484–488 (2011).

170. Roy, R., Hohng, S. & Ha, T. A practical guide to single-molecule FRET. *Nat. Methods* **5**, 507–516 (2008).

171. Lamichhane, R., Solem, A. & Rueda, D. Single Molecule FRET: Surface Passivation and Immobilisation. *Methods* **52**, 192–200 (2012).

172. Aggarwal, V. & Ha, T. Single-molecule pull-down (SiMPull) for new-age biochemistry: Methodology and biochemical applications of single-molecule pull-down (SiMPull) for probing biomolecular interactions in crude cell extracts. *BioEssays* **36**, 1109–1119 (2014).

173. Hoelzel, C. A. & Zhang, X. Visualizing and Manipulating Biological Processes Using HaloTag and SNAP-Tag Technologies. *ChemBioChem* cbic.202000037 (2020). doi:10.1002/cbic.202000037

174. Castoldi, M. & Popov, A. V. Purification of brain tubulin through two cycles of polymerization- depolymerization

in a high-molarity buffer. *Protein Expr. Purif.* **32**, 83–88 (2003).

175. Subramanian, M. *et al.* G-quadruplex RNA structure as a signal for neurite mRNA targeting. *EMBO Rep.* **12**, 697–704 (2011).

176. Schindelin, J. *et al.* Fiji: An open-source platform for biological-image analysis. *Nat. Methods* **9**, 676–682 (2012).

177. Tinevez, J. Y. *et al.* TrackMate: An open and extensible platform for single-particle tracking. *Methods* **115**, 80–90 (2017).

178. Sjekloća, L., Pauwels, K. & Pastore, A. On the aggregation properties of FMRP - A link with the FXTAS syndrome? *FEBS J.* **278**, 1912–1921 (2011).

179. Tsang, B. *et al.* Phosphoregulated FMRP phase separation models activity-dependent translation through bidirectional control of mRNA granule formation SUPP. *Proc. Natl. Acad. Sci.* **116**, 4218–4227 (2019).

180. Das, U. *et al.* Inhibition of protein aggregation: Supramolecular assemblies of Arginine hold the key. *PLoS One* **2**, (2007).

181. Maurin, T. *et al.* The FMRP/GRK4 mRNA interaction uncovers a new mode of binding of the Fragile X mental retardation protein in cerebellum. *Nucleic Acids Res.* **43**, 8540–8550 (2015).

182. Manuscript, A. & Expression, R. B. Recombinant Bacterial Expression and Purification of Human Fragile X Mental Retardation Protein Isoform 1. **74**, 242–247 (2011).

183. Stolt-Bergner, P. *et al.* Baculovirus-driven protein expression in insect cells: A benchmarking study. *J. Struct. Biol.* **203**, 71–80 (2018).

184. Schneider, C. P., Shukla, D. & Trout, B. L. Arginine and the Hofmeister Series: The Role of Ion-Ion Interactions in Protein Aggregation Suppression. *J. Phys. Chem. B* **115**, 7447–7458 (2011).

185. Yamaguchi, H. & Miyazaki, M. Refolding techniques for recovering biologically active recombinant proteins from inclusion bodies. *Biomolecules* **4**, 235–251 (2014).

186. Vagenende, V., Yap, M. G. S. & Trout, B. L. Mechanisms of protein stabilization and prevention of protein aggregation by glycerol. *Biochemistry* **48**, 11084–11096 (2009).

187. Alberti, S. *et al.* A User's Guide for Phase Separation Assays with Purified Proteins. *J. Mol. Biol.* **430**, 4806–4820 (2018).

188. Patel, A. *et al.* Biochemistry: ATP as a biological hydrotrope. *Science (80-.).* **356**, 753–756 (2017).

189. John R.Giudicessi, BA.Michael J.Ackerman., 2013. The variable detergent sensitivity of proteases that are utilized for recombinant protein affinity tag removal. *Bone* **23**, 1–7 (2008).

190. Mohanty, A. K., Simmons, C. R. & Wiener, M. C. Inhibition of tobacco etch virus protease activity by detergents. *Protein Expr. Purif.* **27**, 109–114 (2003).

191. Hinrichs, M. H. *et al.* Tau protein diffuses along the microtubule lattice. *J. Biol. Chem.* **287**, 38559–38568 (2012).

192. Chernov, K. G. *et al.* Atomic force microscopy reveals binding of mRNA to microtubules mediated by two major mRNP proteins YB-1 and PABP. *FEBS Lett.* **582**, 2875–2881 (2008).

193. Minoura, I., Katayama, E., Sekimoto, K. & Muto, E. One-dimensional brownian motion of charged nanoparticles along microtubules: A model system for weak binding interactions. *Biophys. J.* **98**, 1589–1597 (2010).

194. Andreasson, J. O. L., Shastry, S., Hancock, W. O. & Block, S. M. The mechanochemical cycle of mammalian kinesin-2 KIF3A/B under load. *Curr. Biol.* **25**, 1166–1175 (2015).

195. Turner-Bridger, B. *et al.* Single-molecule analysis of endogenous β-actin mRNA trafficking reveals a

mechanism for compartmentalized mRNA localization in axons. *Proc. Natl. Acad. Sci. U. S. A.* **115**, E9697–E9706 (2018).

196. Bensel, B. M. *et al.* Common general anesthetic propofol impairs kinesin processivity. *Proc. Natl. Acad. Sci. U. S. A.* **114**, E4281–E4287 (2017).

197. Yang, J. S. *et al.* rec-YnH enables simultaneous many-by-many detection of direct protein–protein and protein–RNA interactions. *Nat. Commun.* **9**, (2018).

198. Study, I. M. Protein Denaturation in Foam. *J Colloid Interface Sci* **332**, 323–332 (1999).

199. Clarkson, J., Cui, Z. & Darton, R. Protein Denaturation in Foam II. Surface Activity and Conformational Change. *J. Colloid Interface Sci.* **215**, 333–338 (1999).

200. Zanetti-Domingues, L. C., Martin-Fernandez, M. L., Needham, S. R., Rolfe, D. J. & Clarke, D. T. A Systematic Investigation of Differential Effects of Cell Culture Substrates on the Extent of Artifacts in Single-Molecule Tracking. *PLoS One* **7**, (2012).

201. Zanetti-Domingues, L. C., Tynan, C. J., Rolfe, D. J., Clarke, D. T. & Martin-Fernandez, M. Hydrophobic Fluorescent Probes Introduce Artifacts into Single Molecule Tracking Experiments Due to Non-Specific Binding. *PLoS One* **8**, (2013).

202. Lepe-Zuniga, J. L., Zigler, J. S. & Gery, I. Toxicity of light-exposed Hepes media. *J. Immunol. Methods* **103**, 145 (1987).

203. Goyena, R. & Fallis, A. . Analysis of the cytotoxic effects of light-exposed hepes-containing culture medium. *J. Chem. Inf. Model.* **53**, 1689–1699 (2019).

204. Simpson, J. A., Cheeseman, K. H., Smith, S. E. & Dean, R. T. Free-radical generation by copper ions and hydrogen peroxide. Stimulation by Hepes buffer. *Biochem. J.* **254**, 519–523 (1988).

205. Grady, J. K., Chasteen, N. D. & Harris, D. C. Radicals from ‘Good’s’ buffers. *Anal. Biochem.* **173**, 111–115

(1988).

206. Park, H. Y. & Hyungsik Lim, 3 Young J. Yoon, 1 Antonia Follenzi, 4, 5 Chiso Nwokafor, 1, 3, 6 Melissa Lopez-Jones, 1 Xiuhua Meng, 1 Robert H. SingerHye Yoon Park, 1, 2 Hyungsik Lim, 3 Young J. Yoon, 1 Antonia Follenzi, 4, 5 Chiso Nwokafor, 1, 3, 6 Melissa Lopez-Jones, 1 Robert H. Singer. Visualization of Dynamics of Single Endogenous mRNA Labeled in Live Mouse. *Science (80-.).* **343**, 422–424 (2014).

207. Miller, L. C. *et al.* Combinations of DEAD box proteins distinguish distinct types of RNA: Protein complexes in neurons. *Mol. Cell. Neurosci.* **40**, 485–495 (2009).

208. Ruhnow, F. & Diez, S. Challenges in estimating the motility parametersn of single processive motor proteins. *bioRxiv* 1–32 (2017). doi:10.1016/j.bpj.2017.09.024

209. Jankovics, F. & Brunner, D. Transiently Reorganized Microtubules Are Essential for Zippering during Dorsal Closure in Drosophila melanogaster. 375–385 (2006). doi:10.1016/j.devcel.2006.07.014

210. Wang, H. *et al.* Dynamic association of the fragile X mental retardation protein as a messenger ribonucleoprotein between microtubules and polyribosomes. *Mol. Biol. Cell* **18**, 3250–3263 (2007).

211. Adinolfi, S. *et al.* The N-terminus of the fragile X mental retardation protein contains a novel domain involved in dimerization and RNA binding. *Biochemistry* **42**, 10437–10444 (2003).

212. Blice-baum, A. C. & Mihailescu, M. R. Biophysical characterization of G-quadruplex forming FMR1 mRNA and of its interactions with different fragile X mental retardation protein isoforms Biophysical characterization of G-quadruplex forming FMR1 mRNA and of its interactions with different fragi. *Rna* 103–114 (2013). doi:10.1261/rna.041442.113.1

213. Evans, T. L., Blice-Baum, A. C. & Mihailescu, M. R. Analysis of the Fragile X mental retardation protein isoforms 1, 2 and 3 interactions with the G-quadruplex

forming semaphorin 3F mRNA. *Mol. Biosyst.* **8**, 642–649 (2012).